EFFECTS OF OXIDATIVE FUNCTIONALIZED AND AMINOSILANIZED CARBON NANOTUBES ON THE BEHAVIOURS OF POLYAMIDE-6 NANOCOMPOSITES

A THESIS SUBMITTED TO
THE GRADUATE SCHOOL OF NATURAL AND APPLIED SCIENCES
OF
MIDDLE EAST TECHNICAL UNIVERSITY

BY

SEÇİL ŞANKAL

IN PARTIAL FULFILLMENT OF THE REQUIREMENTS
FOR
THE DEGREE OF MASTER OF SCIENCE
IN
MICRO AND NANOTECHNOLOGY

MARCH 2013

Approval of the Thesis:

EFFECTS OF OXIDATIVE FUNCTIONALIZED AND AMINOSILANIZED CARBON NANOTUBES ON THE BEHAVIOURS OF POLYAMIDE-6 NANOCOMPOSITES

submitted by **SEÇİL ŞANKAL** in partial fulfillment of the requirements for the degree of **Master of Science in Department of Micro and Nanotechnology, Middle East Technical University** by,

Prof. Dr. Canan Özgen
Dean, Graduate School of **Natural and Applied Sciences** _____

Prof. Dr. Tayfun Akın
Head of Department, **Micro and Nanotechnology** _____

Prof. Dr. Cevdet Kaynak
Supervisor, **Metallurgical and Materials Engineering Dept., METU** _____

Assoc. Prof. Dr. Burcu Akata Kurç
Co-Supervisor, **Micro and Nanotechnology Department., METU** _____

Examining Committee Members:

Prof. Dr. Göknur Bayram
Chemical Engineering Department, METU _____

Prof. Dr. Cevdet Kaynak
Metallurgical and Materials Engineering Department, METU _____

Assoc. Prof. Dr. Burcu Akata Kurç
Micro and Nanotechnology Department, METU _____

Prof. Dr. Necati Özkan
Micro and Nanotechnology Department, METU _____

Assist. Prof. Dr. İrem Erel
Chemistry Department, METU _____

Date: **27.03.2013**

I hereby declare that all information in this document has been obtained and presented in accordance with academic rules and ethical conduct. I also declare that, as required by these rules and conduct, I have fully cited and referenced all material and results that are not original to this work.

Name, Last name: Seçil Şankal

Signature:

ABSTRACT

EFFECTS OF OXIDATIVE FUNCTIONALIZED AND AMINOSILANIZED CARBON NANOTUBES ON THE BEHAVIOURS OF POLYAMIDE-6 NANOCOMPOSITES

Şankal, Seçil
M.Sc., Department of Micro and Nanotechnology
Supervisor: Prof. Dr. Cevdet Kaynak
Co-supervisor: Assoc. Prof. Dr. Burcu Akata Kurç

March 2013, 80 pages

The first aim of this dissertation was to modify carbon nanotubes to be used as nano-reinforcements in the polyamide-6 matrix. Surfaces were first oxidative functionalized by sulphuric acid/nitric acid mixture, then aminosilanized by γ-aminopropyltriethoxysilane. Chemical groups formed on carbon nanotubes due to these surface treatments were characterized by X-ray photoelectron spectroscopy, Fourier-transform infrared spectroscopy and also energy dispersive spectroscopy. Morphological changes and crystal structure of surface-treated carbon nanotubes were analyzed by scanning electron microscopy and X-ray diffraction, respectively. Thermogravimetric analysis was also used to observe thermal degradation of the chemical groups formed on the nanotube surfaces.

Then, unmodified, oxidative functionalized and aminosilanized carbon nanotubes with three different loading levels (0.1, 0.5 and 1.0 wt%) were melt mixed with polyamide-6 matrix via laboratory size twin-screw extruder, followed by specimen shaping via injection molding. As the second aim of this dissertation, morphology and dispersion states of carbon nanotubes in polyamide-6 matrix was investigated by scanning and transmission electron microscopy; which revealed more homogeneous dispersion of functionalized and aminosilanized carbon nanotubes due to their increased chemical interactions with the matrix.

The third aim of this dissertation was to investigate effects of oxidative functionalized and aminosilanized carbon nanotubes on the (i) isothermal and (ii) non-isothermal crystallization kinetics of polyamide-6 by DSC analyses, and (iii) crystal structure of injection molded specimens by XRD analyses. Due to basically very effective heterogeneous nucleation effect, both increasing amount and surface functionalization of carbon nanotubes by oxidation and aminosilanization resulted in higher relative crystallinity for all three cases. The increases were as much as 40% for the isothermal and non-isothermal crystallization, and it was up to more than two times in the injection molding. Crystallization parameters and Avrami constants indicated that crystallization rate increases in isothermal crystallization while it decreases in non-isothermal crystallization due to the delayed conformational mobility of polymer chains via physical hinderance of carbon nanotubes. Parameters also revealed that growth mechanism of crystallites might change during isothermal crystallization while there was no significant change during non-isothermal crystallization. XRD deconvolution analyses indicated that during injection molding, due to the constraints of carbon nanotubes only α-crystal structure was formed.

Finally, as the fourth aim of this dissertation, effects of oxidative functionalized and aminosilanized carbon nanotubes on the mechanical and thermal properties of polyamide-6 nanocomposites were investigated. Flexural and tensile tests indicated that, increases in the flexural strength and tensile yield strength were 30% and 20%, while in the flexural modulus and Young's modulus were 40% and 23%, respectively, with only 1 wt% aminosilanized carbon nanotubes; due to very efficient load transfer from the matrix to covalently bonded carbon nanotubes. Both dynamic mechanical analysis and thermogravimetric analysis showed that surface modified carbon nanotubes improve all thermal

properties due to decreased matrix mobility and physical barrier formation. For example, increases in the storage modulus values were as much as 25%, while the increase in the thermal degradation temperatures were as much as by 5°C in the specimens with only 1wt% aminosilanized carbon nanotubes. Increases in the mechanical and thermal properties should be also due to the increased crystallinity of polyamide-6 matrix via carbon nanotubes acting as heterogeneous nucleation sites.

Keywords: Polyamide-6, Carbon Nanotubes, Oxidative Functionalization, Aminosilanization, γ-aminopropyltriethoxysilane, Crystallization Behaviour, Mechanical and Thermal Properties

ÖZ

OKSİDATİF FONKSİYONELLEŞTİRİLEN VE AMİNOSİLANLANAN KARBON NANOTÜPLERİN POLİAMİD-6 NANOKOMPOZİTLERİNİN DAVRANIŞLARINA ETKİLERİ

Şankal, Seçil
Yüksek Lisans, Mikro ve Nanoteknoloji Bölümü
Tez Yöneticisi: Prof. Dr. Cevdet Kaynak
Ortak Tez Yöneticisi: Doç. Dr. Burcu Akata Kurç

Mart 2013, 80 sayfa

Bu tezin ilk amacı, karbon nanotüplerin poliamid-6 matrisinde takviye malzemesi olarak kullanılması amacıyla yüzey modifikasyonunu yapmaktır. Nanotüplerin yüzeylerine öncelikle sülfürik asit/nitrik asit karışımı ile oksidatif fonksiyonelleştirme işlemi uygulanmış, sonrasında γ-aminopropiltrietoksisilan kullanılarak yüzeyler aminosilanlanmıştır. Bu işlemlere bağlı olarak karbon nanotüp yüzeylerinde oluşan kimyasal gruplar X-ışınları foto-elektron spektroskopisi, Fourier dönüşümlü kızıl ötesi spektroskopisi, enerji dağınımlı X-ışınları spektroskopisi ile karakterize edilmiştir. Yüzey işlemi uygulanan karbon nanotüplerin morfolojilerindeki değişimler ve kristal yapıları sırasıyla taramalı elektron mikroskopu ve X-ışını kırınımı ile incelenmiştir. Karbon nanotüplerin yüzeyleri üzerinde oluşturulan kimyasal grupların ısıl bozunumunu gözlemlemek için ise termogravimetrik analiz kullanılmıştır.

Sonrasında, poliamid-6 matris ile işlem görmeyen, oksidatif fonksiyonelleştirilen ve aminosilanlanan karbon nanotüpler üç farklı ağırlık yüzdesinde (ağ.% 0.1, 0.5 ve 1.0) çift vidalı ekstrüderde eriyik halde karıştırma yöntemi ile nanokompozitler üretilmiş, ardından enjeksiyon kalıplama yöntemiile numuneler şekillendirilmiştir. Bu tezin ikinci amacı olarak, karbon nanotüplerin poliamid-6 matris içerisindeki morfolojileri ve dağılımları taramalı ve geçirimli elektron mikroskobu ile incelenmiştir. Sonuçlar, matris ile kimyasal etkileşimlerinin artışına bağlı olarak, fonksiyonelleştirilen ve aminosilanlanan karbon nanotüplerin matris içerisinde daha homojen dağıldığını göstermiştir.

Bu tezin üçüncü amacı, oksidatif fonksiyonelleştirilen ve aminosilanlanan karbon nanotüplerin poliamid-6 matrisinin (i) eşısıl ve (ii) eşısıl-olmayan kristallenme kinetiği üzerine etkilerini DSC analizleriyle ve (iii) enjeksiyon kalıplama ile şekillendirilen numunelerin kristal yapıları üzerine etkilerini XRD analizleri ile incelemektir. Karbon nanotüplerin heterojen çekirdeklendirici olarak etki etmesi nedeniyle, hem karbon nanotüp miktarının artması hem de oksidasyon ve aminosilanlama yöntemleri kullanılarak yüzey fonksiyonelleştirmelerinin yapılması, üç durum için de göreceli kristallenme değerlerinin artmasını sağlamıştır. Eşısıl ve eşısıl-olmayan kristallenme için artışlar yaklaşık olarak %40 iken, enjeksiyon kalıplamada iki kattan daha fazlaya kadar iyileşmeler gözlemlenmiştir. Kristallenme parametreleri ve Avrami sabitleri, eşısıl kristallenmede kristallenme hızınınn arttığını buna rağmen eşısıl-olmayan kristallenmede karbon nanotüplerin fiziksel engel oluşturarak polimer zincir hareketliliğini kısıtlaması nedeniyle kristallenme hızının düştüğünü göstermektedir. Parametreler ayrıca kristal büyüme mekanizmasının eşısıl-kristallenme sırasında değişebileceğini ancak eşısıl-olmayan kristallenme sırasında önemli bir değişikliğin olmadığını göstermektedir. XRD dekonvolusyon analizleri enjeksiyon kalıplama sırasında karbon nanotüplerin fiziksel kısıtlamalarına bağlı olarak sadece α-kristal yapısının oluştuğunu göstermektedir.

Bu tezin dördüncü amacı olarak, oksidatif fonksiyonelleştirilen ve aminosilanlanan karbon nanotüplerin poliamid-6 nanokompozitlerinin mekanik ve ısıl özellikleri üzerine etkileri incelenmiştir. Eğme ve çekme testlerinden elde edilen sonuçlar, ağ.% 1.0 oranında aminosilanlanan karbon nanotüpler kullanılarak üretilen nanokompozitlerin eğme dayanımı ve çekmedeki akma dayanımı

değerlerindeki artışların sırasıyla %30 ve %20 olduğunu, bununla birlikte eğme modülü ve Young modülü değerlerinde ise sırasıyla %40 ve %23 artış olduğunu göstermektedir. Mekanik özelliklerdeki bu artışlar matristen kovalent olarak bağlanan karbon nanotüplere etkin yük transferi sağlanmış olması ile ilgilidir. Dinamik mekanik analizler ve termogravimetrik analizler, matris hareketliliğinin düşmesi ve fiziksel bariyer oluşumuna bağlı olarak, yüzey modifikasyonu yapılan karbon nanotüplerin eklenmesinin poliamid-6 matrisinin tüm ısıl özelliklerini iyileştirdiğini göstermektedir. Örneğin, ağ.% 1.0 oranında aminosilanlanan karbon nanotüp içeren numuneler için depolama modülü değerlerindeki artışlar %25 iken ısıl bozunum sıcaklıklarındaki artışlar 5ºC civarındadır. Mekanik ve ısıl özelliklerdeki artışların bir başka nedenin, heterojen çekirdeklendirici olarak etki eden karbon nanotüplerin poliamid-6 matrisinin kristallenme derecesini arttırmasıyla ilgili olduğu düşünülmektedir.

Anahtar Sözcükler: Poliamid-6**,** Karbon Nanotüpler, Oksidatif Fonksiyonelleştirme, Aminosilanlama, γ-aminopropiltrietoksisilan, Kristallenme Davranışı, Mekanik ve Isıl Özellikler

to my beloved family

ACKNOWLEDGEMENTS

I would like to express my sincere gratitude to my supervisor Prof. Dr. Cevdet Kaynak for his guidance, advice and patience at every stage of this dissertation. He provided me an opportunity to conduct a TUBITAK project that was my major purpose during my graduate studies. I would also acknowledge my co-supervisor Assoc. Prof. Dr. Burcu Akata Kurç for her advices during my experimental works.

I am very grateful to TUBITAK, the Scientific and Technological Research Council of Turkey, for their financial support of this research as a part of the Project 111M460. I would like to acknowledge all the technical staff and administrative board of the Metallurgical and Materials Engineering Department for supplying all the research facilities required in this thesis. I would also like to thank to METU Wind Energy Center sincerely for allowing extensive use of DSC, TGA and DMA equipment; and to METU Central Laboratory for XPS, FT-IR and TEM analyses.

I want to thank my laboratory mates, Ayşe Çağıl Özkaraca, Esin İbibikcan, Bengü Melike Sipahioğlu and Yelda Meyva for their sincere friendship, support and encouragement. I also want to thank Duygu Kozanoğlu, Elçin Dertli, Salar Habibpur and Zhanar Sholanbayeva from Micro and Nanotechnology Department for their valuable friendship. This academic journey would have been more difficult without their positive approach.

My sincere thanks go to the very best of friends, Caner Ural, Derya Çetecioğlu, Emir Bozkırlı, Gözde Begüm Akyol, Melike Baladın, Orçun Çınar, Öncü Tatar and Pelin Tonka for helping me get through the difficult times, and for all the support, entertainment and caring they have provided for many years.

I would like to express my deepest gratitude to my mother, my father and my little sister, Göksu Şankal. They have been a constant source of love and encouragement in every step of my life. This thesis would certainly be not possible without their support.

My special thanks go to my love Sarper Ünen who has completely changed my life. Words are not enough to express my deep gratitude; just I can thank him from the bottom of my heart for being in my life. I am sincerely longing for his endless existence throughout the rest of my life.

TABLE OF CONTENTS

.

LIST OF TABLES

TABLES

LIST OF FIGURES

FIGURES

NOMENCLATURE

(1-X_T)	**:**	amorphous phase fraction with respect to temperature
(1-X_t)	**:**	amorphous phase fraction with respect to time
2θ	**:**	XRD diffraction angle
β	**:**	cooling rate during non-isothermal crystallization
$dH(t)/dt$	**:**	rate of heat evolution
ΔH_f	**:**	measured heat of fusion of the specimens
ΔH_f^0	**:**	heat of fusion of 100% crystalline polymer
ΔH_c	**:**	heat of crystallization
APTES	**:**	γ-aminopropyltriethoxysilane
CCVD	**:**	catalytic carbon vapor deposition
CNTs	**:**	unmodified carbon nanotubes
f-CNTs	**:**	oxidative functionalized carbon nanotubes
K	**:**	crystallization rate constant
K_c	**:**	modified Avrami rate constant
MWCNTs	**:**	multi-walled carbon nanotubes
n	**:**	Avrami exponent
OR^1	**:**	hydrolyzable alkoxy group
PA6	**:**	polyamide-6
R	**:**	functional organic group
RO	**:**	reverse osmosis
s-CNTs	**:**	oxidative functionalized and then aminosilanized carbon nanotubes
SWCNTs	**:**	single-walled carbon nanotubes
$t_{1/2}$	**:**	half crystallization time
t_{max}	**:**	maximum rate of crystallization
t_∞	**:**	end time of the crystallization
$T_{1/2}$	**:**	half crystallization temperature
$T_{5wt\%}$	**:**	thermal degradation temperature at 5 wt% mass loss
$T_{10wt\%}$	**:**	thermal degradation temperature at 10 wt% mass loss
$T_{25wt\%}$	**:**	thermal degradation temperature at 25 wt% mass loss
T_g	**:**	primary transition temperature
T_{max}	**:**	maximum degradation rate temperature
$T_{MLR\text{-}max}$	**:**	maximum mass loss rate peak
T_o	**:**	onset crystallization temperature
T_p	**:**	peak temperature of crystallization
T_R	**:**	temperature range of crystallization
T_∞	**:**	end crystallization temperature
X_c	**:**	degree of crystallinity
X_t	**:**	fractional crystallinity
w_m	**:**	weight fraction of polymer

CHAPTER 1

INTRODUCTION

1.1 Polyamide-6 and Its Crystallization Behavior

Polyamides, also known as nylons, are known as one of the most important class of thermoplastic polymers and are subject of consistent interest because of their utility in a very wide range of engineering applications. The combination of mechanical and electrical properties associated with good chemical resistance, fire resistance, stability at elevated temperatures, drawability, good appearance and good processibility are key properties of polyamides.

Polyamide was first synthesized in 1935 by Wallace Carothers, a scientist at the laboratories of DuPont Company. The first commercial use was in 1938 with the production of tooth brush filaments by using polyamide 6,6. Consequently, Paul Schlack synthesized polyamide-6 from caprolactam in 1938 at I.G. Farbenindustrie in Germany. Since then, the commercial use of polyamides continues to rise and become indispensable in today's society. Polyamides have found miscellaneous application areas in automotive components, electrical/electronic devices, consumer products and packaging.

Polyamides contain amide groups (–CONH–) in their mer structure. There is a broad range of polyamide materials depending on the monomers employed. Semi-crystalline polyamides are the most significant commercial polyamides which represent more than 90% of global use. Figure 1.1 shows chemical structure of polyamide-6 with the repeating mer unit enclosed in brackets.

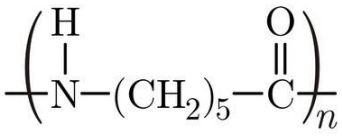

Figure 1.1 Chemical Structure of Polyamide-6

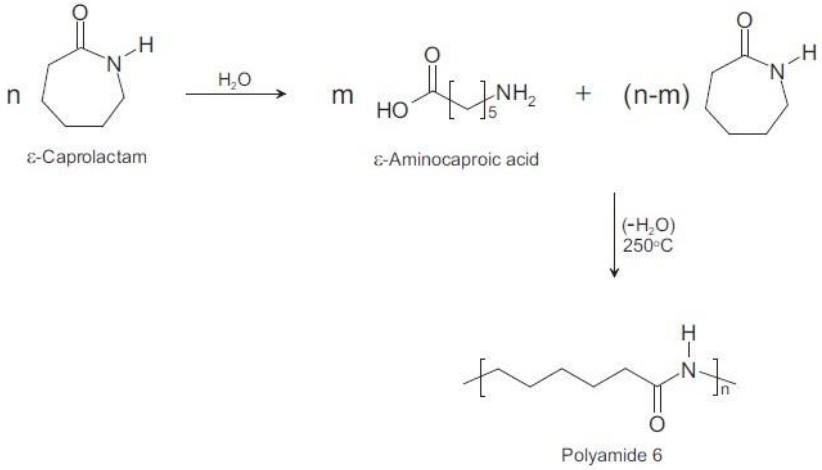

Figure 1.2 Synthesis of Polyamide-6 from ε-caprolactam [1]

In industry, polyamide-6 is today generally synthesized by a step-growth mechanism following the ring-opening polymerization of ε-caprolactam, as shown in Figure 1.2. ε-caprolactam is a ring structured molecule which polymerizes itself. Synthesized polyamide is called polyamide-6 as caprolactam has six carbon atoms. Polymerization process of polyamide-6 is said to be a step-growth polymerization because each bond in the polymer is formed independently. Step-growth polymerization generally proceeds with a condensation reaction in which a water or an alcohol molecule is eliminated in each step [1].

In the first step, ε-caprolactam reacts with water, then a few percent of the ε-caprolactam hydrolyzes to ε-aminocaproic acid. NH_2 groups of the ε-aminocaproic acid initiate the ring-opening polymerization of the ε-caprolactam. After that polycondensation reaction takes place between the NH_2 and COOH endgroups of the ring-opening polymerization reaction which results in a high molecular weight product. In the final step, water is eliminated [1].

Crystal structure and hydrogen bonding are significant concepts in the polymer field. An ideal polymer crystal is formed from an ordered, identical structural units and infinite repetition of these units in space which refers to crystalline state. The polymer is in the amorphous state when no order is present. Polymer molecules have great length and irregularity, so in general they do not have an ideal crystal structure. Certain polymers do not indicate any crystalline structure and remain in the amorphous state. Most polymers, including polyamides, contain crystalline and amorphous regions which are called semicrystalline polymers [1]. Crystal structure of polymers are thin and lamellar. Molecular chains of the polymer are folded back and forth between the main surface of each lamella. Figure 1.3 shows folded chains in a crystalline structure and a schematic unit cell for polyamide [1].

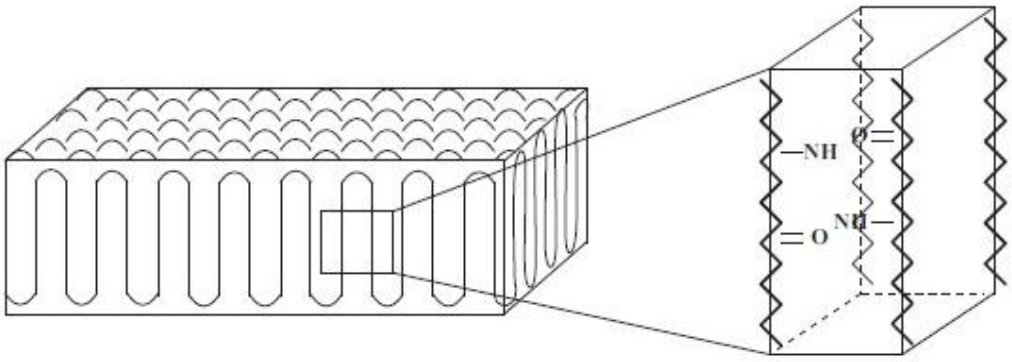

Figure 1.3 Chain Folding in a Crystalline Structure (on the left), and a Schematic Unit Cell for Polyamide (on the right) [1]

Polyamides occupy a prominent place in the thermoplastic polymer family thanks to their good mechanical properties, excellent chemical resistance, and their stability at high temperatures. The underlying qualities of polyamides are related to their crystallinity and high melting points. In addition, it has been stated that their ability to form strong hydrogen bonds between the chains affects their properties. Any structural changes that influence interchain hydrogen bonding ability will have a significant impact on the properties [2].

Hydrogen bonding takes place between the carbonyl and NH groups in adjacent sections of the polyamide chains. For polyamide-6, when chains are aligned together, a high degree of hydrogen bonding develops which results in enhanced crystalline structure in that area. These polyamides are semicrystalline materials that consist of a combination of ordered crystalline areas having a much higher concentration of hydrogen bonding and more random amorphous areas. Good balance of properties can be achieved for semicrystalline structured polymers. Crystalline areas contribute to the

strength, stiffness, creep resistance, electrical properties, chemical resistance, temperature stability whereas the amorphous areas make contribution to the impact resistance and high elongation [3].

Polyamide-6 has two major crystalline structures, α-phase and γ-phase as indicated in Figure 1.4. Polyamide chains adopt either a fully extended or twisted configuration in order to enhance hydrogen bonding in the crystalline areas. In the fully extended configuration, namely α-phase, polymer chains are formed in an anti-parallel orientation. In anti-parallel chains, amide linkages and methylene units lie within the same plane and hydrogen bonding takes place between adjacent anti-parallel chains. Whereas, γ-phase of polyamide-6 takes place when hydrogen bonding occurs between parallel polyamide chains. In this case, amide linkages should twist approximately 60° out of the plane of these molecular layers in order to form hydrogen bonding. Otherwise, only half of the hydrogen bonds would be formed. Monoclinic α-phase is the thermodynamically stable crystalline form usually obtained by slow cooling from the melt while pseudohexagonal γ-phase is the less stable one usually forming by fast cooling [4].

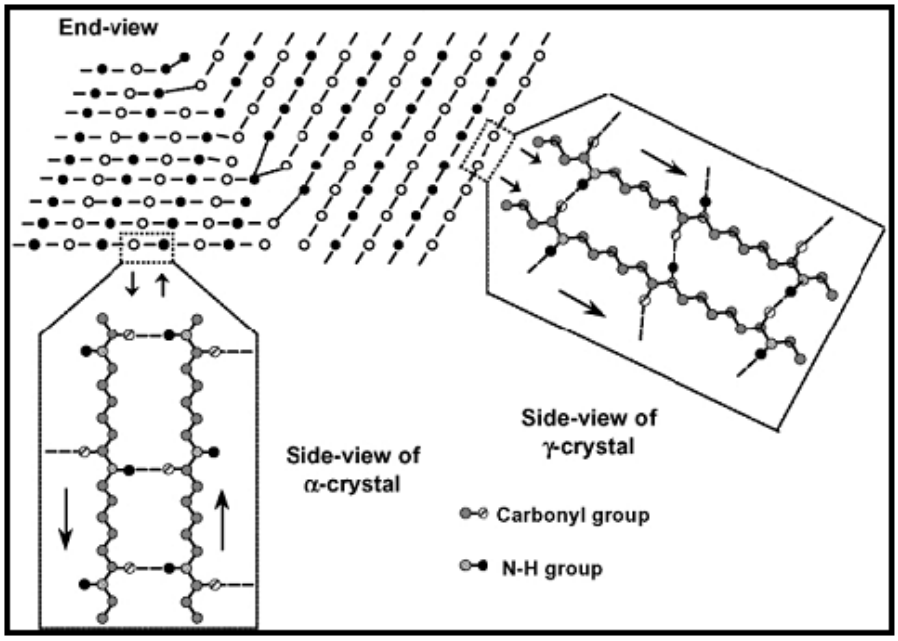

Figure 1.4 End-view and Side-view of the α- and γ- Crystalline Structures of Polyamide-6 [4]

One of the characteristics of polyamide is the ability to absorb significant amount of water. Water absorption usually become intense in the amorphous areas of the polymer which is again related to the polar amide groups. Higher proportion of amide groups leads to higher water adsorption when degree of crystallinity is inadequate. Increased content of water has similar effect to that of increased temperature. This property interrupts the polymer hydrogen bonding thus plasticizing the material, making it more flexible and increasing the impact strength. In addition, increase in water content leads to a decrease in stiffness and tensile strength values. However, water stiffens the polyamide at very low temperatures. Both the degree of crystallinity and the density of amide groups are responsible for the water absorption [2, 3].

The greatest application area for polyamides is automotive industry. The number of new applications rapidly increases and strongly contributes to the overall growth rate for this type of polymer. Polyamides are considered to replace metal components due to their lower weight (and hence higher fuel efficiency) and decreased manufacturing costs. During 1990s, air intake manifolds made from polyamide had replaced aluminum and utility of polyamides had extended to fans, thermostat housings, valve and engine covers. Polyamides have been utilised for handles, seat belt components and switches. New applications comprise air bag containers (in order to resist the explosive inflation

forces, very tough materials are needed), pedals and pedal boxes. Polyamides have also been used to replace metals in seat systems. The greatest exterior application for polyamides is probably the wheel covers which made from polyamide composites in order to get the required degree of dimensional stability and flatness. Other exterior applications involve door handles, sun roof surrounds, fuel filler flaps, etc. [3].

Electrical and electronic industry is another important application area of polyamides due to their electrical insulating properties, stability at high temperatures, toughness, and inherent low flammability. Significant applications include cable ties, plugs, switches, connectors and light housings [3].

Moreover, polyamides have been used in a number of consumer applications. Sporting goods is another area in which polyamide use has expanded significantly. Polyamide has been used in ice/roller skates, sports shoe soles, ski boots and tennis rackets (polyamide composites with carbon fiber reinforcement). Lighters, kitchen utensils, toothbrush filaments, spectacle frames, sewing thread, and packaging film are other miscellaneous applications of polyamide [3].

1.2. Carbon Nanotubes

The groundbreaking discovery of carbon nanotubes (CNTs) [5] have stimulated considerable scientific interest due to their extraordinary properties. CNTs not only have unique atomic structure, low density, nanoscale diameter and high aspect ratio but also they exhibit exceptional mechanical properties, high electrical and thermal conductivities [6-9]. The combination of these intrinsic characteristics makes them excellent candidates in the production of high-performance and multifunctional polymer nanocomposites [10, 11].

There are two main types of carbon nanotubes depending on the production process. Single-walled carbon nanotubes (SWCNTs) consist of a single graphene layer rolled seamlessly to form a cylinder whereas multi-walled carbon nanotubes (MWCNTs) consist of two or more concentric cylindrical graphene layers coaxially arranged around a central hollow core with van der Waals forces between adjacent layers. Figure 1.5 shows TEM images of MWCNTs with different graphene layers [12].

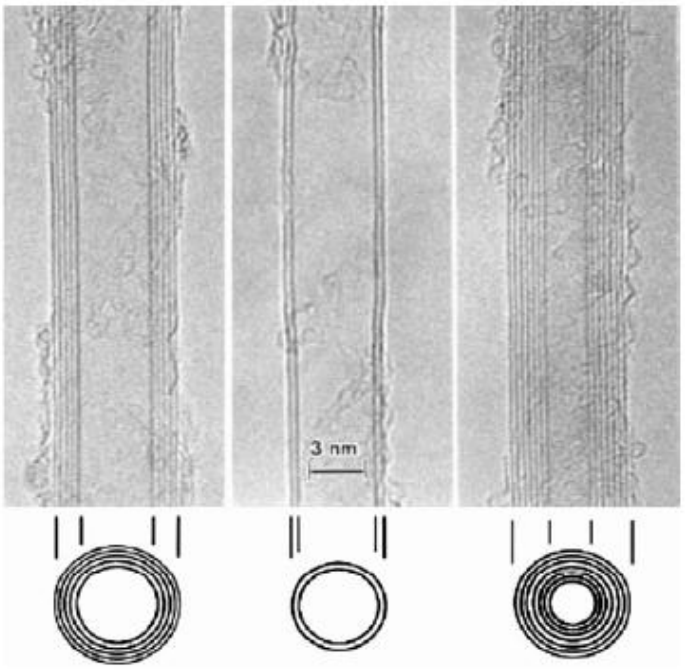

Figure 1.5 TEM Images of MWCNTs with 5, 2, 7 Layers of Graphene [12]

Structure of carbon nanotubes can be described by means of nanotube chirality. Rolling angle of the graphene layer determines the tube chirality. Carbon nanotubes have three chiralities, namely, armchair, zigzag and chiral. Chirality is identified by the chiral vector, $C_h = na_1 + ma_2$, where the integers (n, m) are the number of steps along the carbon bonds and a_1 and a_2 are unit vectors of the hexagonal lattice, as shown in Figure 1.6. Using these integers (n, m) three types of chiralities are specified. If $n = m$, the nanotubes are called ‘‘armchair”. If $m = 0$, the nanotubes are called ‘‘zigzag”. Otherwise, they are called ‘‘chiral” [12].

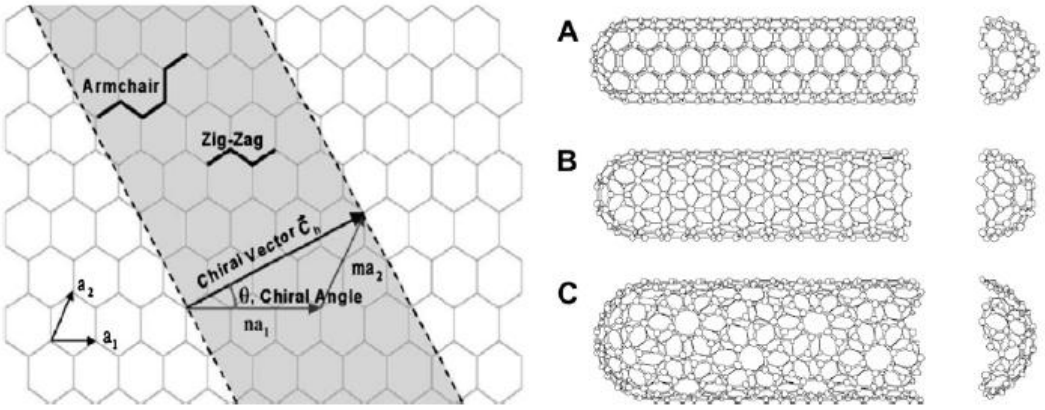

Figure 1.6 Carbon Nanotubes with Different Chiralities: (A) Armchair, (B) Zigzag, and (C) Chiral [12]

Diameter of carbon nanotubes ranges from 1 to 100 nm whereas they have lengths up to millimetres. Their densities can be as low as ~1.3 g/cm^3 [13]. The chemical bonding of carbon nanotubes consist of sp^2 carbon–carbon bonds which is stronger than the sp^3 bonds found in diamond. Extremely high mechanical properties of carbon nanotubes are originated from this bonding structure [12]. Their Young’s modulus are greater than that of all carbon fibers with values higher than 1 TPa. Multi-walled carbon nanotubes have strengths of almost 60 GPa which is an order of magnitude higher than that of carbon fibers. Even the weakest measured strength for a carbon nanotube was several GPa. These exceptional mechanical properties make carbon nanotubes one of the strongest and stiffest materials on earth [13]. Typical properties of carbon nanotubes are summarized in Table 1.1 [14].

Primary production techniques for single and multi-walled carbon nanotubes are arc discharge, laser ablation, and chemical vapor decomposition (CVD) from hydrocarbons. In arc discharge and laser ablation techniques, solid carbon is evaporated and then condensated carbon atoms are used in order to produce carbon nanotubes [10, 13, 15].

Chemical vapor decomposition includes catalytic decomposition of a gaseous carbon source (hydrocarbon, CO) and deposition of nanotubes on a substrate or growing from a substrate. Chemical vapor decomposition might suggest more control over the length and structure of the produced nanotubes compared with arc discharge and laser ablation [10, 13, 15].

Large quantities are required for application of carbon nanotubes as reinforcing materials in composites. Compared to the very low yield of the arc discharge and laser ablation techniques, CVD method suggests the highest potential for large-scale production of carbon nanotubes [10, 13, 15]. It is also well known that production techniques of carbon nanotubes generate impurities such as non-tubular fullerenes, amorphous carbon and catalyst particles. Therefore, in order to seperate these impurities, purification steps are required after production process. CVD process tend to produce nanotubes with fewer impurities [10].

Table 1.1 Typical Properties of Carbon Nanotubes [14]

Property	**SWCNT**	**MWCNT**
Tensile Strength (GPa)	50 - 500	10 - 60
Elastic Modulus (TPa)	~1	0.3 - 1
Elongation at Break (%)	5.8	-
Density (g/cm^3)	1.3 - 1.5	1.8 - 2.0
Electrical Conductivity (S/m)	$\sim 10^6$	$\sim 10^6$
Thermal Stability (in air)	>700°C	>700°C
Typical Diameter (nm)	1	20

1.3 Functionalization Techniques of Carbon Nanotubes

In the last 20 years, there has been a strong emphasis on the development of polymeric nanocomposites, where at least one of the dimensions of the filler material is in the order of a nanometer. The potential of carbon nanotubes as reinforcement materials in polymer nanocomposites is based not only on the extraordinary mechanical properties of carbon nanotubes, but also on their relatively high aspect ratio and surface area-to-volume ratio. Structures with high high aspect ratio are known to be more load-carrying efficient, while high surface area-to-volume ratio means more surface area at the same volume. For composite materials, this results in an increase of the surface area of the reinforcing phase, and thus an increase of the region for load transfer from matrix to carbon nanotubes.

Carbon nanotubes have a great tendency to form bundles and entanglements due to the presence of strong van der Waals attractions between them. Figure 1.7 shows entangled carbon nanotube agglomerates observed during SEM analysis of unmodified CNTs in this thesis. Additionally, CNT surfaces are usually hydrophobic and chemically inert, which leads to poor interfacial adhesion with many polymer matrices. In this regard, two major challenges encountered in developing high-performance polymer/CNT nanocomposites are first to obtain uniform dispersion of CNTs throughout the polymer matrix without formation of bundles and second sufficient interfacial adhesion between CNTs and polymer matrix required for the efficient load transfer from the matrix to the reinforcing nanotubes.

Different methods have been reported for the functionalization of CNT surfaces in order to improve debundling of CNTs and interfacial bond with polymer matrices. Among them, introduction of functional groups on the surface of CNTs via oxidative functionalization is considered as one of the most effective route.

In the literature, several oxidizing agents have been employed including H_2O_2 [16–18], $KMnO_4$ [19, 20], O_3 [21, 22], HNO_3 [23–28], H_2SO_4 [29], and mixture of HNO_3/H_2SO_4 [30–35]. With oxidative functionalization, defect sites are created on the surface of CNTs and these are stabilized by covalent attachment of carboxylic acid (–COOH) or hydroxyl (–OH) functional groups. Oxygen-containing functional groups can be used as linkers for further chemical reactions, such as silanization.

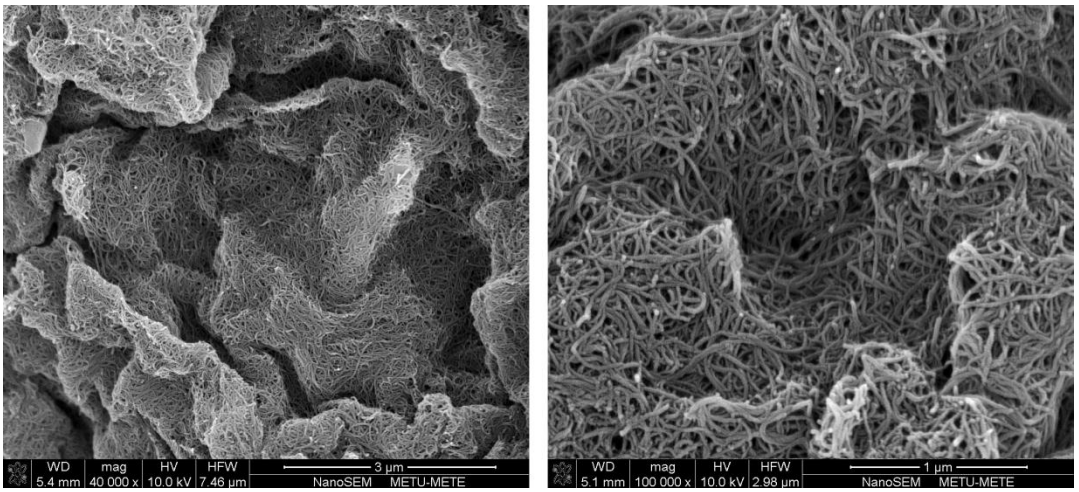

Figure 1.7 SEM Images of Unmodified Carbon Nanotube Entanglements Observed in this Thesis

Silanization of CNTs is one of the most effective strategies employed to enhance both dispersion and interfacial adhesion with the polymer matrix. Most commonly used silane coupling agents are organosilanes that are represented by the following formula:

$$R - (CH_2)_n - Si(OR^1)_3$$

where n = 0–3, OR^1 is the hydrolyzable alkoxy group, and R is the functional organic group. The selection of the R group depends on the matrix being used. The $(OR^1)_3$ is generally trimethoxy $(OCH_3)_3$ or triethoxy $(OC_2H_5)_3$.

As illustrated in Figure 1.8, silanization reaction involves four steps. First, hydrolysis of the unstable $(OR^1)_3$ groups forming trihydroxy silanols followed by condensation to siloxane oligomers. Then, these oligomers form hydrogen bonding with the hydroxyl groups present on the nanotube surfaces which were produced via previous oxidative treatments. Finally, covalent bonding can be formed with nanotube surfaces after dehydration and condensation.

1.4 Literature Survey

1.4.1 Studies on the Characterization of Functionalized Carbon Nanotubes

Kathi et al. [36] functionalized CNTs with H_2SO_4/HNO_3 (3:2)(v:v) acid mixture and then silanized using 3-aminopropyltriethoxysilane (APTES). FT-IR spectrum of oxidized nanotubes presented two new bands at 1716 cm^{-1} and 1162 cm^{-1} which corresponds to C=O and C–O stretching vibrations of the carboxylic groups (–COOH). FT-IR spectrum of silanized nanotubes indicated characteristic absorption peaks at 1070 cm^{-1} and 803 cm^{-1} which correspond to Si–O vibration and Si–OH stretching, respectively.

Zhou et al. [37] coated CNTs with inorganic silica by a sol–gel process and then grafted with 3-methacryloxypropyltrimethoxysilane (3-MPTS). Their deconvolution of Si2p peak from XPS analysis revealed typical peaks for –Si–O–Si– and –Si–O–C– bonds at binding energies of 103.6 and 106.1 eV, respectively. XRD diffractograms indicated that both silica-coating and 3-MPTS functionalization had no influence on the diffraction peak of CNTs. TGA curves showed that maximum degradation rate temperature (T_{max}) of unmodified CNTs is at about 700°C whereas after 3-MPTS functionalization, T_{max} decreased to 666°C.

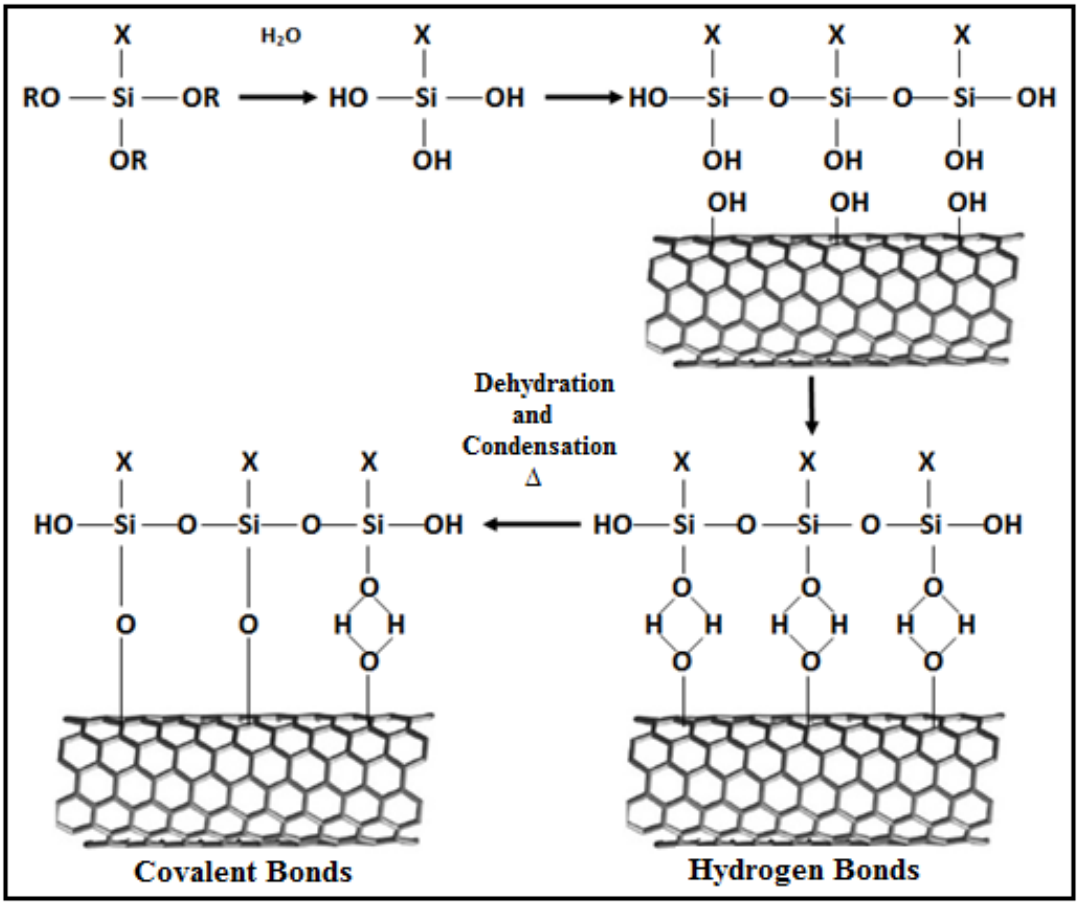

Figure 1.8 Silanization Process of Carbon Nanotubes

Ma et al. [38] conducted a combined process of UV/O_3 treatment and silanization reaction using 3-glycidoxypropyltrimethoxy silane (GPTMS) for the functionalization of CNTs. Their XPS analysis revealed that the atomic percentage of oxygen increased from 1.35% to 8.74% which can be attributed to the generated functional groups on CNT surfaces. Deconvoluted Si2p peak from XPS analysis at a binding energy of 101.6 eV indicated the bond of silicon with oxygen originating from CNTs (–Si–O–C–) whereas the bond at 103.3 eV was attributed to siloxane (–Si–O–Si–) resulting from the partial hydrolysis of GPTMS molecules.

Yu et al. [39] functionalized CNTs with H_2SO_4/HNO_3 (3:1)(v:v) acid mixture and then silanized using n-octyltriethoxysilane (OTES). Their SEM images indicated that pristine CNTs were encapsulated by foreign substances containing excessive impurities. However, it was stated that acid treatment of CNTs removed metal catalyst particles, graphite fragments and amorphous carbons. Their FT-IR results revealed formation of surface functional groups, e.g. the broad peak at ~3429 cm^{-1} was attributed to O-H stretching vibration, while the peak at 1730 cm^{-1} was assigned to stretching vibrations of carbonyl groups (C=O).

Shanmugharaj et al. [40] treated CNTs with H_2SO_4 in the presence of potassium dichromate ($K_2Cr_2O_7$) and then silanized with 3-aminopropyltriethoxysilane (APTES). Their SEM-EDS analyses showed only a carbon peak for unmodified CNTs while two peaks of carbon and oxygen were observed for functionalized CNTs. The presence of silane molecules was confirmed from the peak appeared at around 1.8 eV. This evidence was further supported by the relative increase in O/C ratio with silanization. It was also observed from TGA curves that for unmodified CNTs, the residual weight at 750°C was 90%, while this value was about 45% for silanized CNTs which was attributed to the degradation of chemically attached aminosilane molecules.

Li et al. [41] treated CNTs with H_2SO_4/HNO_3 (3:1)(v:v) acid mixture and then functionalized by 1,6-hexamethylenediamine (HMD) via acid-thionyl chloride. Their SEM images showed that the stacking behavior of pure (p-CNTs), acid-treated (a-CNTs) and functionalized (f-CNTs) nanotubes were different from each other. It was stated that p-CNTs were randomly and loosely entangled together while a-CNTs were compact and massive. Under higher magnification, agglomeration of a-CNTs was observed. It was found that in the agglomerated structure, some CNTs were adhered together and almost no interspace remains. After functionalization with HMD, it was observed that f-CNTs became loose again.

Aviles et al. [42] conducted chemical functionalization of CNTs by means of acid oxidation with HNO_3/H_2O_2 (Ox-CNTs), direct silanization of the as-received CNTs by using 3-methacryloxypropyltrimethoxysilane (MPTMS) (Sil-CNTs), and a sequential treatment based on oxidation and silanization (Ox-Sil-CNTs). FT-IR spectrum of Ox-CNTs showed an intensity at 1714–1726 cm^{-1}, which corresponded to the stretching vibrations of carbonyl groups (C=O). FT-IR spectrum of Ox-Sil-CNTs indicates characteristic absorption bands at 1160 and 817 cm^{-1} associated with the –Si–O–C– functional group and Si–OH stretching, respectively.

Yuen et al. [43] modified CNTs by refluxing with an acid mixture of H_2SO_4/HNO_3 (3:2)(v:v) and silanized with 3-aminopropyltriethoxysilane (APTES). XPS spectrum of silane-modified CNTs revealed main C1s and O1s peaks at binding energies of 285 and 531 eV, respectively. Additional peaks were observed at 103 and 400 eV corresponding to the Si2p and N1s. FT-IR spectrum of acid-oxidized CNTs indicated carboxylic group stretching (COOH) at 1720 cm^{-1}. It was also observed that COO^- asymmetric stretching and $^-COO^-$ stretching corresponded to the wavenumbers 1610 cm^{-1} and 3430 cm^{-1}, respectively.

1.4.2 Studies on the Crystallization Behaviour of Polyamide-6 Reinforced with Carbon Nanotubes

The degree of crystallinity and crystalline structure of thermoplastic polymers have profound effects on their physical, chemical and mechanical properties, thus it is very important to study the influences of reinforcing fillers especially their size, amount, and surface characteristics on the crystallization behavior of micro- and nanocomposites.

In this respect, researchers have significant interest to enhance degree of crystallinity of polyamide-6 to achieve desired nanocomposite properties. In the literature, apart from micron sized fillers, there are several reports investigating the effects of nano-fillers such as nanoclays [44-47], foliated graphite [48], nano-Ag [49], nano-SiO_2 [50], nano-$CaCO_3$ [51], nano-ZnO [52], etc. on the crystallization behaviour of polyamide-6. Limited number of investigations [53-56] on the influences of carbon nanotubes are summarized below:

Chen et al. [53] prepared polyamide-6 (PA6) nanocomposites with acid treated carbon nanotubes (CNTs) by solution mixing technique. Isothermal crystallization kinetics revealed that the addition of 0.25 and 1.0 wt% treated CNTs significantly speed up the crystallization rate of PA6. The Avrami exponent, *n* values for neat PA6 was found in the range of 3.1-3.2 while it was in the range of 2.0-2.4 for PA6/CNT nanocomposites. Non-isothermal crystallization kinetics also showed that at the same cooling rate, peak temperature *(T_p)* slightly shifted to higher temperatures for the PA6/CNT nanocomposites, compared to neat PA6. They claimed that these improvements were due to treated CNTs acting as heterogeneous nucleation sites.

Li et al. [54] investigated non-isothermal crystallization kinetics of PA6/CNT nanocomposites. They showed that PA6/CNT nanocomposites have higher T_p and broader crystallization temperature range *(D)* than neat PA6 at all cooling rates. It is noted that *n* values of neat PA6 vary from 4.5 to 6.7, while they range from 4.0 to 4.7 for the nanocomposites which means that introduction of CNTs influences the nucleation and growth mechanisms of PA6 crystallites. However, they also indicated that the crystallization rate of nanocomposites were lower compared to neat PA6.

In their another work, Li et al. [55] studied isothermal crystallization kinetics of PA6 nanocomposites filled with pristine CNTs and 1,6-hexamethylenediamine (HMD) grafted CNTs through melt blending. They simply showed that at all crystallization temperatures nanocomposites have higher crystallization rate than that of neat PA6 due to the nucleating effects of CNTs. The *n* values of the nanocomposites with pristine CNTs and grafted CNTs were 1.5–1.7 and 2.1–2.5, respectively.

Qiu et al. [56] studied monomer casting PA6 nanocomposites with toluene 2,4-diisocyanate functionalized CNTs via in situ anionic ring opening polymerization. Non-isothermal crystallization kinetics were modeled with Avrami equation modified by Jeziorny. It was stated that the Avrami-Jeziorny model could well correspond to the non-isothermal crystallization data of neat PA6. On the other hand, for the nanocomposites, the deviation from the plot in the final stage of crystallization was attributed to the secondary crystallization, and the change of *n* values from 4.12 to 4.68 resulting from a change in the nucleation mechanism.

1.4.3 Studies on the Effects of Silanized Carbon Nanotubes on the Mechanical and Thermal Properties of Polymer Matrices

Mukherjee et al. [57] investigated effects of vinyltriacetoxy silane treated carbon nanotubes on the properties of Polycarbonate (PC)/Liquid Crystalline Polymer (LCP) system. They revealed that incorporation of silane coupling agent enhanced thermal stability and storage modulus of the PC/LCP system as much as 14% and 50%, respectively. They claimed that these results are due to the better dispersion and enhanced interaction of CNTs with the matrix system.

Yuen et al. [58] prepared polyimide nanocomposites with γ-aminopropyltriethoxysilane (APTES) treated CNTs. They indicated that glass transition temperature (Tg) of polyimide increased from 281°C to 304°C when 4.8 wt% APTES treated CNTs were used, while tensile strength of polyimide increased 26% with only 1.0 wt% APTES treated CNTs.

Wu et al. [59] produced DGEBA type epoxy matrix nanocomposites with 3-isocyanatopropyltriethoxysilane (IPTES) treated CNTs. Their SEM analysis revealed that silane treated CNTs were well dispersed and embedded in the matrix, while tensile strength of epoxy increased 41% with only 1.0 wt.% of these CNTs.

Kim et al. [60] compared the effects of acid treated and γ-aminopropyltriethoxysilane modified carbon nanotubes on the flexural properties of CNT/epoxy/basalt composites. They indicated that 1 wt.% silane-treated CNTs lead to 10% higher flexural modulus, 14% higher flexural strength and 40% higher fracture toughness G_{IC} compared to acid treated CNTs.

Lee et al. [61] produced carbon/CNT/epoxy composites containing 1 wt.% unmodified, acid-treated, and γ-aminopropyltriethoxysilane -modified CNTs. It was shown that silane-modified CNTs resulted in 8% and 16% higher tensile strength compared to acid-modified and unmodified CNTs, respectively. For the storage modulus values, these increases were 14% and 61%, respectively.

Zhou et al. [62] investigated polypropylene matrix nanocomposites reinforced with 3-methacryloxypropyltrimethoxysilane (3-MPTS) treated CNTs and they concluded that using silane treated CNTs lead to 4% higher tensile strength compared to untreated CNTs.

Jiang et al. [63] used bis(3-triethoxysilylpropyl) tetrasulfide (TESPT) as a silane coupling agent to modify CNT surfaces. Then, they developed natural rubber/CNT nanocomposites by solvent casting. It was revealed that using 3 wt% silane modified CNTs resulted in 33% higher storage modulus compared to unmodified CNTs.

1.5 Aim of the Study

Carbon atoms on carbon nanotube walls are chemically stable because of the aromatic nature of the bond. Thus, carbon nanotubes are inert and can interact with the surrounding matrix mainly through van der Waals interactions, which is not enough to provide an efficient load transfer from matrix to carbon nanotubes. It is also difficult to obtain uniform dispersion of carbon nanotubes throughout polymer matrix. This difficulty is related to the poor interfacial adhesion with polymer matrix and the inevitable bundle and entanglement formation because of strong van der Waals attraction between nanotubes.

Therefore, the first aim of this study was to modify CNT surfaces with oxidative functionalization and aminosilanization. For this purpose, carboxylic and hydroxyl functional groups on CNT surfaces were formed by a concentrated acid solution treatment. Then, aminosilanization of the surfaces were conducted by using γ-aminopropyltriethoxysilane (APTES). As stated in the literature review part, there are several studies [64-66] employing oxidative functionalization followed by aminosilanization of multi-walled CNTs with certain characterization methods. Thus, in this part, it was also aimed to contribute these investigations by using more characterization techniques such as X-ray photoelectron spectroscopy (XPS), Fourier-transform infrared spectroscopy (FTIR), scanning electron microscopy-energy dispersive spectroscopy (SEM-EDS), X-ray diffraction (XRD), thermogravimetric analysis (TGA) etc.

After performing oxidative functionalization and silanization of CNTs, what is important is to investigate influences of these treatments on the dispersion and interaction of CNTs with the polymer matrix. In the literature, although there are some studies indicating the effects of these CNT surface treatments in the matrices of polyethylene [67, 68], polypropylene [69, 70], epoxy [71-73], rubber [74-76] etc., to the best of our knowledge, there seems to be no work for polyamides. Therefore, the second aim of this study was to explore the effects of oxidative functionalization and aminosilanization of CNTs on the debundling and dispersion state of CNTs in PA6 matrix. For this second purpose, scanning and transmission electron microscopy (SEM and TEM) were conducted.

Since the degree of crystallinity and crystalline structure of thermoplastic polymers have profound effects on their physical, chemical and mechanical properties, it is very important to study the influences of reinforcing fillers especially their size, amount, and surface characteristics on the crystallization behavior of micro- and nanocomposites. However, as stated in the literature survey, there are very limited number of investigations [53-56] on the influences of unmodified and oxidative functionalized CNTs. Moreover, although silanizationhas been one of the most effective surface treatment of CNTs, to the best of our knowledge, there seems to be no particular investigation exploring the influences of silanized CNTs on the crystallization behaviour of polyamide-6. Therefore, the third purpose of this study was to investigate the effects of first oxidative functionalized and then aminosilanized carbon nanotubes on the isothermal and non-isothermal crystallization kinetics of polyamide-6, including the effects on the crystalline structure of injection molded specimens. For this third aim, crystallization kinetics were investigated by using differential scanning calorimetry (DSC) under both isothermal and non-isothermal conditions, then data were evaluated with basic and modified equations of Avrami. Different crystal structures of polyamide-6 (i.e. α and γ phases) and their percentages were determined by using X-ray diffraction (XRD) method.

After functionalization and silanization, what is also important is to study the effects of these surface treatments on the properties of polymer/CNT nanocomposites as discussed in the literature review part by several investigations [57-63] for other polymer matrices. Although, polyamide-6 is one of the most significant thermoplastic polymer, to the best of our knowledge, there seems to be no work investigating the effects of CNT surface treatments on the properties of polyamide matrices. Therefore, the fourth aim of this study was to contribute this field by revealing the influences of oxidative functionalization and aminosilanization of CNTs on the mechanical and thermal properties of polyamide-6. For this fourth purpose, specimens were compared by conducting tensile and flexural tests, dynamic mechanical analyses (DMA) and thermogravimetric analyses (TGA).

CHAPTER 2

EXPERIMENTAL WORK

In this thesis, there were basically four experimental stages. First, functionalization and silanization of CNTs followed by characterization of these surface treatments. Second, compounding and shaping of PA6/CNT nanocomposites followed by distribution analysis of CNTs in the matrix. In the third stage, effects of surface treated CNTs on the crystallization behaviour of PA6 matrix, while in the fourth stage effects on the mechanical and thermal properties of PA6/CNT nanocomposites were investigated. Experimental procedures and the equipment used during these four stages are explained below:

2.1 Materials Used

In this study, matrix material used was polyamide-6 (PA6) (EMS Griltex D1894A) having a melting range of 220-225°C and density of 1.14 g/cm^3, while the nanoreinforcement was multi-walled carbon nanotubes (MWCNTs) (Nanocyl NC7000) produced via catalytic carbon vapor deposition (CCVD) process. The physical properties of carbon nanotubes are given in Table 2.1. Oxidative functionalization was conducted with sulfuric acid (H_2SO_4) (97%, Fluka) and nitric acid (HNO_3) (67%, Sigma-Aldrich). For aminosilanization, γ-aminopropyltriethoxysilane (APTES) (%99, Sigma–Aldrich) and ethanol (99.5%, Sigma–Aldrich) were used. Figure 2.1 shows chemical structure of γ-aminopropyltriethoxysilane.

Table 2.1 Physical Properties of Carbon Nanotubes Used

Property	Value	Method of Measurement
Average diameter (nm)	9.5	TEM
Average length (μm)	1.5	TEM
Carbon purity (%)	90	TGA
Metal oxide (%)	10	TGA
Amorphous carbon (%)	-	HRTEM
Surface area (m^2/g)	250-300	BET

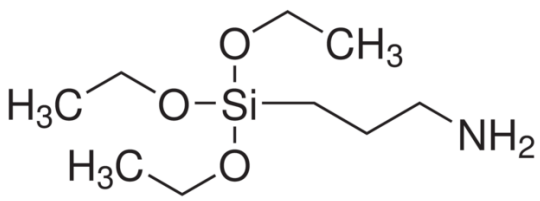

Figure 2.1 Chemical Structure of γ-aminopropyltriethoxysilane (APTES)

2.2 Oxidative Functionalization and Aminosilanization of Carbon Nanotubes

For oxidative functionalization, one gram of unmodified (as received) carbon nanotubes (CNTs) were dispersed in 100 mL acid solution (60:40 H_2SO_4/HNO_3) followed by refluxing for 4 hours in a 50°C ultrasonic bath (Bandelin Sonopuls, 220 W), as shown in Figure 2.2. Then, the slurry was filtered (using filter funnels with porosity 4) and washed thoroughly with reverse osmosis (RO) H_2O in order to neutralize CNTs (i.e. ph=7), as shown in Figure 2.3. Finally, the material was dried under vacuum for 12 hours at 80°C. This sample is named as oxidative functionalized carbon nanotubes and designated with f-CNT.

Figure 2.2 Oxidative Functionalization of Unmodified Carbon Nanotubes (CNTs) by Refluxing in an Ultrasonic Bath

Figure 2.3 Filtering and Washing of Carbon Nanotubes After Oxidative Functionalization Treatment

For aminosilanization, 1.8 g of f-CNTs were dispersed in 100 mL solution of RO H_2O: APTES (98:2)(v:v) and then this mixture was added to a solution of 300 mL ethanol: RO H_2O (95:5)(v:v) and ultrasonicated for 30 minutes, as shown in Figure 2.4. After that the mixture was placed onto a magnetic stirrer and refluxed for 4 hours at 70°C to conduct aminosilanization reaction (Figure 2.5). Finally, the material was dried under vacuum for 12 hours at 80°C. This sample is named as oxidative functionalized and then aminosilanized carbon nanotubes and designated as s-CNT.

Figure 2.4 Ultrasonication of Oxidative Functionalized Carbon Nanotubes (f-CNTs) Before Aminosilanization

Figure 2.5 Aminosilanization of Oxidative Functionalized Carbon Nanotubes by Refluxing

2.3 Characterization Techniques Used for Oxidative Functionalized and Aminosilanized Carbon Nanotubes

(i) X-ray Photoelectron Spectroscopy (XPS)
XPS was used for the surface chemistry of CNTs. Analysis were performed by using PHI 5000 VersaProbe with scanning monochromatic A1 anode. The XPS curve fitting of Si 2p peak was accomplished by XPSPEAK 4.1 software.

(ii) Fourier Transform-Infrared Spectroscopy (FT-IR)
FTIR was used for the identification of the surface functional groups of CNTs. Analysis were recorded with KBr pellets by using Bruker IFS 66/S FTIR spectrometer. A minimum of 32 scans were signal-averaged with a resolution of 4 cm^{-1} in the wavenumber range of 400 to 4000 cm^{-1}.

(iii) Scanning Electron Microscopy - Energy Dispersive X-Ray Spectroscopy (SEM-EDS)
SEM-EDS was done in order to observe surface morphology and elemental analysis of CNTs by using FEI Nova Nano 430 with an EDS detector.

(iv) X-Ray Diffraction Analysis (XRD)
XRD analysis were conducted to observe whether there is a change or not in the crystalline structure of CNTs by using Rigaku D-Max 2200 X-ray diffractometer with monochromatic CuKα radiation. The anode voltage and current were set at 40 kV and 30 mA, respectively. The diffraction angle 2θ is scanned from 10° to 60° at a scanning speed of 1°/min.

(v) Thermogravimetric Analysis (TGA)
TGA were done in order to observe especially thermal degradation behavior of the modifiers on the CNT surfaces. Analysis were performed via Perkin Elmer TGA 4000 with a heating rate of 10°C/min from 30° to 700°C under N_2 flow.

2.4 Compounding and Shaping of Polyamide-6 Nanocomposites

(i) Compounding by Melt Mixing with Twin Screw Extruder
CNTs and PA6 granules were first premixed in a high energy ball mill (RETSCH Pulverisette 6) at 300 rpm for 5 minutes. Then, specimens were compounded by melt mixing method via laboratory size twin-screw extruder (Rondol Microlab 400) having screw diameter of 10 mm and L/D ratio of 20. During extrusion process, temperature profile was 185 – 220 – 230 – 225 – 205°C and screw speed was 68 rpm.

(ii) Shaping by Injection Moulding
Specimens were dried under vacuum for 24 hours at 80°C prior to shaping via injection molding (DSM Xplore Micro 10 cc). Barrel and mold temperatures were 240°C and 70°C, respectively, and heating time was 4 minutes.

(iii) Designation of the Specimens
Nanocomposites were produced with unmodified carbon nanotubes (CNTs), with oxidative functionalized carbon nanotubes (f-CNTs), and with oxidative functionalized and then aminosilanized carbon nanotubes (s-CNTs). For each carbon nanotubes three different amounts (0.1, 0.5, 1.0 wt%) were used giving a total number of 9 different nanocomposites. In order to designate these specimens the format of PA/*x*-CNT*y* is used, where PA represents polyamide-6 matrix, while *x*- represents the type of CNT surface functionalization and *y* represents the amount of CNT in wt%. Designation and composition of all these specimens are given in Table 2.2.

2.5 Dispersion Analysis of Carbon Nanotubes by Electron Microscopy

(i) Scanning Electron Microscopy (SEM)
SEM was done in order to observe distribution and morphology of CNTs on the fracture surfaces of nanocomposites by using FEI Nova Nano 430. The sample surfaces were sputtered with a thin layer of gold to avoid electrostatic charging and provide conductive surfaces.

(ii) Transmission Electron Microscopy (TEM)
TEM was used in order to observe dispersion state of CNTs in PA6 matrix. Specimens were first ultramicrotomed into 75 nm sections by Lecia EM UC 6 with a diamond knife at room temperature. Analysis were conducted via FEI Tecnai G2 Spirit BioTWIN at an acceleration of 80 kV.

Table 2.2 Designations and Compositions (wt%) of the Specimens

Specimen	PA	CNT	f-CNT	s-CNT
PA	100	-	-	-
PA/CNT 0.1	99.9	0.1	-	-
PA/CNT 0.5	99.5	0.5	-	-
PA/CNT 1.0	99.0	1.0	-	-
PA/f-CNT 0.1	99.9	-	0.1	-
PA/f-CNT 0.5	99.5	-	0.5	-
PA/f-CNT 1.0	99.0	-	1.0	-
PA/s-CNT 0.1	99.9	-	-	0.1
PA/s-CNT 0.5	99.5	-	-	0.5
PA/s-CNT 1.0	99.0	-	-	1.0

2.6 Techniques Used for the Crystallization Behaviour of Polyamide-6 and Its Nanocomposites

(i) Differential Scanning Calorimetry (DSC) for Isothermal and Nonisothermal Crystallization Kinetics
DSC was performed in order to investigateisothermal and non-isothermal crystallization kinetics of polyamide-6 and its nanocomposites. Analyses were conducted via Perkin Elmer DSC 4000 with an average sample weight of 8 mgunder nitrogen purge at a constant flow rate of 20 mL/min.

For isothermal melt crystallization behaviour samples were first heated from 25°C to 250°C, above the melting temperature, at a rate of 20°C/min and held at that temperature for 3 min to eliminate any previous thermal history, and then cooled to crystallization temperature (195°C) rapidly at a rate of 50°C/min; and held at this temperature for 30 min until isothermal crystallization was complete. The chosen crystallization temperature of 195°C was determined as an optimum value after a few trials. Heat flow curves as a function of crystallization time were used to study isothermal crystallization kinetics.

For non-isothermal melt crystallization behaviour samples were first held at -10°C for 2 min then heated to 250°C at a rate of 20°C/min and held at that temperature for 3 min to erase any previous thermal history, followed by cooling to -10°C at a cooling rate of 20°C/min. The chosen non-isothermal cooling rate of 20°C/min was also determined as an optimum value after a few trials. Heat flow curves as a function of temperature during cooling were used to study non-isothermal crystallization kinetics.

(ii) X-Ray Diffraction (XRD) for Crystal Structure Analysis
XRD were performed in order to investigate crystalline structure of polyamide-6 and its nanocomposites by using Rigaku D-Max 2200 X-ray diffractometer with monochromatic CuKα radiation. The anode voltage and current were set at 40 kV and 30 mA, respectively. Diffraction angle 2θ is scanned from 5° to 45° at a scanning speed of 1°/min. In order to deconvolute the amorphous and crystalline phases (α and γ), X-ray intensity versus 2θ data were analyzed by using the profile fitting software PeakFit v.4.11 (SYSTAT Software Inc.).

2.7 Techniques Used for the Mechanical and Thermal Properties of Polyamide-6 and Its Nanocomposites

(i) Bending and Tension Tests
In order to observe effects of oxidative functionalization and aminosilanization of CNTs on the mechanical performance of PA6, three-point bending and tension tests were conducted by 5 kN Universal Testing Machine (Instron 5565 A), at a crosshead speed of 1 mm/min according to ISO 178 and ISO 527-2 standards, respectively.

(ii) Dynamic Mechanical Analysis (DMA)
DMA were performed in order to investigate thermomechanical behavior of the specimens. Analysis were performed for the specimens of 40 x10 x 4 mm^3 via Perkin Elmer DMA 8000 in three-point bending mode at a frequency of 1 Hz. The temperature program was run from -50°C to 150°C at a heating rate of 2°C/min.

(iii) Thermogravimetric Analysis (TGA)
TGA were done in order to determine levels of thermal degradation in the specimens. Analysis were conducted via Perkin Elmer TGA 4000 with a heating rate of 10°C/min from 30° to 700°C under N_2 flow.

CHAPTER 3

RESULTS AND DISCUSSION

As stated before, since this dissertation has four experimental stages, their results are presented and discussed successively in the following four subsections:

3.1 Characterization of Oxidative Functionalized and Aminosilanized Carbon Nanotubes

Details of oxidative functionalization and aminosilanization procedures of CNTs were given in the previous chapter, here only the characterization of these treatments by different techniques will be discussed.

3.1.1 X-Ray Photoelectron Spectroscopy

The first characterization method performed to get information on the elemental compositions of functional groups that might be formed on the surfaces of unmodified CNTs, f-CNTs and s-CNTs was XPS analysis. Figure 3.1 shows that XPS spectra of unmodified CNTs basically consists of carbon peak, i.e. C1s peak at a binding energy of 283 eV. For the f-CNTs new sharp peaks appear for oxygen, for instance O1s peak at 533 eV. For s-CNTs, additional peaks are observed at binding energies 101, 152 and 400 eV, which are attributed to Si2p, Si2s and N1s, respectively.

XPS elemental compositions of CNT surfaces in Table 3.1 also indicate that after oxidative functionalization the atomic percentage of oxygen becomes 7.6%. This should be due to the formation of functional groups such as –OH and –COOH on CNT surfaces. The reduction of carbon atoms on f-CNTs compared to unmodifed ones could be attributed to the bonding of oxygen atoms on the CNT surface. For s-CNTs, the atomic percentages of silicon and nitrogen are found to be 2.0%, which should be due to the attachment of silane and amino groups.

Table 3.1 XPS Elemental Analysis (at%) of Carbon Nanotube Surfaces

	CNT	**f-CNT**	**s-CNT**
C1s	99.4	92.0	86.5
O1s	-	7.6	9.5
Si2p	-	-	2.0
N1s	-	-	2.0

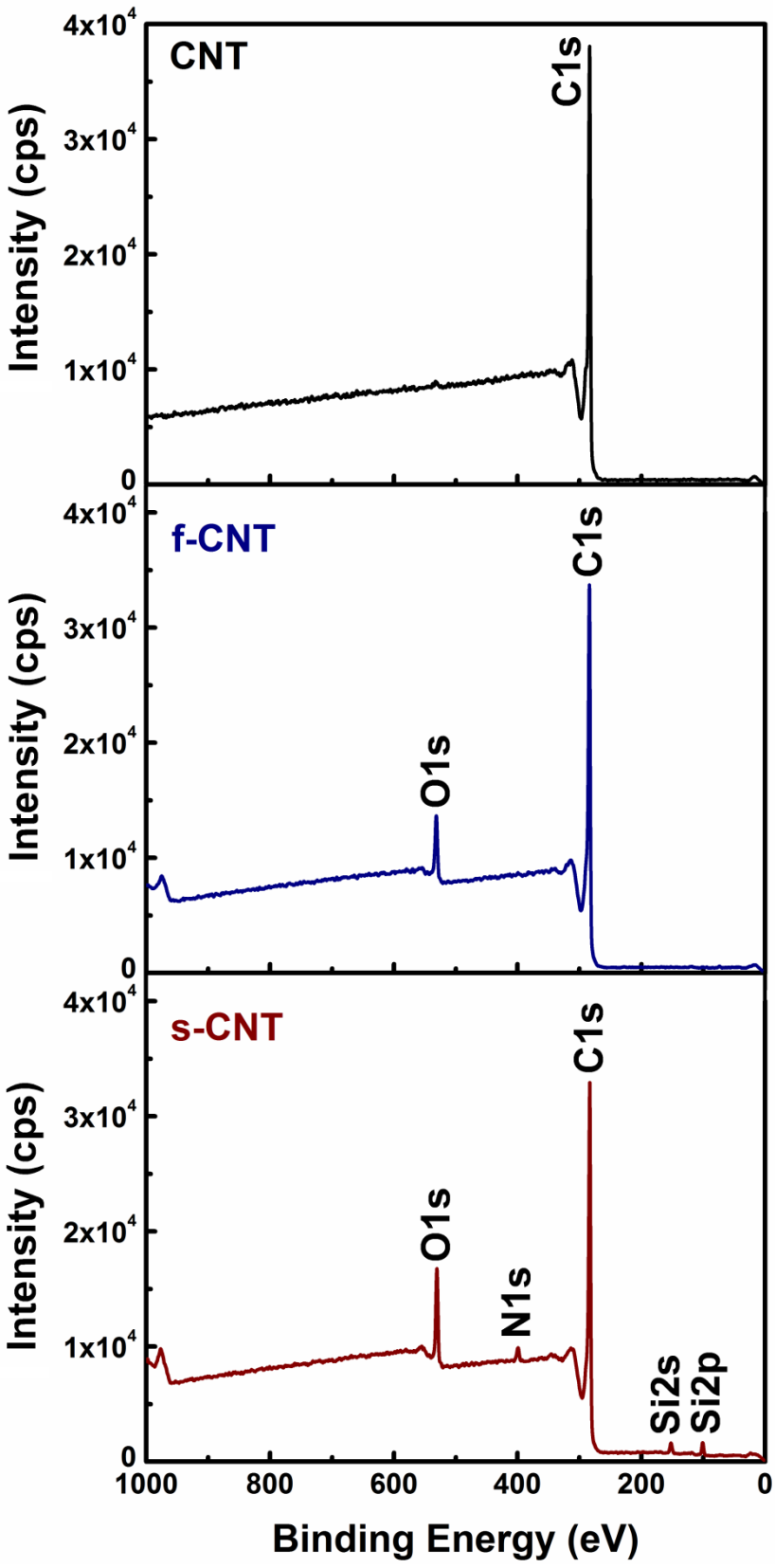

Figure 3.1 XPS Spectrum of Unmodified (CNT), Oxidative Functionalized (f-CNT) and Aminosilanized (s-CNT) Carbon Nanotubes

In order to have additional information from the surfaces of s-CNTs, Si2p peak was also deconvoluted. Figure 3.2 shows that Si2p peak is composed of two peaks for two different Si functionalities at 101.3 and 102.8 eV. The peak at 101.3 eV corresponds to silicon atoms bonded to oxygen atoms on carbon nanotube surfaces (Si-O-C), whereas the peak at 102.8 eV is attributed to Si-O-Si bonds originated from hydrolysis and then condensation of aminosilane molecules to silanol oligomers.

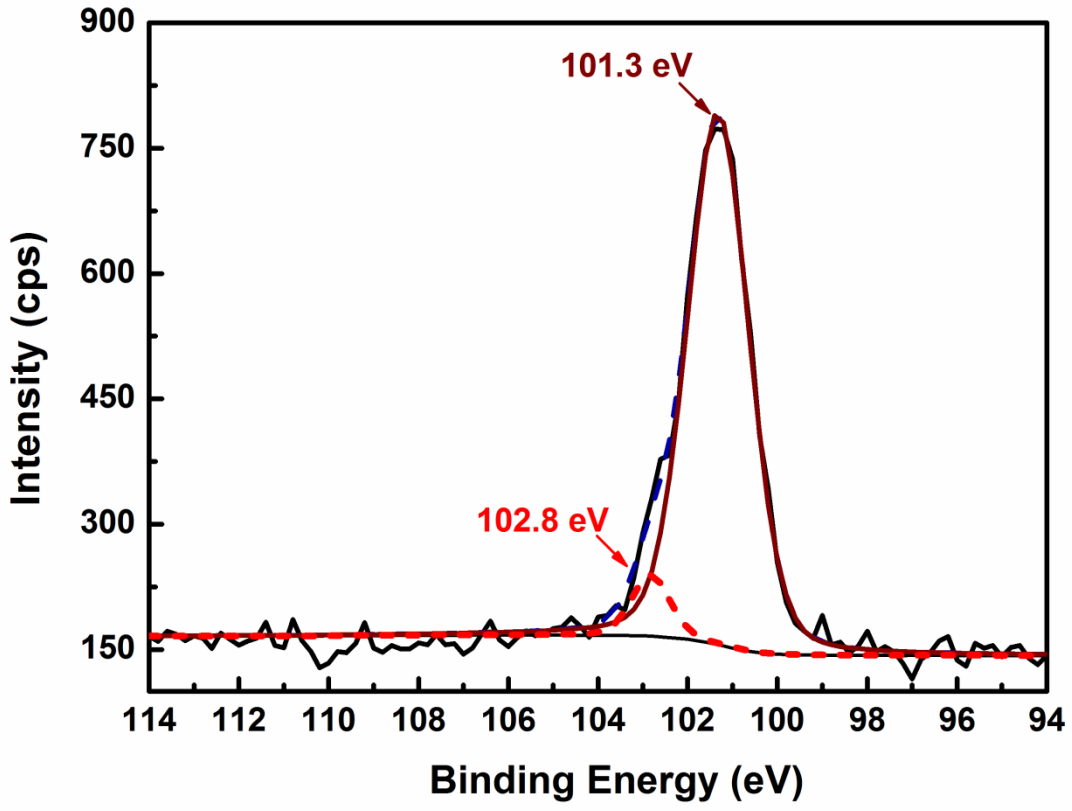

Figure 3.2 Deconvoluted Form of Si2p Peak from XPS Analysis

3.1.2 Fourier Transform-Infrared Spectroscopy

FTIR spectroscopy is used for the identification of the surface functional groups formed by functionalization of CNTs through oxidation and aminosilanization. Figure 3.3 compares FTIR spectra of unmodified CNTs, f-CNTs and s-CNTs.

Absorption band at 3436 cm^{-1} is attributed to the presence of hydroxyl groups (–OH) on the surface of unmodified CNTs, which is believed to be resulted from either ambient atmospheric moisture or oxidation during purification of CNTs, which was also discussed by Ramanathan et al. [77]. Since the moisture in the KBr powder could not be completely eliminated, it could be assumed that most of the O-H vibrations originate from moisture in KBr powder rather than from the functional groups attached to the surface of the CNTs during purification. Another band at 1632 cm^{-1} is assigned to the conjugated C=C stretching related to CNT nature. The incidence of 2942 and 2894 cm^{-1} bands are attributed to asymmetric and symmetric methylene stretching bands, respectively. The presence of these functional groups demonstrates that unmodified CNTs already have several functional groups which could be introduced during the production and/or purification processes of CNTs.

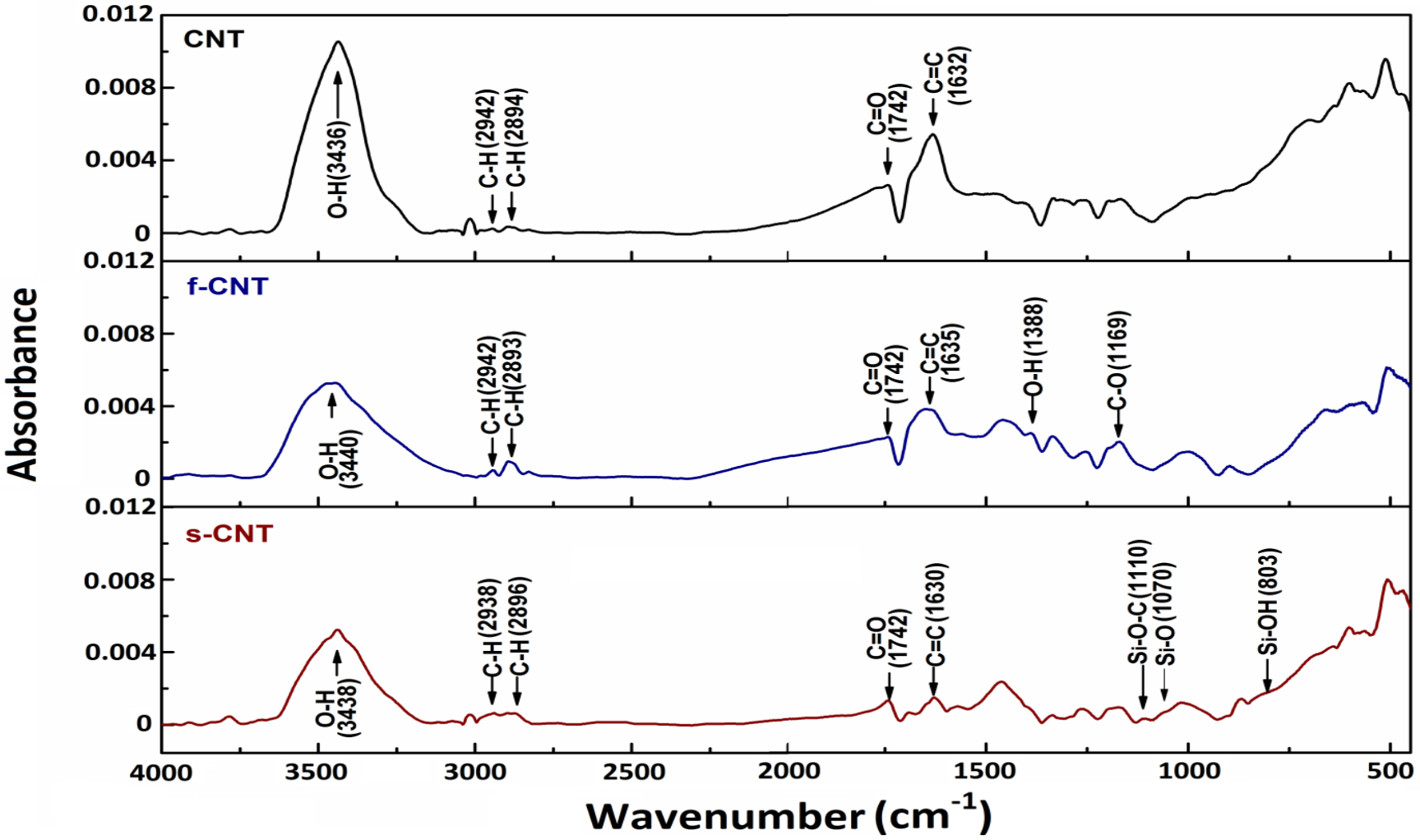

Figure 3.3 FTIR Spectra of Unmodified (CNT), Oxidative Functionalized (f-CNT) and Aminosilanized (s-CNT) Carbon Nanotubes

For f-CNTs, an absorption peak at 3440 cm^{-1} is attributed to the O-H stretching vibration. The band at 1742 cm^{-1} might be assigned to stretching vibrations of carbonyl groups (C = O) due to carboxylic groups formed during the oxidation of hydroxyl compounds, similar observations were made by Aviles et al. [78] FTIR spectra of f-CNTs also show some additional features. For instance, new band appeared at 1169 cm^{-1} corresponds to the C-O stretching vibrations of the carboxylic groups as also confirmed by Kuznetsova et al. [79] Appearance of an additional peak at 1388 cm^{-1} can be attributed to the bending vibrations of O-H groups found in carboxylic groups as evaluated by Grossiord et al. [80]. FTIR spectra of f-CNTs constitute direct evidences for the covalent attachment of carboxylic acid groups on the CNT surfaces. These observations indicate that oxidation with concentrated H_2SO_4/HNO_3 acid solution could introduce surface functional groups on the CNTs and enhance surface activity of CNTs for further chemical reaction with aminosilane molecules.

For s-CNTs, chemical interaction of aminosilane molecules with CNT surfaces is confirmed by the presence of Si–O–C stretching at 1110 cm^{-1}, Si–O vibration peak at 1070 cm^{-1} and Si–OH stretch mode at 803 cm^{-1}, as also indicated by Satyanarayana et al. [81]. Compared to f-CNTs, s-CNTs display relatively weak absorption of carboxyl groups at 1742 cm^{-1}. The band at 1388 cm^{-1} which is attributed to O–H bending vibration found in carboxylic groups almost disappeared. The reduction of these groups on the surface of CNTs further support chemical interactions between CNTs and aminosilane.

3.1.3 Scanning Electron Microscopy - Energy Dispersive X-Ray Spectroscopy

SEM is first of all used to observe surface morphology of CNTs. SEM images in Figure 3.4 show that unmodified CNTs tend to formation of bundles and entanglements because of the van der Waals forces of attraction. In additon to this, CNT surfaces are usually hydrophobic and chemically inert, which leads to poor interfacial adhesion with many polymer matrices. Oxidative functionalization and aminosilanization decrease hydrophobicity of CNTs leading to debundling and disentanglement and also some fragmentation of individual CNTs. Figure 3.4 also shows that there is no severe damage in the structure of CNTs. This indicates that CNTs are strong enough to withstand oxidative functionalization with concentrated acid solution.

SEM is further used to confirm oxidation and aminosilanization of CNTs with EDS analysis. One example (s-CNT) of the SEM-EDS spectrum is given in Figure 3.4, while elemental compositions (wt% and at%) of all CNT surfaces by EDS are tabulated in Table 3.2. It is seen that unmodified CNTs are mainly composed of carbon and oxygen elements. Certain amount of aluminium element detected should be originating from the production and/or purification processes of CNTs via certain metal catalysts. Table 3.2 shows that the weight percent of oxygen atoms on the surfaces of unmodified CNTs is 3.58%, while it is 9.88% and 9.76% for f-CNT and s-CNT surfaces, respectively. These increments (more than 100%) confirm the success of oxidative functionalization process. After oxidative functionalization of CNTs, most of the aluminium impurity is removed by H_2SO_4/HNO_3 acid solution.

For s-CNTs, the presence of silicon atom confirmed by the peak at around 1.8 keV could be an evidence of covalent attachment of aminosilane molecules on the surfaces of f-CNTs. Aminosilanization can be further evaluated by the relative increase of O/C at% ratio which is found to be 0.085 for f-CNTs and 0.089 for s-CNTs. This increase could be related to the extra oxygen atoms of aminosilane molecules on s-CNT surfaces.

Table 3.2 SEM-EDS Elemental Analysis (wt% and at%) of Carbon Nanotube Surfaces

	CNT		f-CNT		s-CNT	
	wt%	**at%**	**wt%**	**at%**	**wt%**	**at%**
C	88.99	93.69	86.33	90.46	82.47	88.54
O	3.58	2.83	9.88	7.77	9.76	7.86
Al	7.43	3.48	3.79	1.77	1.20	0.58
Si	0.00	0.00	0.00	0.00	6.57	3.02

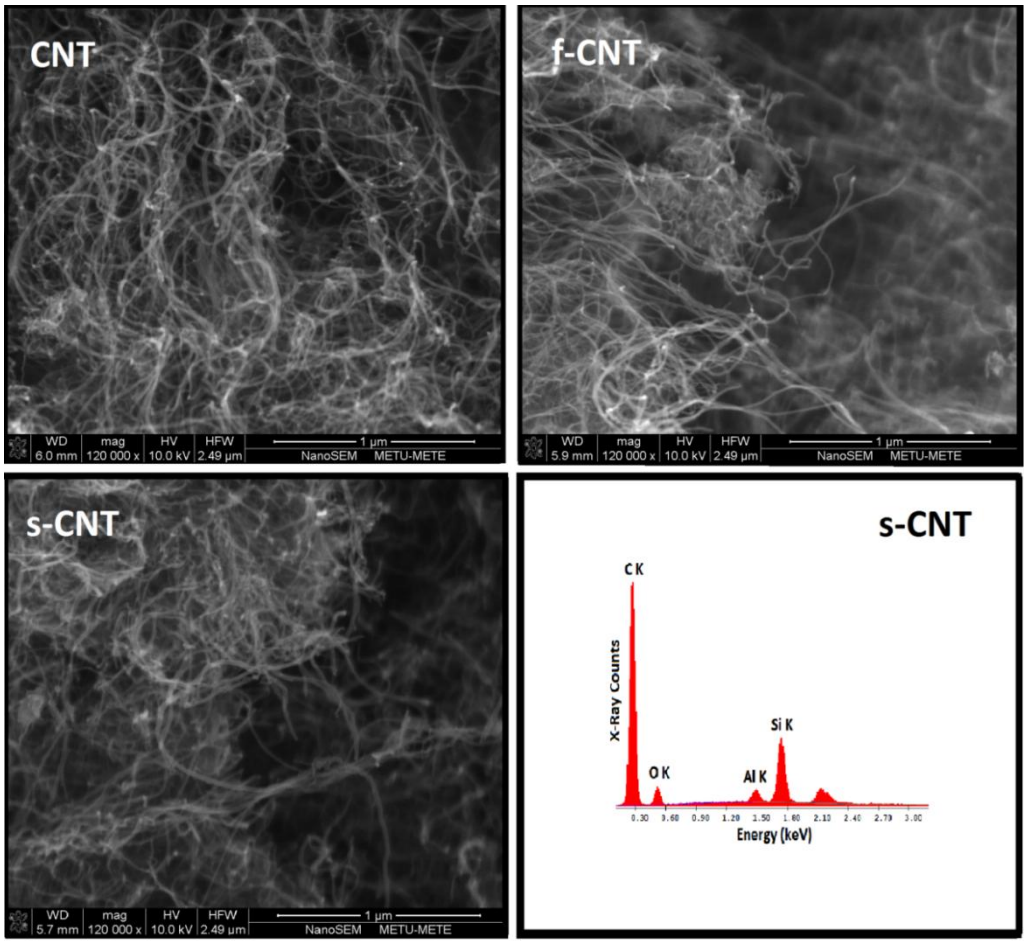

Figure 3.4 SEM Images of Unmodified (CNT), Oxidative Functionalized (f-CNT) and Aminosilanized (s-CNT) Carbon Nanotubes Including EDS Spectra of s-CNT

3.1.4 X-Ray Diffraction Analysis

XRD studies were conducted in order to clarify whether there is a change in the crystal structure of f-CNTs and s-CNTs. Figure 3.5 shows that XRD patterns of all CNTs have almost the same first order diffraction peak at a 2θ of 25.6°, which corresponds to a *d*-spacing of 0.34 nm according to Bragg's equation. This means that oxidative functionalization and aminosilanization lead to no significant change in the crystalline structure of CNTs.

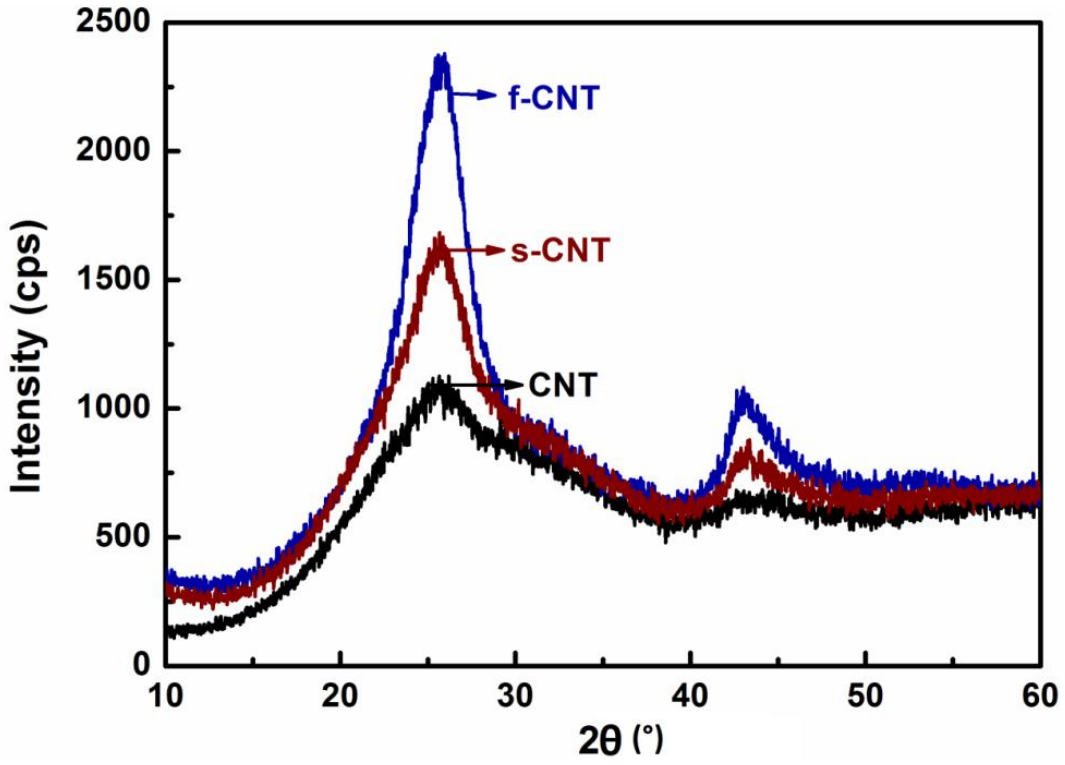

Figure 3.5 XRD Patterns of Unmodified (CNT), Oxidative Functionalized (f-CNT) and Aminosilanized (s-CNT) Carbon Nanotubes

The main difference in the XRD patterns of CNTs is the intensity of the first order diffraction peaks. This difference could be due to the different absorption coefficients of the elements present in the functional groups on f-CNTs and aminosilane groups on s-CNTs. Another reason for this difference could be related to the transformation of amorphous carbon leading to an increase of the graphitization degree after oxidative functionalization of CNTs as discussed in the literature [82].

3.1.5 Thermogravimetric Analysis

Figure 3.6 shows thermogravimetric curves of unmodified CNTs, f-CNTs and s-CNTs. Additionally, 5 wt% and 10 wt% decomposition temperatures of CNTs are tabulated in Table 3.3. Figure 3.6 simply reveals that significant thermal degradation of unmodified CNTs starts around 550°C, while there is gradual decrease for f-CNTs and s-CNTs.

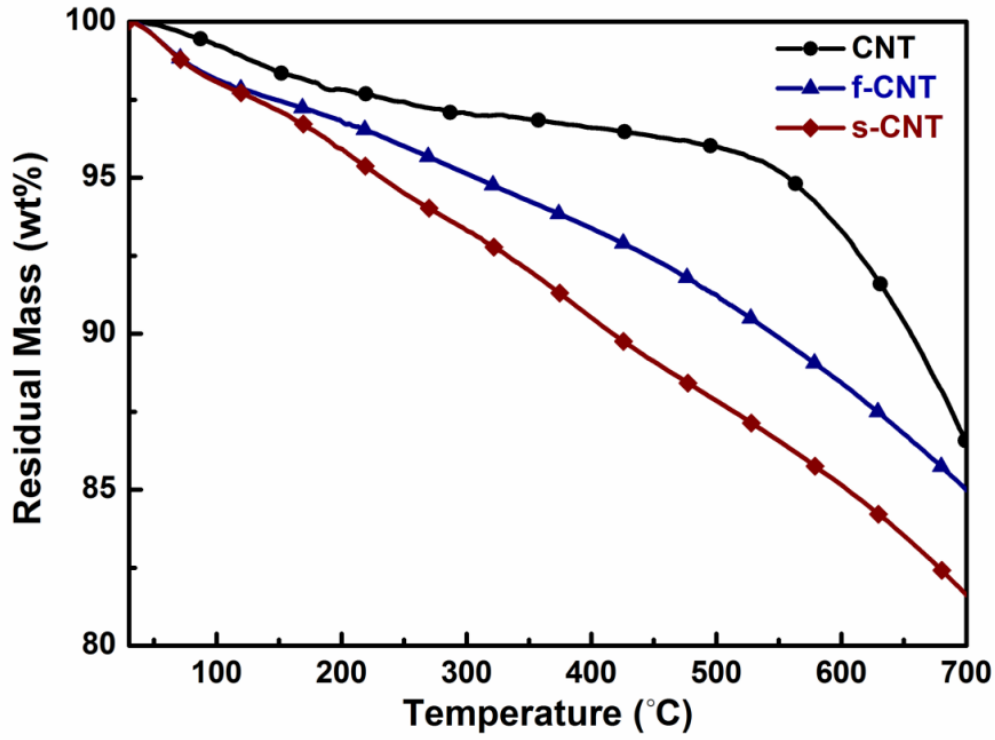

Figure 3.6 TGA Curves of Unmodified (CNT), Oxidative Functionalized (f-CNT) and Aminosilanized (s-CNT) Carbon Nanotubes

Table 3.3 also shows that 5 wt% and 10 wt% thermal decomposition temperatures ($T_{5wt\%}$ and $T_{10wt\%}$) for unmodified CNTs are 558°C and 656°C, respectively. These temperatures are 307°C and 545°C for f-CNTs and 232°C and 417°C for s-CNTs, respectively. Therefore, it can be also stated that the gradual increase in the mass loss of s-CNTs are higher than that for f-CNTs, which can be explained as the lower temperature resistance of aminosilane groups on s-CNTs compared to the carboxylic and hydroxy groups on f-CNTs.

Table 3.3 TGA Thermal Decomposition Temperatures of Carbon Nanotubes

	$T_{5wt\%}$ (°C)	$T_{10wt\%}$ (°C)
CNT	558	656
f-CNT	307	545
s-CNT	232	417

3.2 Effects of Oxidative Functionalization and Aminosilanization on the Dispersion of Carbon Nanotubes in Polyamide-6

3.2.1 Morphology and Dispersion Analysis by SEM

SEM images of the fracture surfaces of nanocomposites with 1.0 wt% CNTs, f-CNTs and s- CNTs are shown in Figure 3.7. First of all this figure shows that CNTs are all oriented with the injection molding axes, so that only pulled-out tips of CNTs are seen in the fractographs.It is seen that unmodified CNTs are unevenly distributed while oxidative functionalization (f-CNTs) lead to more even distribution. Figure 3.7 shows that the most homogeneous distribution was obtained with aminosilanization (s-CNTs).

It is known that dispersion of CNTs in polymer matrices takes place in two stages, first wetting of CNTs by the matrix and then diffusion of individual CNTs into the matrix. Unmodified CNTs cannot be wetted properly due to the poor interfacial interactions between nanotube surfaces and polyamide molecules. Thus, uniform diffusion of CNTs into polyamide matrix becomes very difficult.

Oxidative functionalization enhance hydrophilicity of CNTs resulting in stronger interfacial interactions between CNTs and polyamide. Thus, this treatment increases wetting of CNTs by polyamide matrix leading to enhanced dispersion of CNTs. Another reason for the more uniform dispersion of f-CNTs could be due to the decreased length of CNTs with acid treatment. Because, degree of formation of CNT bundles will decrease with decreased lengths.

Aminosilanization of CNTs provide the strongest interfacial interactions due to the covalent attachment of aminosilane molecules with surface functional groups of f-CNTs. Therefore, s- CNTs can be sufficiently wetted making uniform diffusion into the polyamide matrix properly.

Therefore, Figure 3.7 also shows that lengths of the pulled-out tips of unmodified CNTs are much longer due to their insufficent chemical bonding with the matrix. On the other hand, lengths of the pulled-out tips of s-CNTs are very short due to hydrogen bonding and even possibility of covalent attractions between their surfaces and the matrix.

3.2.2 Dispersion Analysis by TEM

Figure 3.8 shows TEM micrographs of 1.0 wt% unmodifed CNTs, f-CNTs and s-CNTs in polyamide-6 matrix. In terms of dispersion, TEM images were all consistent with the images obtained under SEM. Figure 3.8 simply shows that unmodified CNTs were unevenly distributed due to the poor interfacial interactions between nanotube surfaces and polyamide molecules. On the other hand, oxidative functionalization (f-CNTs) lead to more even distribution due to stronger interfacial interactions. Aminosilanization of f-CNTs, i.e. s-CNTs, result in much stronger interfacial interactions because of the covalent attachment of aminosilane molecules with surface functional groups of f-CNTs. Therefore, Figure 3.8 shows that the most homogeneous distribution was obtained with s-CNTs.

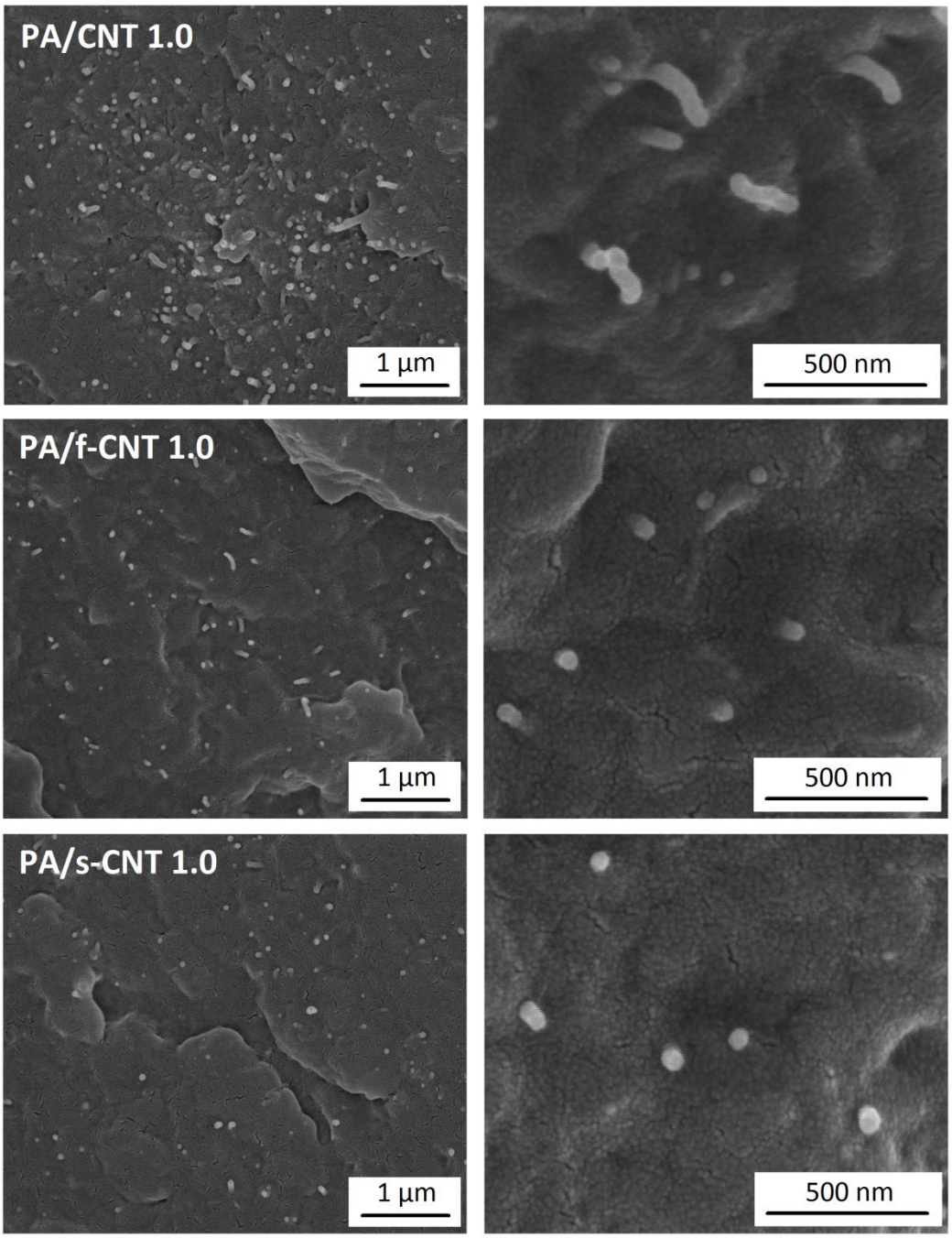

Figure 3.7 SEM Images Showing Dispersion State (Images on the Left) and Pull-out Morphologies (Images on the Right) of 1.0 wt% Unmodifed (CNT), Oxidative Functionalized (f-CNT) and Aminosilanized (s-CNT) Carbon Nanotubes in Polyamide-6 Matrix

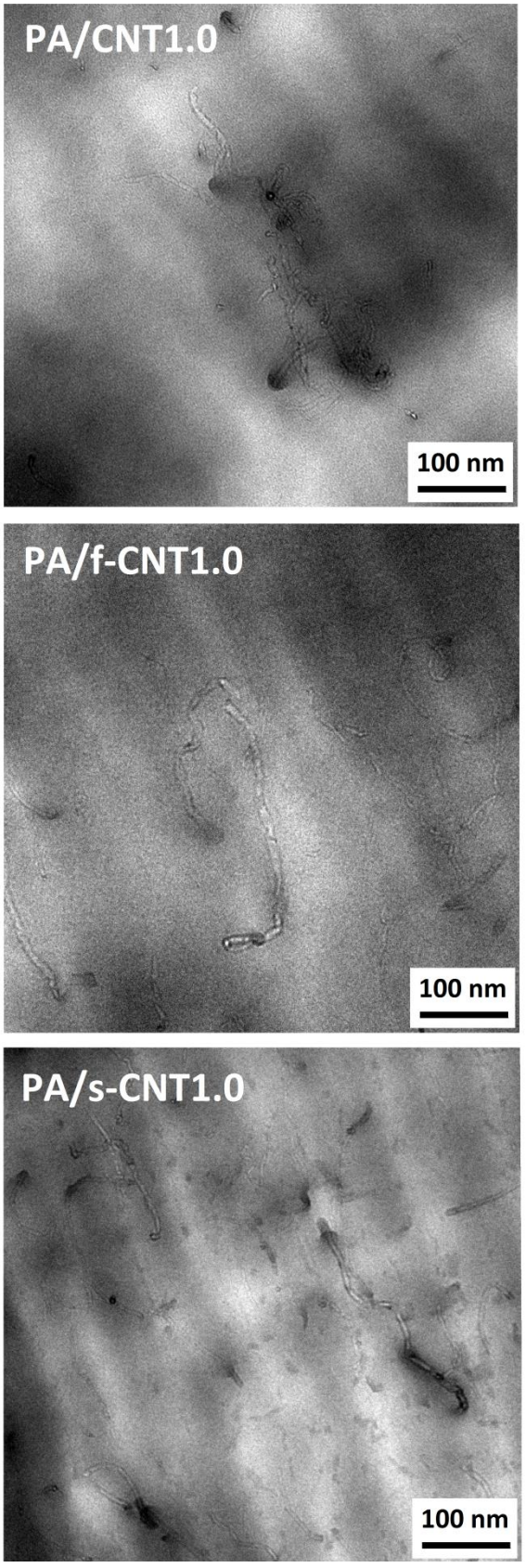

Figure 3.8 TEM Images Showing Dispersion State of 1.0 wt% Unmodifed (CNT), Oxidative Functionalized (f-CNT) and Aminosilanized (s-CNT) Carbon Nanotubes in Polyamide-6 Matrix

3.3 Effects of Oxidative Functionalized and Aminosilanized Carbon Nanotubes on the Crystallization Behaviour of Polyamide-6 Nanocomposites

Results of crystallization behaviour of all specimens were presented and discussed in the following subsections. Note that all data obtained for neat PA6 and its nine different nanocomposites are given in the tables in detail. However, in order to prevent complicated figures, plots are shown only for PA6 matrix and the nanocomposites with 1 wt% carbon nanotubes. Other plots for the nanocomposites with 0.1 and 0.5 wt% carbon nanotubes are given in Appendix A.

3.3.1 Isothermal Crystallization Kinetics by DSC

In order to reveal effects of unmodified CNTs, f-CNTs and s-CNTs on the isothermal crystallization kinetics of polyamide-6, DSC procedures explained in the experimental part were applied for all specimens.

Figure 3.9 presents examples of DSC heating thermograms (at 20°C/min) for polyamide-6 and its nanocomposites with 1.0 wt% carbon nanotubes. It is apparent that these thermograms exhibit double melting peaks at around 204°C and 220°C, respectively. It is supposed that these melting peaks should correspond to the melting of especially α-crystal phase of PA6 as discussed in the following XRD results. Multiple peaks might be due to the different size spherulites which melt and recrystallize during heating.

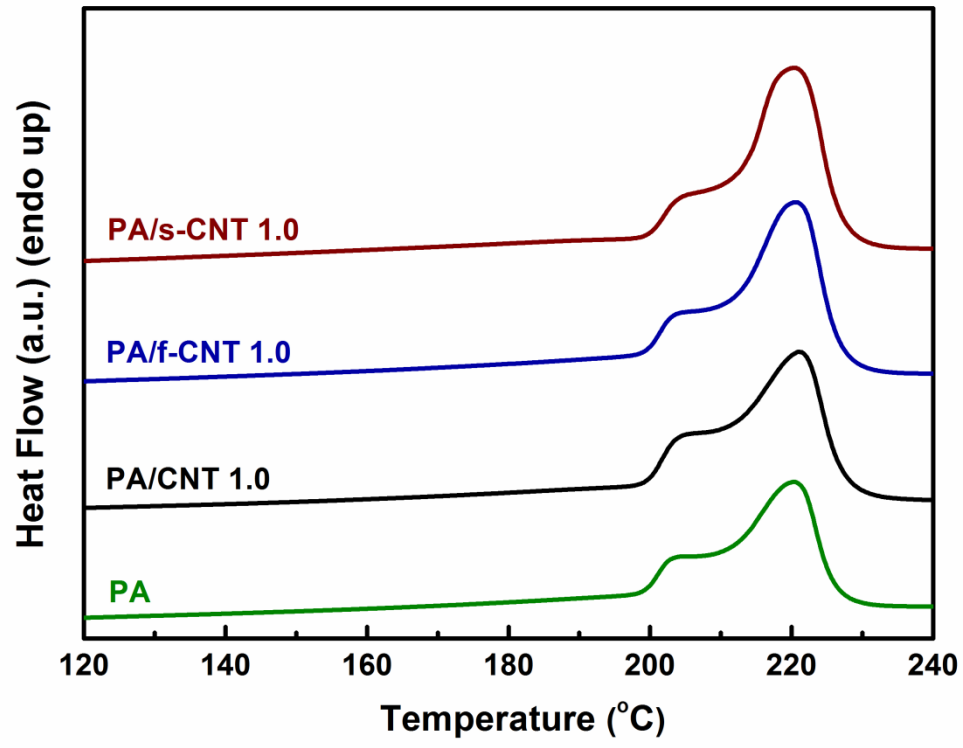

Figure 3.9 DSC Heating Thermograms (at 20°C/min) for PA-6 and its Nanocomposites with 1.0 wt% Carbon Nanotubes

Heat of fusion of each specimen was determined by calculating the area under the melting peaks to compare the degree of crystallinity (X_c) of PA6 and its nanocomposites by using the following equation:

$$X_c(\%) = \frac{\Delta H_f}{w_m \Delta H_f^0} 100$$

where ΔH_f is the measured heat of fusion of the specimens, ΔH_f^0 is the heat of fusion of 100% crystalline PA6, and w_m is the weight fraction of the PA6 matrix. In the literature [4], the heat of fusion for the formation of α- and γ- crystal phases of PA6 are given as 241 and 239 J/g, respectively. In this study, an average of these values 240 J/g was used.

The degree of crystallinity together with other isothermal crystallization parameters for PA6 and its all nanocomposites are given in Table 3.4. It is known that just like other micro- and nano-fillers, CNTs also act as heterogeneous nucleation agents. Thus, Table 3.4 shows that the degree of crystallinity $X_c$increases with increasing CNT content. It is seen that $X_c$also increases with oxidative functionalization and aminosilanization treatments of CNTs due to more uniform distribution. For instance, compared to neat PA6, $X_c$increases as much as 40% in the nanocomposite specimen PA/s-CNT 1.0.

Table 3.4 Isothermal Crystallization Parameters and Avrami Constants for PA6 and its Nanocomposites

Specimens	ΔH_f **(J/g)**	X_c **(%)**	t_{max} **(min)**	$t_{1/2}$ **(min)**	***n***	***K***
PA	53.10	22.13	0.60	1.06	3.72	0.16
PA/CNT 0.1	60.75	25.34	0.40	0.94	1.57	1.14
PA/f-CNT 0.1	61.06	25.47	0.36	0.66	2.14	2.21
PA/s-CNT 0.1	64.98	27.10	0.34	0.55	2.33	3.47
PA/CNT 0.5	61.94	25.94	0.35	0.79	1.60	1.20
PA/f-CNT 0.5	61.62	25.80	0.33	0.64	2.15	2.34
PA/s-CNT 0.5	69.41	29.07	0.31	0.54	2.39	3.67
PA/CNT 1.0	62.62	26.36	0.34	0.69	1.72	1.28
PA/f-CNT 1.0	63.94	26.91	0.31	0.63	2.22	2.56
PA/s-CNT 1.0	73.47	30.92	0.28	0.52	2.48	3.89

Figure 3.10 shows examples of isothermal crystallization curves (at 195°C) for PA6 and its nanocomposites with CNT content of 1.0 wt %. Exothermic peaks in this figure represent t_{max}which is the time to reach the maximum rate of crystallization. Table 3.4 indicates that t_{max}decreases with increasing CNT content and also with oxidative functionalization and aminosilanization, such as $t_{max}$for neat PA6 decreases from 0.60 min down to 0.28 min for PA/s-CNT1.0, which means a decrease of more than two times.

Figure 3.11 indicates examples of fractional crystallinity,X_t as a function of isothermal crystallization time for PA6 and its nanocomposites with 1.0 wt% unmodified CNTs, f-CNTs and s-CNTs. X_t can be determined as a function of time by using the following equation:

$$X_t = \frac{\int_0^t \frac{dH(t)}{dt} dt}{\int_0^{t_\infty} \frac{dH(t)}{dt} dt}$$

where *dH(t)/dt* is the rate of heat evolution and t_∞ is the end time of the crystallization. In this equation, integral at the numerator indicates generated crystallization enthaply up to time *t*, while integral at the denominator shows total crystallization enthalpy at time t_∞.

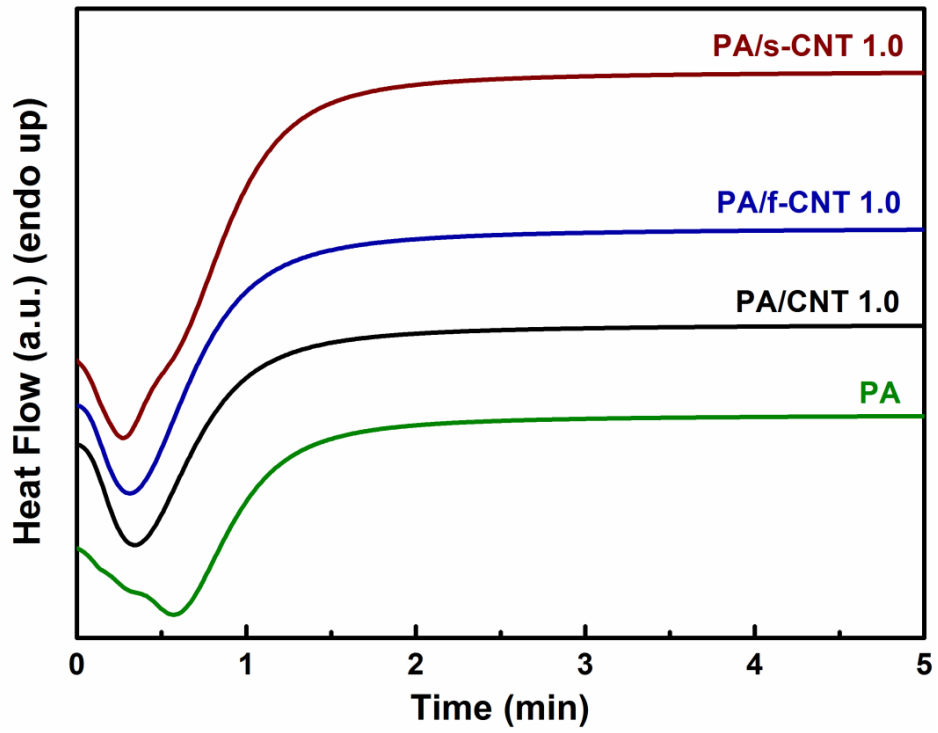

Figure 3.10 Isothermal Crystallization Thermograms (at 195°C) for PA6 and its Nanocomposites with 1.0 wt% Carbon Nanotubes

It is seen in Figure 3.11 that isothermal crystallization curves of PA6 and its nanocomposites have characteristic sigmoidal isotherms. In order to characterize rate of isothermal crystallization process, the time at which half crystallization occurs, i.e. $t_{1/2}$ can be used. The larger the $t_{1/2}$ value the slower the crystallization rate. Thus, $t_{1/2}$ values were determined from the onset of crystallization to the point where the crystallization is half completed. Then, all $t_{1/2}$ data obtained were tabulated in Table 3.4.

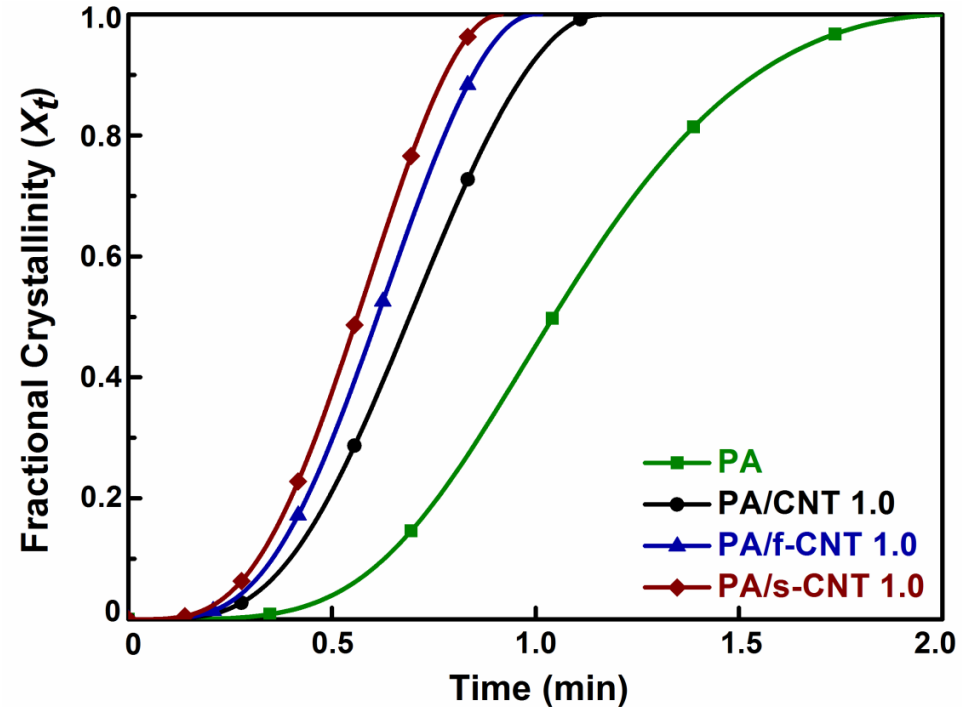

Figure 3.11 Fractional Crystallinity versus Isothermal Crystallization Time Curves for PA6 and its Nanocomposites with 1.0 wt% Carbon Nanotubes

It can be seen in Table 3.4 that $t_{1/2}$ of PA6 is much larger compared to its nanocomposites which indicates a much slower crystallization rate. Again, just like t_{max} , $t_{1/2}$ decreases with increasing CNT content and with oxidative functionalization and aminosilanization. For example, compared to neat PA6, the decrease in $t_{1/2}$ for the nanocomposite specimen with 1 wt% s-CNT is almost two times, i.e. from 1.06 min down to 0.52 min.

Then, isothermal crystallization kinetics of all specimens were evaluated by using the well established Avrami equation:

$$1 - X_t = \exp[-Kt^n]$$

In this equation, X_t is the fractional crystallization at different crystallization times t, whereas K is the crystallization rate constant and n is the Avrami exponent. It is well known that Avrami constants are related to the rate and different mechanisms of nucleation and growth of crystalline phases.

Avrami equation can be rearranged by taking the double logarithm of both sides:

$$\ln\,[-\ln\,(1 - X_t)] = n \ln t + \ln K$$

This equation is especially used to describe the initial stage of crystallization, i.e. "Primary Crystallization", because of almost having no deviation from linearity in this stage. On the other hand, Avrami equation may not obey to describe the late stages of crystallization, i.e. "Secondary Crystallization" due to the deviation from the linearity.

Figure 3.12 shows examples of Avrami plots of ln [– ln (1 – X_t)]versus ln t for PA6 and its nanocomposites with 1.0 wt% carbon nanotubes. Generally, Avrami constants n and K can be determined by fitting isothermal crystallization data at $X_t < 0.5$. Because, up to 50% relative crystallinity degree, Avrami plots obey linearity.

Similarly in this study, since primary crystallization stage comprised above 50% relative crystallinity, values of n and K were determined as the slopes and intercepts of each curve by using the linear regression analysis at $X_t < 0.5$ for all specimens. Then, these Avrami constants were tabulated in Table 3.4.

Table 3.4 shows that Avrami exponent n for neat PA6 is 3.72 which could be attributed to thermally nucleated spherulites followed by three-dimensional growth mechanism of these crystallites. However, nucleation and growth mechanisms of PA6 spherulites were influenced by the incorporation of all types of CNTs, leading to a decrease of n values down to a range of 1.57-2.48 for the PA6 nancomposites. Since there would be so many numbers of heterogeneous nucleation sites by the addition of CNTs, the decrease of exponent n could be attributed to the change of crystal growth mechanism from three-dimensional spherulite growth into two-dimensional spherulite growth.

Table 3.4 also shows that Avrami rate constant K for neat PA6 is 0.16, however it increases with increasing CNT content and with oxidative functionalization and aminosilanization drastically; for example to a value of 3.89 in the specimen PA/s-CNT 1.0, i.e. an increased rate constant K of more than 24 times, again due to their very effective heterogeneous nucleation.

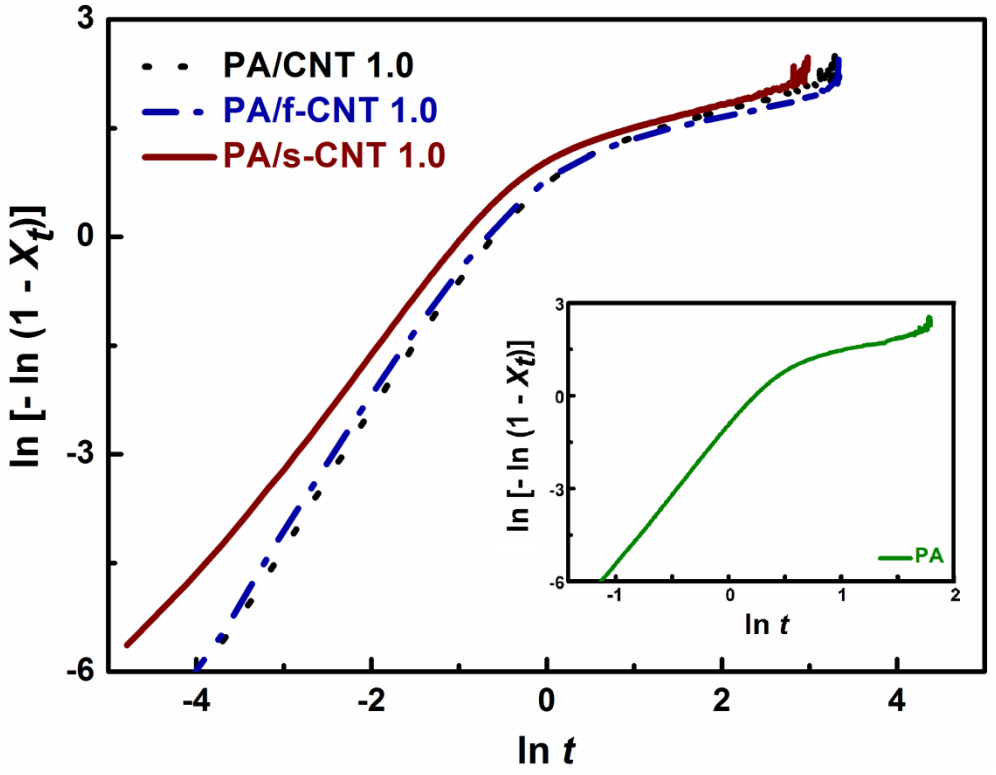

Figure 3.12 Avrami Plots ln [– ln (1 – X_t)] versus ln t during Isothermal Crystallization of PA6 (inset) and its Nanocomposites with 1.0 wt% Carbon Nanotubes

3.3.2 Non-Isothermal Crystallization Kinetics by DSC

In order to investigate influences of unmodified CNTs, f-CNTs and s-CNTs on the non-isothermal crystallization kinetics of polyamide-6, DSC procedures explained in the experimental part were applied for all specimens.

Figure 3.13 gives examples of DSC non-isothermal crystallization thermograms for PA6 and its nanocomposites with 1.0 wt% carbon nanotubes at a cooling rate of 20°C/min. From these curves,

apart from heat of crystallization (ΔH_c), onset temperature of crystallization (T_o), peak temperature of crystallization (T_p), and temperature range of crystallization (T_R) can be also determined.

After determining ΔH_c of each specimen by integrating the area under the crystallization peaks, degree of crystallinity (X_c) of PA6 and its all nanocomposites were compared by using the following equation:

$$X_c(\%) = \frac{\Delta H_c}{w_m \Delta H_f^0} \, 100$$

In this case, ΔH_c is the measured heat of crystallinity of the specimens, while ΔH_f^0 and w_m are the same as discussed in the previous section.

Then, the degree of crystallinity (X_c) together with other non-isothermal crystallization parameters (T_o, T_p, T_R) for PA6 and its all nanocomposites are tabulated in Table 3.5. Just like in the previous isothermal case, Table 3.5 shows that incorporation of carbon nanotubes increases degree of crystallinity of PA6 also during non-isothermal cooling. Due to their nano-size and very high aspect ratio, carbon nanotubes have very good ability to reduce nucleation activation energy which makes them very efficient heterogeneous nucleation agents.

Table 3.5 indicates that degree of crystallinity (X_c) of PA6 increases not just with increasing CNT content, but also with oxidative functionalization and aminosilanization of CNTs due to more uniform distribution. It can be seen that X_c of neat PA6 increases more than 40% by adding only 1 wt% s-CNTs.

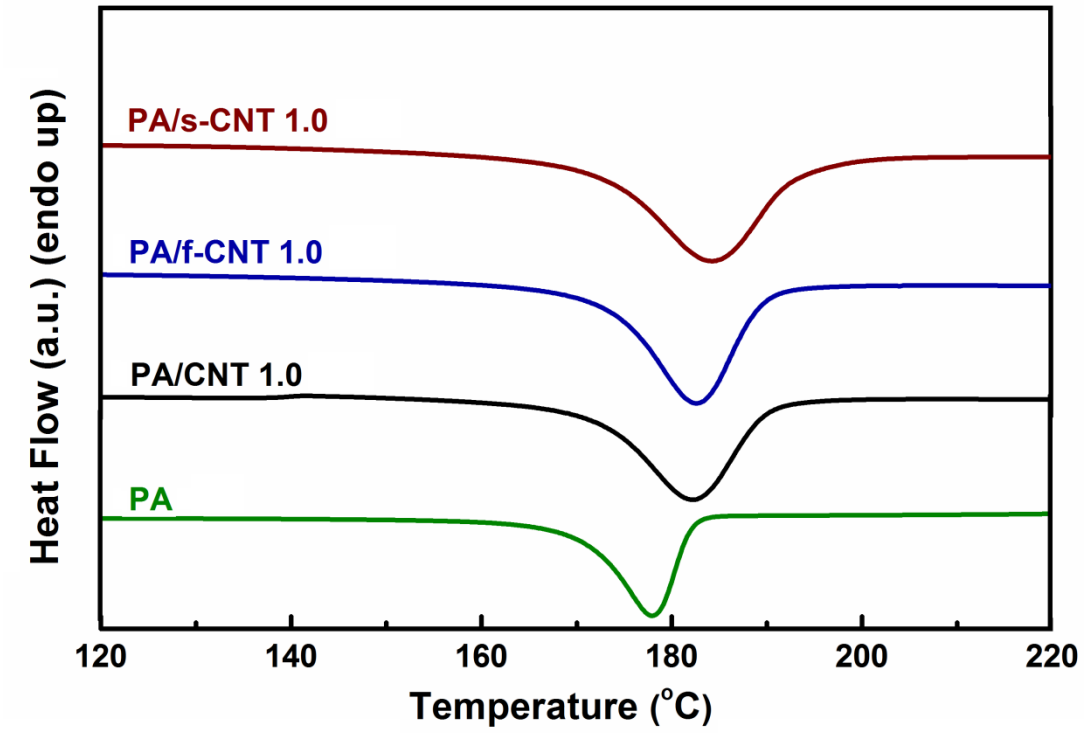

Figure 3.13 DSC Cooling Thermograms (at 20°C/min) for PA6 and its Nanocomposites with 1.0 wt% Carbon Nanotubes

Due to their heterogeneous nucleation effects, Table 3.5 also shows that for all nanocomposites both onset (T_o) and peak (T_p) temperatures of non-isothermal crystallization shifts to higher temperatures. Similarly, temperature range (T_R) of the exothermic peaks of all nanocomposites are much broader compared to neat PA6. This means that incorporation of carbon nanotubes lead to start of crystallization of PA6 chains at higher temperatures and continuation of crystallization in broader ranges.

For the non-isothermal crystallization case, fractional crystallinity X_T can be determined as a function of temperature by using the following equation:

$$X_T = \frac{\int_{T_0}^{T} \frac{dH(T)}{dT} dT}{\int_{T_0}^{T_\infty} \frac{dH(T)}{dT} dT}$$

where T_o and T_∞ are the onset and end crystallization temperatures, respectively. In this equation, integral at the numerator indicates generated crystallization enthaply up to crystallization temperature T, while integral at the denominator shows total crystallization enthalpy at temperatureT_∞. Figure 3.14 shows examples of amorphous phase fraction (1-X_T) versus non-isothermal crystallization temperature T curves for PA6 and its nanocomposites with 1.0 wt% unmodified CNTs, f-CNTs and s-CNTs.

It is seen in Figure 3.14 that compared to neat PA6 sigmoidal curves of crystallization for all nanocomposites shifts to higher temperatures. From these curves it is also possible to determine $T_{1/2}$ values, i.e. the temperature at which half crystallization occurs.

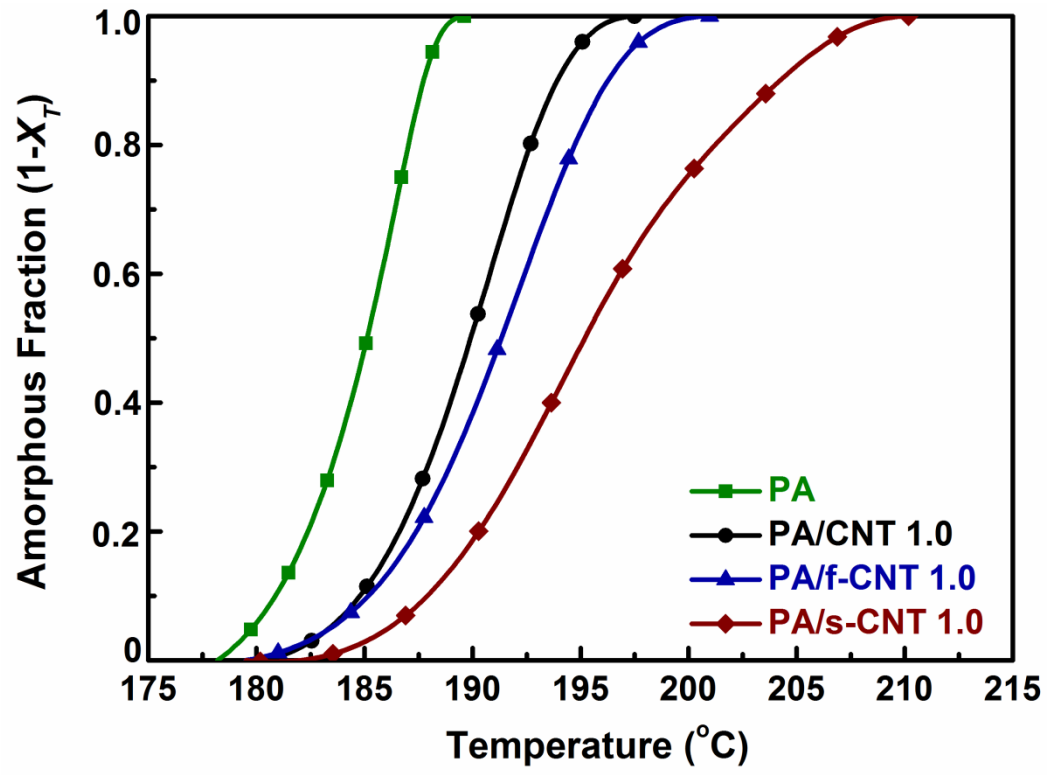

Figure 3.14 Amorphous Phase Fraction versus Non-isothermal Crystallization Temperature Curves for PA6 and its Nanocomposites with 1.0 wt% Carbon Nanotubes

Similar to the values of T_o, T_p, T_R determined from non-isothermal cooling thermograms, values of $T_{1/2}$ given in Table 3.5 indicates that crystallization for all nanocomposites takes place at higher temperatures than neat polyamide-6 matrix. For example, $T_{1/2}$ of neat PA6 (185°C) increases by 10°C reaching to a value of 195°C for the nanocomposite PA/s-CNT 1.0.

Then, in order to obtain sigmoidal crystallization curves with respect to time, the following relationship between crystallization temperature, T and crystallization time, t

$$t = \frac{T_o - T}{\beta}$$

can be used; where β is the cooling rate during non-isothermal crystallization. Figure 3.15 shows examples of amorphous phase fraction (1-X_t) versus non-isothermal crystallization time t curves for neat PA6 and its nanocomposites with 1.0 wt% carbon nanotubes. Just like Figure 3.14, Figure 3.15 also indicates that crystallization curves for nanocomposites shifts to longer times compared to neat polyamide-6 matrix. From these curves it is again possible to characterize rate of non-isothermal crystallization by determining the values of $t_{1/2}$, i.e. the time at which half crystallization occurs.

Table 3.5 shows that compared to neat polyamide-6, all nanocomposites have much slower crystallization rate. For instance, values of $t_{1/2}$ increases from 0.25 min for neat PA6 up to 0.76 min for the nanocomposite with 1 wt% s-CNT, i.e. an increase of 3 times.

Under non-isothermal condition, as discussed by other researchers in the literature [53,54], carbon nanotubes act as physical obstacles, thus delaying the necessary conformational mobility of polyamide-6 chains to crystallize in a regular manner.

In order to evaluate Avrami constants of non-isothermal crystallization kinetics, the basic Avrami relation

$$1 - X_t = \exp[-K\, t^n]$$

should be modified, because the rate of non-isothermal crystallization depends on the cooling rate. In the literature, one of the most widely used modification of Avrami relation was made by Jeziorny [83]. He suggested that the rate constant K should be corrected by cooling rate β to obtain the modified rate constant K_c, i.e.:

$$\ln K_c = \frac{\ln K}{\beta}$$

Thus, by taking the double logarithm of both sides of basic Avrami equation, and introducing the modification of Jeziorny, the final form of modified Avrami equation becomes:

$$\ln\,[-\ln\,(1 - X_t)] = n \ln\, t + \beta\, \ln K_c$$

By using the above relation, modified Avrami plots of ln [– ln (1 – X_t)] versus ln t were constructed for all specimens. Figure 3.16 shows examples of these curves for PA6 and its nanocomposites with 1.0 wt% carbon nanotubes.

In this study, just like in the previous case of isothermal crystallization, modified Avrami plots all obeyed linearity beyond 50% relative crystallinity, X_t. Therefore, modified Avrami constants n, K and K_c were determined in this range (i.e. X_t< 0.5) for all specimens, and tabulated in Table 3.5.

Table 3.5 Non-isothermal Crystallization Parameters and Modified Avrami Equation Constants for PA6 and its Nanocomposites

Specimens	ΔH_c **(J/g)**	X_c **(%)**	T_o **(°C)**	T_p **(°C)**	T_R **(°C)**	$T_{1/2}$ ***(°C)***	$t_{1/2}$ **(min)**	***n***	***K***	K_c
PA	65.64	27.35	182	177	18	185	0.25	4.23	12.47	1.134
PA/CNT 0.1	68.94	28.75	187	182	20	189	0.43	3.87	1.89	1.032
PA/f-CNT 0.1	69.17	28.85	187	182	21	191	0.49	3.85	1.72	1.027
PA/s-CNT 0.1	70.98	29.60	189	183	21	192	0.51	3.82	1.63	1.025
PA/CNT 0.5	74.47	31.19	188	182	23	190	0.39	3.82	1.70	1.027
PA/f-CNT 0.5	79.69	33.37	188	183	24	191	0.51	3.80	1.62	1.024
PA/s-CNT 0.5	83.70	35.05	190	184	25	192	0.54	3.77	1.49	1.020
PA/CNT 1.0	80.93	34.06	190	183	27	190	0.39	3.79	1.56	1.022
PA/f-CNT 1.0	82.51	34.73	189	184	30	191	0.49	3.73	1.47	1.019
PA/s-CNT 1.0	91.23	38.40	191	185	31	195	0.76	3.68	1.26	1.012

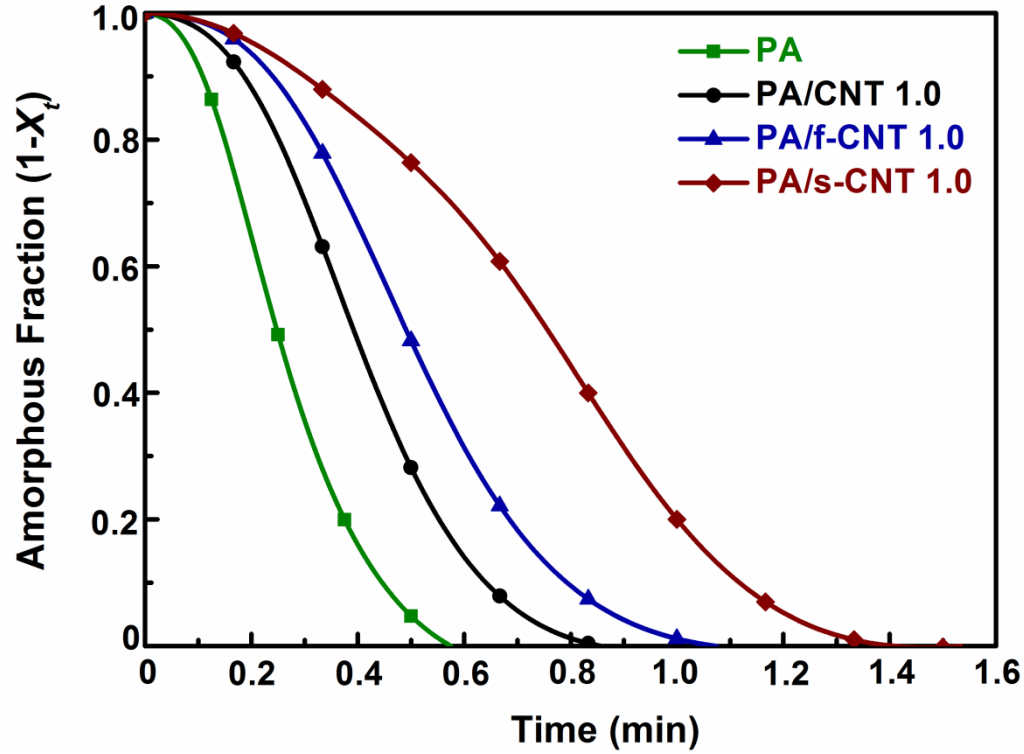

Figure 3.15 Amorphous Phase Fraction versus Non-isothermal Crystallization Time Curves for PA6 and its Nanocomposites with 1.0 wt% Carbon Nanotubes

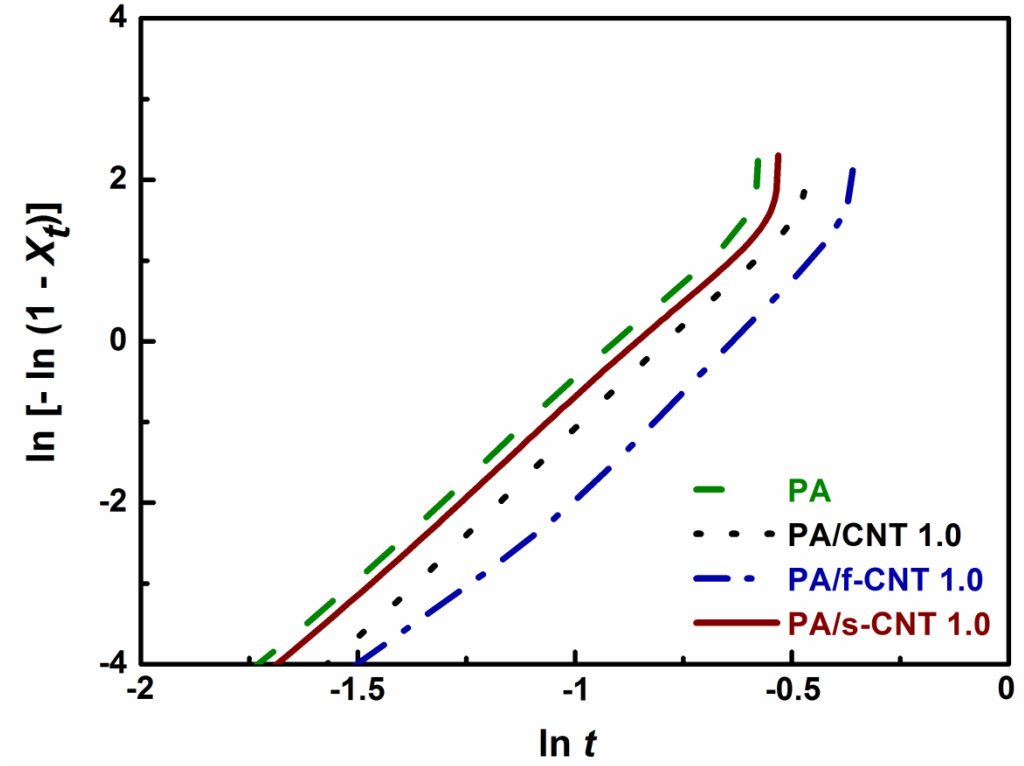

Figure 3.16 Avrami Plots of ln [– ln (1 – X_t)] versus ln t during Non-isothermal Crystallization of PA6 and its Nanocomposites with 1.0 wt% Carbon Nanotubes

Table 3.5 shows that there is no significant changes in the values of modified Avrami exponent *n*, which reveals that under non-isothermal condition growth mechanisms of spherulustic crystallites for neat polyamide-6 and nanocomposites are similar. On the other hand, compared to neat PA6 values of modified Avrami rate constants K and K_c decreases for all nanocomposites. As discussed for the values of $t_{1/2}$ above, the decreases in the rate constants are due to the physical barrier effects of carbon nanotubes delaying the conformational arrangements of polymer chains for crystallization. These findings agree well with the other studies [53,54] in the literature.

3.3.3 Crystal Structure Analysis by XRD

Injection molding is one of the most common method to shape thermoplastic components in the industry. During this process, molten polymer is injected into a mold or cavity under high pressure. The temperature of mold which is well below the melting point influences the crystalline structure, and consequently mechanical and physical properties of the component.

Therefore, in this part of the study, crystal structure of the nanocomposites were compared with neat PA6 by XRD analysis as explained in the experimental part. It was observed that XRD patterns of all nanocomposites were different compared to neat PA6; in which they all had double crystallization peaks. Figure 3.17 shows examples of these curves for the nanocomposites with 1 wt% carbon nanotubes.

It is known that PA6 crystallize predominantly as α- and γ-crystalline morphologies depending on the processing parameters and presence of nucleation agents. In the α-phase, chains are in extended conformation arranged in an anti-parallel manner, while in the γ-phase chains have parallel arrangement and amide groups on the chains are rotated about 60° from the planar extended conformation. In order to investigate these different structures, all XRD peaks were deconvoluted as stated in the experimental part.

In the literature [55,84-86], the 2θ locations for the α- and γ-phases are well established. α-phase crystallizes at two diffraction peaks of 20.3° and 23.5° assigned to (200) and (002/202) planes, on the other hand γ-phase crystallizes at 21.4° assigned to (001) and (200/201) planes.

During deconvolution analysis, the peak locations of α- and γ-phases were held constant, while the peak heights and widths were allowed to vary. For the amorphous phase, the peak location was allowed to float around 22°. In order to start curve fitting algorithm reasonably, heights and breadths of each peak were adjusted manually, then they were modeled using a Gaussian-Lorentzian peak shape. Figure 3.18 shows examples of these deconvoluted XRD peaks for neat PA6 and its nanocomposites with 1 wt% carbon nanotubes.

In order to estimate the degree of crystallinity for each phase, the ratio of the areas of the crystalline phases to that of total area of the curve (amorphous+crystalline) was used. The data and the model predictions agreed well with determination coefficients, R^2 being above 0.99. Then, results of these deconvolution analyses were tabulated in Table 3.6 for all specimens.

Table 3.6 clearly shows that, just like in the isothermal and non-isothermal crystallization cases discussed above, the degree of total crystallinity of injection molded PA6 increases significantly after incorporation of CNTs due to basically their heterogeneous nucleation site effect. Crystallinity of nanocomposites increases again both by increasing the amount of nanotubes and also by oxidative functionalization and aminosilanization treatments leading to more homogeneous dispersion. For example, total crystallinity of injection molded neat PA6 increases from 36% up to almost 80% (an increase of more than two times) by only adding 1 wt% s-CNT.

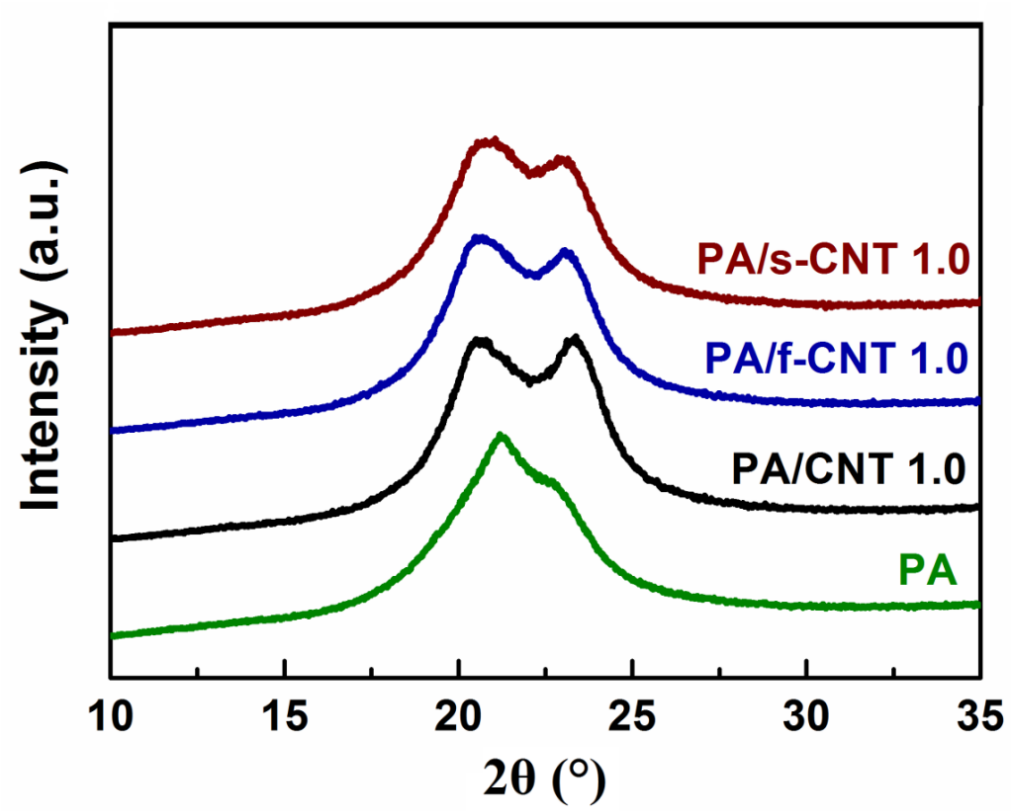

Figure 3.17 XRD Patterns of Injection Molded PA6 and its Nanocomposites with 1.0 wt% Carbon Nanotubes

Table 3.6 also shows that crystalline structure of injection molded neat PA6 was composed of almost 60% α-phase and 40% γ-phase. On the other hand, it is seen in Table 3.6 that addition of all types of CNTs resulted in transformation of γ-phase into α-phase, or better to say, constraints from CNTs imposed on the polymeric chains of PA6 favored formation of the α-phase crystals. It is known that α-phase is more thermodynamically stable and exhibit better mechanical properties than γ-phase.

In the literature, it is discussed that due to the different constraints imposed on the polymer chains, there is a role of dimensionality of nano-fillers on the crystalline structure. For instance, it is claimed that one-dimensional carbon nanotubes promote formation of α-phase [84,86], while two-dimensional nanoclays promote γ-phase [44-47].

Table 3.6 Crystallinity and Phase Structure of Injection Molded PA6 and its Nanocomposites Estimated by Theoretical Fitting of XRD Patterns

Specimens	Total Crystallinity (%)	% α-phase of Total	% γ-phase of Total
PA	36.05	59.45	40.55
PA/CNT 0.1	49.80	100	0
PA/f-CNT 0.1	56.55	100	0
PA/s-CNT 0.1	71.30	100	0
PA/CNT 0.5	51.43	100	0
PA/f-CNT 0.5	57.87	100	0
PA/s-CNT 0.5	76.54	100	0
PA/CNT 1.0	61.86	100	0
PA/f-CNT 1.0	60.85	100	0
PA/s-CNT 1.0	79.93	100	0

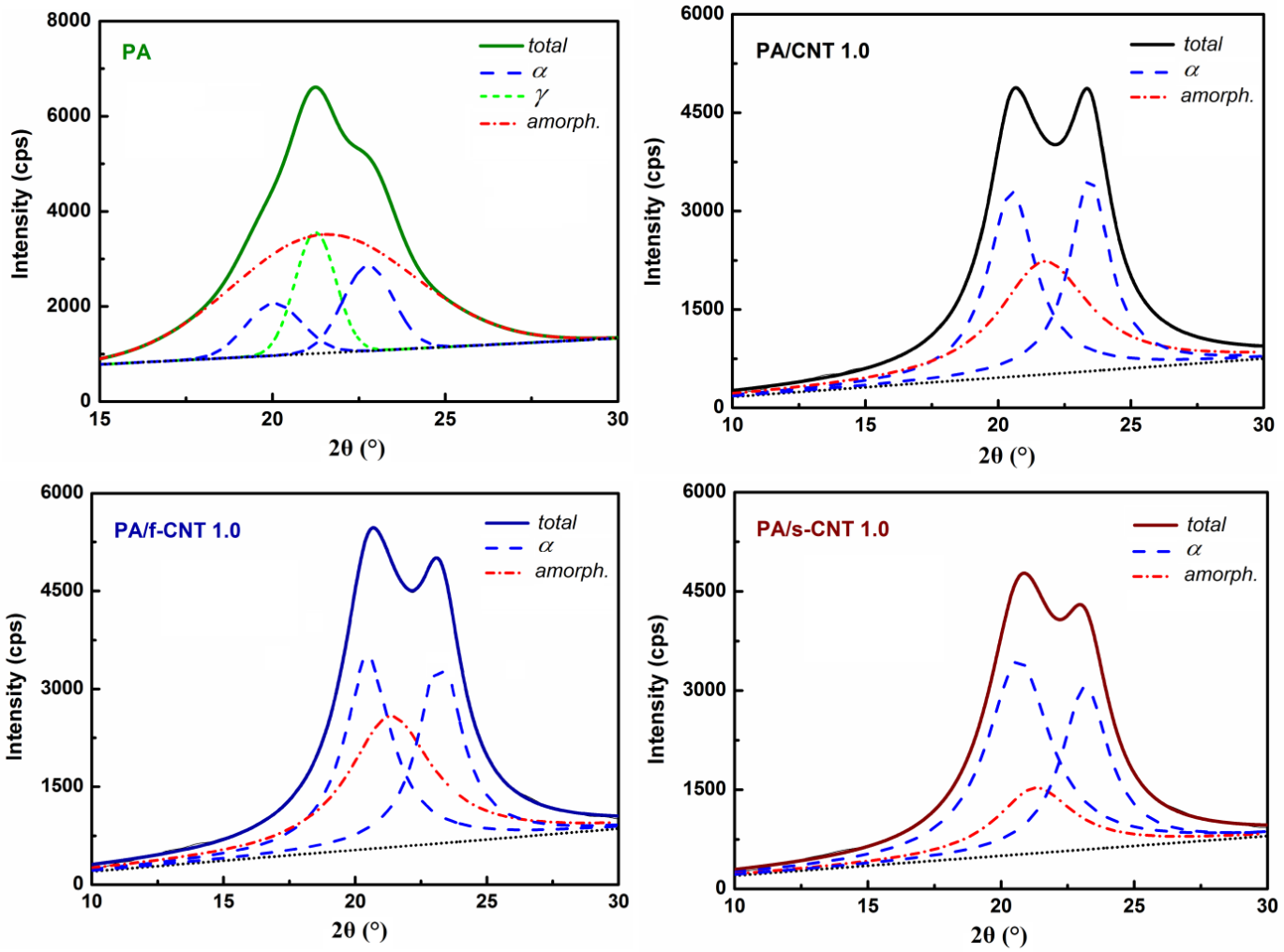

Figure 3.18 Deconvoluted XRD Peaks of PA6 and its Nanocomposites with 1.0 wt% Carbon Nanotubes

3.4 Effects of Oxidative Functionalized and Aminosilanized Carbon Nanotubes on the Mechanical and Thermal Properties of Polyamide-6 Nanocomposites

Results of mechanical and thermal behaviour of all specimens were presented and discussed in the following subsections. Note that all data obtained for neat PA6 and its nine different nanocomposites are given in the tables in detail. However, in order to prevent complicated figures, plots are shown only for PA6 matrix and the nanocomposites with 1 wt% carbon nanotubes. Other plots for the nanocomposites with 0.1 and 0.5 wt% carbon nanotubes are given in Appendix B.

3.4.1 Flexural Properties by Bending Tests

Flexural tests were conducted for neat PA6 and three groups of PA6 nanocomposites with three different loading levels of CNTs (0.1, 0.5, 1.0 wt%). Examples of flexural stress versus flexural strain curves are given in Figure 3.19 for the specimens with 1 wt% CNTs. Flexural strength and flexural modulus of all specimens are illustrated in Figure 3.20 and tabulated with standard deviations in Table 3.7.

Figure 3.20 and Table 3.7 show that even the use of unmodified CNTs increases flexural strength and modulus values to a certain extent. This should be especially due to the decreased mobility of PA6 molecular chains. Therefore, increasing CNT loading increases these properties.

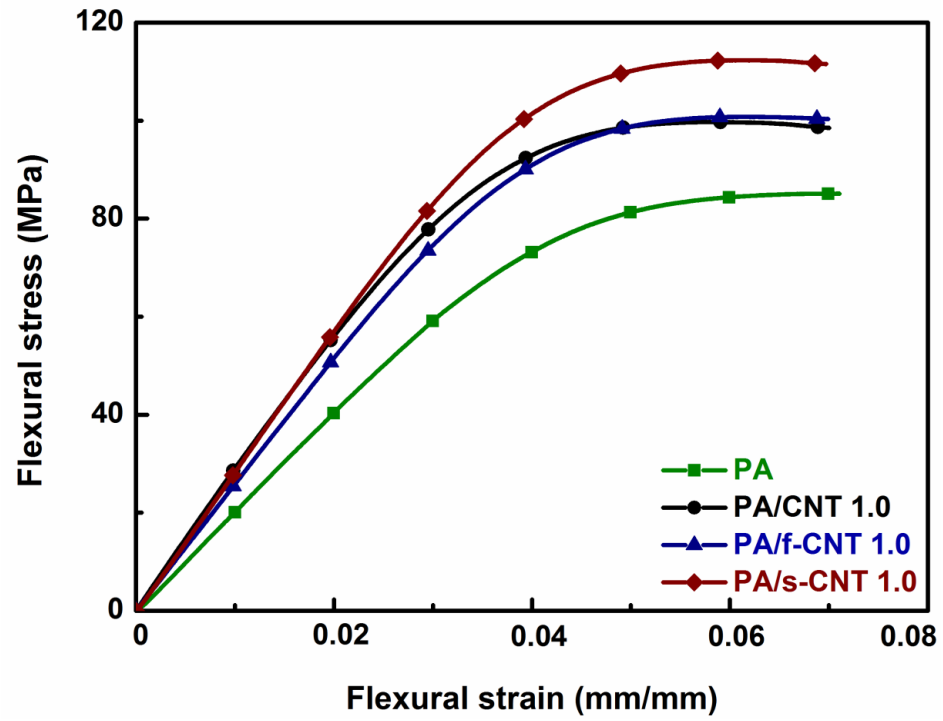

Figure 3.19 Flexural Stress versus Flexural Strain Curves of PA6 and its Nanocomposites with 1.0 wt% Carbon Nanotubes

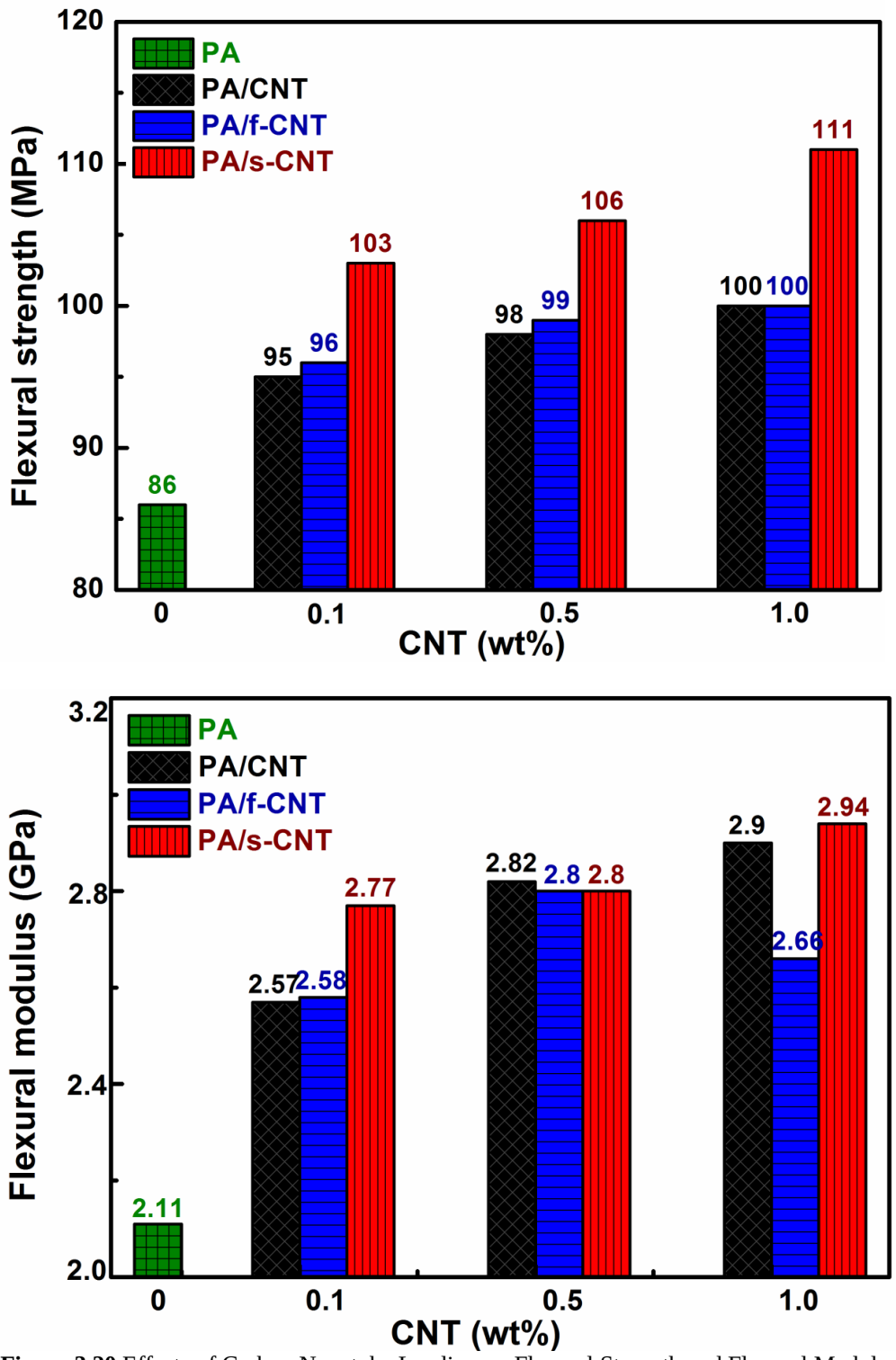

Figure 3.20 Effects of Carbon Nanotube Loading on Flexural Strength and Flexural Modulus of PA6 Nanocomposites

When CNTs are functionalized by oxidation (f-CNT) and then aminosilanization (s-CNT), flexural strength and modulus values increase further. Because, these treatments increase interfacial interactions between the CNT surfaces and PA6 molecules leading to formation of either hydrogen bonding or covalent bonding at the interface. Then, the load transfer mechanism from the matrix to the reinforcement works efficiently.

In this respect, the highest increases were obtained in the specimen of PA/s-CNT 1.0. For instance, compared to neat PA6, the increases in flexural strength and flexural modulus values were as much as 30% and 40%, respectively.

Table 3.7 Flexural Properties of PA6 and its Nanocomposites

Specimens	Flexural Strength (MPa)	Flexural Modulus (GPa)
PA	86 ± 3.4	2.11 ± 0.08
PA/CNT 0.1	95 ± 1.5	2.57 ± 0.09
PA/f-CNT 0.1	96 ± 1.3	2.58 ± 0.13
PA/s-CNT 0.1	103 ± 0.4	2.77 ± 0.07
PA/CNT 0.5	98 ± 0.3	2.82 ± 0.09
PA/f-CNT 0.5	99 ± 1.8	2.80 ± 0.14
PA/s-CNT 0.5	106 ± 1.4	2.80 ± 0.03
PA/CNT 1.0	100 ± 0.9	2.90 ± 0.02
PA/f-CNT 1.0	100 ± 0.6	2.66 ± 0.10
PA/s-CNT 1.0	111 ± 1.2	2.94 ± 0.05

3.4.2 Tensile Properties by Tension Tests

Apart from bending tests, in order to investigate effects of unmodified CNTs, f-CNTs and s-CNTs on the mechanical performance of polyamide-6, tensile tests were also conducted with three different loading levels (0.1, 0.5, 1.0 wt%) of each. Examples of tensile stress-strain curves are given in Figure 3.21 for polyamide-6 and its nanocomposites with 1.0 wt% carbon nanotubes, while yield strength and Young's modulus values with respect to all carbon nanotube loadings are shown in Figure 3.22. All the tensile properties including tensile strength and % strain at break data with standard deviations are tabulated in Table 3.8.

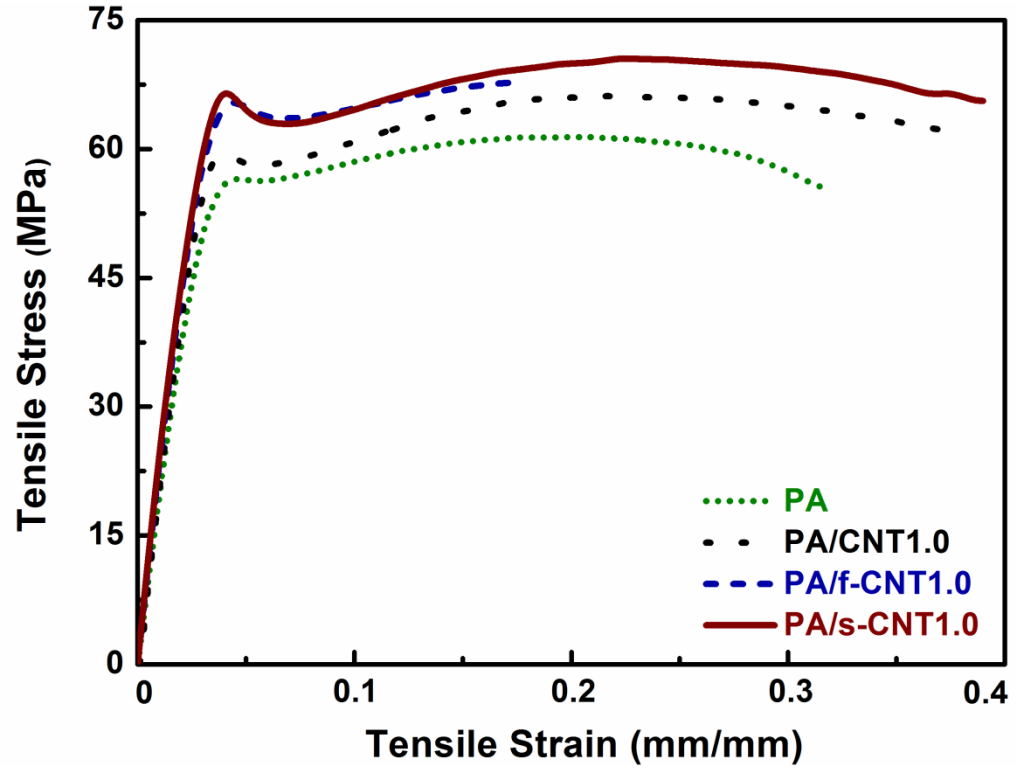

Figure 3.21 Tensile Stress versus Tensile Strain Curves of PA6 and its Nanocomposites with 1.0 wt% Carbon Nanotubes

Just like in the bending tests, Figure 3.21 and Table 3.8 show that even the use of unmodified CNTs increases yield strength and Young's modulus values to a certain extent, again especially due to the decreased mobility of matrix chains. Thus, increasing CNT content increases these properties.

After oxidative functionalization and aminosilanization of CNTs, yield strength and Young's modulus values increase further; due to the increased interfacial interactions between CNT surfaces and matrix chains by hydrogen or covalent attraction at the interface. Then, the load transfer mechanism from the matrix to the reinforcement works efficiently.

Therefore, the highest increases were again obtained in PA/s-CNT 1.0 specimen; compared to neat PA6, the increases in yield strength and Young's modulus values were as much as 20% and 23%, respectively.

Table 3.8 also shows that use of unmodified CNTs and s-CNTs increases tensile strength and % elongation at break values of neat PA6. For instance, these increases in the specimens of PA/s-CNT 1.0 are as much as 16% for tensile strength, while 25% for % elongation at break values, respectively.

As discussed in the previous crystallization section, it should be noted that, all the increases in the mechanical properties were also originating from the increased degree of crystallinity due to the heterogeneous nucleation effect of carbon nanotubes.

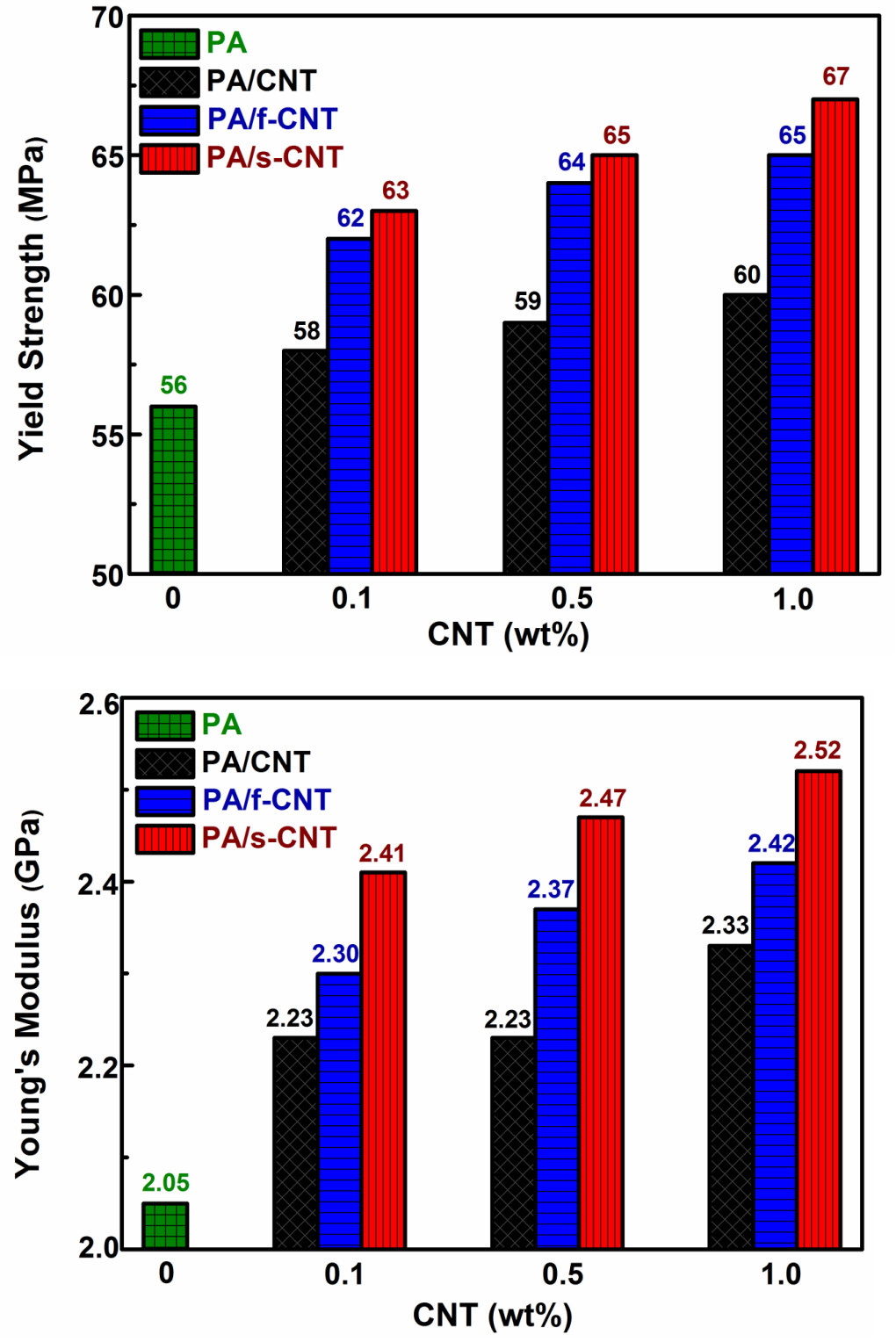

Figure 3.22 Effects of Carbon Nanotube Loading on Yield Strength and Young's Modulus of PA6 and its Nanocomposites

Table 3.8 Tensile Properties of PA6 and its Nanocomposites

Specimens	Yield Strength (MPa)	Young's Modulus (GPa)	Tensile Strength (MPa)	% Strain at Break
PA	56 ± 1.0	2.05 ± 0.05	61 ± 0.9	32 ± 1.2
PA/CNT 0.1	58 ± 1.2	2.23 ± 0.05	66 ± 1.4	36 ± 1.3
PA/f-CNT 0.1	62 ± 0.8	2.30 ± 0.02	62 ± 1.2	8 ± 1.0
PA/s-CNT 0.1	63 ± 1.5	2.41 ± 0.07	68 ± 1.7	40 ± 1.1
PA/CNT 0.5	59 ± 1.4	2.23 ± 0.06	66 ± 1.3	34 ± 1.4
PA/f-CNT 0.5	64 ± 0.7	2.37 ± 0.03	64 ± 1.1	10 ± 0.9
PA/s-CNT 0.5	65 ± 1.0	2.47 ± 0.04	69 ± 1.5	40 ± 1.7
PA/CNT 1.0	60 ± 1.5	2.33 ± 0.08	66 ± 1.4	38 ± 1.2
PA/f-CNT 1.0	65 ± 0.9	2.42 ± 0.03	68 ± 1.1	18 ± 1.0
PA/s-CNT 1.0	67 ± 1.4	2.52 ± 0.09	71 ± 1.6	40 ± 1.5

3.4.3 Thermomechanical Behaviour by DMA

DMA analyses were conducted in order to investigate thermomechanical properties of the specimens. Examples of storage modulus and *tan* δ curves are given in Figure 3.23 for PA6 and its nanocomposites with 1 wt% CNTs, while Table 3.9 gives the data for all specimens. In this table, results are evaluated as two different storage modulus values at -25° and 25°C, including primary transition temperature (T_g) taken at peak *tan* δ values.

Figure 3.23 and Table 3.9 show that in the glassy plateau region, for example at -25°C, even the use of unmodified CNTs increase storage modulus value of PA6 due to the decreased mobility of the side groups of polyamide backbone. Of course increasing CNT content leads to more improvement in the storage modulus values.

Table 3.9 also indicates that oxidative functionalization (f-CNT) and aminosilanization (s-CNT) increase storage modulus values at -25°C even further. For instance, the increases were as much as 20% and 23% for the specimens with 1.0 wt% f-CNTs and s-CNTs, respectively. Because, these treatments lead to formation of stronger chemical bonding making mobility of side groups even harder.

Table 3.9 Dynamic Thermomechanical Properties of PA6 and its Nanocomposites

Specimens	**Storage Modulus at -25°C (GPa)**	**Storage Modulus at 25°C (GPa)**	**T_g (°C) (peak tan δ)**
PA	2.36	1.66	42
PA/CNT 0.1	2.45	1.80	44
PA/f-CNT 0.1	2.62	1.81	47
PA/s-CNT 0.1	2.77	1.92	58
PA/CNT 0.5	2.48	1.68	45
PA/f-CNT 0.5	2.78	2.01	52
PA/s-CNT 0.5	2.81	2.03	60
PA/CNT 1.0	2.59	1.96	46
PA/f-CNT 1.0	2.84	2.02	57
PA/s-CNT 1.0	2.90	2.07	61

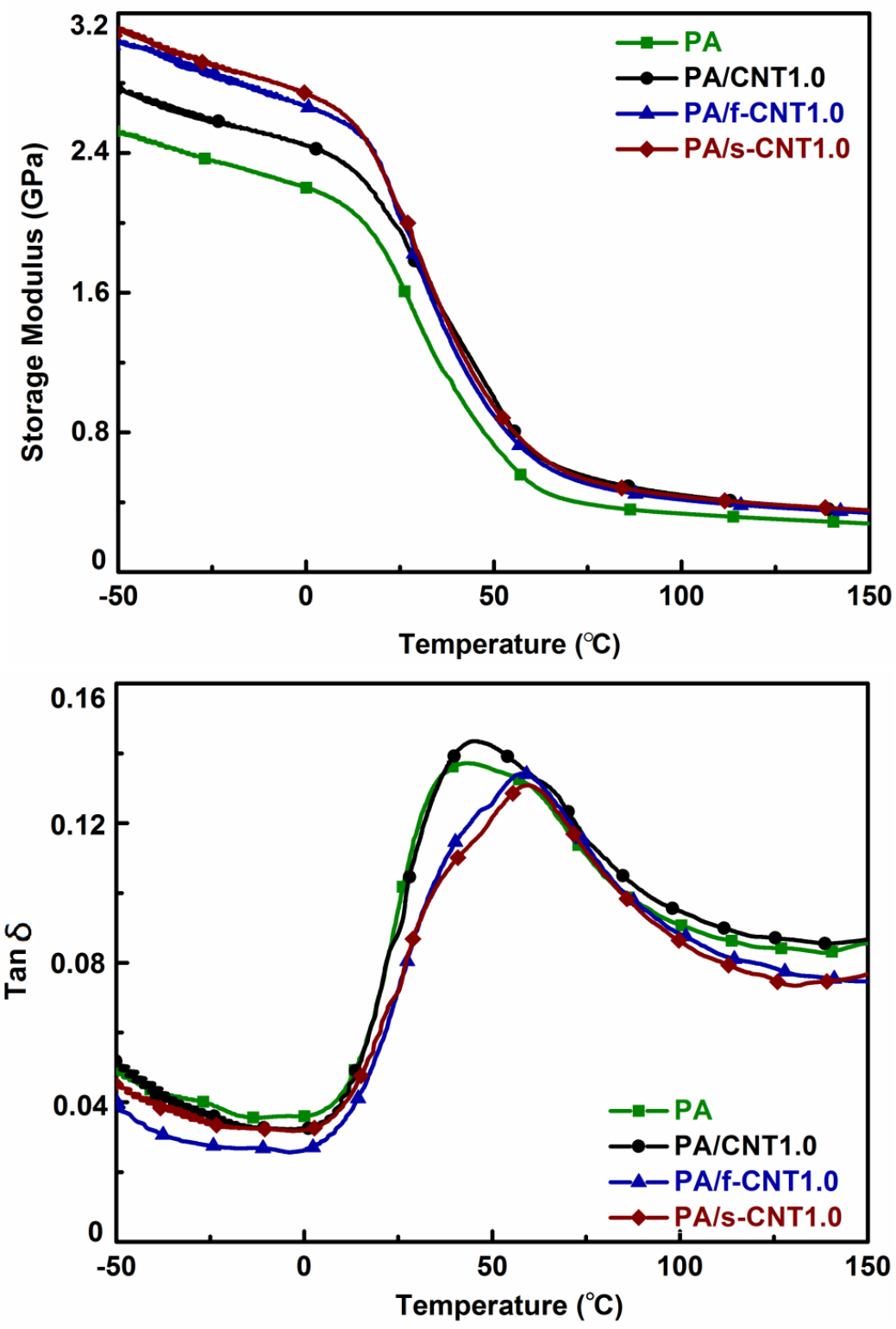

Figure 3.23 Storage Modulus and *tan δ* Curves of PA6 and its nanocomposites with 1.0 wt% Carbon Nanotubes

Tan δ curves in Figure 3.23 show that above 0°C the main backbone of the polyamide chains start to move over each other significantly, which decreases storage modulus values. However, storage modulus data at 25°C given in Table 3.9 indicate that use of unmodified CNTs, f-CNTs and s-CNTs again increase this value of neat PA6. This time, the increases in storage modulus values are 18%, 22% and 25% for the 1.0 wt% unmodified CNTs, f-CNTs and s-CNTs, respectively. This is again due to the uniform dispersion and stronger interfacial interactions between the treated nanotube surfaces and polyamide chains leading to decreased mobility.

It is known that *tan δ* curves make a peak when the temperature reaches to a critical transition where blocks of polymer chain segments move over each other. This primary transition temperature (at *tan δ* peak) can be interpreted as T_g of the specimens. Table 3.9 shows that T_g of neat PA6 increases with the use of all types of CNTs. Again as discussed above, due to more restricted mobility of polyamide chains with functionalized nanotube surfaces, the increases in T_g of neat PA6 were 4°C, 15°C and 19°C for 1.0 wt% unmodified CNTs, f- CNTs and s-CNTs, respectively.

3.4.4 Thermal Degradation by TGA

In order to investigate the effects of CNT surface treatments on the thermal degradation behavior of PA6, TGA data were evaluated in the form of thermogravimetric (TG) and differential thermogravimetric (DTG) curves. Examples of these curves are shown in Figure 3.10 for PA6 and its nanocomposites with 1 wt% CNTs. Table 3.10 also tabulates two data for all specimens; $T_{25wt\%}$ and $T_{MLR\text{-}max}$ which are the thermal degradation temperatures at 25 wt% mass loss and maximum mass loss rate peak, respectively.

Table 3.10 Thermal Degradation Data of PA6 and its Nanocomposites

Specimens	$T_{25wt\%}$ **(°C)**	$T_{MLR\text{-}max}$ **(°C)**
PA	437	455
PA/CNT 0.1	438	457
PA/f-CNT 0.1	438	456
PA/s-CNT 0.1	440	458
PA/CNT 0.5	439	457
PA/f-CNT 0.5	440	458
PA/s-CNT 0.5	441	459
PA/CNT 1.0	439	458
PA/f-CNT 1.0	440	457
PA/s-CNT 1.0	442	460

$T_{25wt\%}$: temperature at 25 wt% mass loss
$T_{MLR\text{-}max}$: temperature at maximum mass loss rate peak

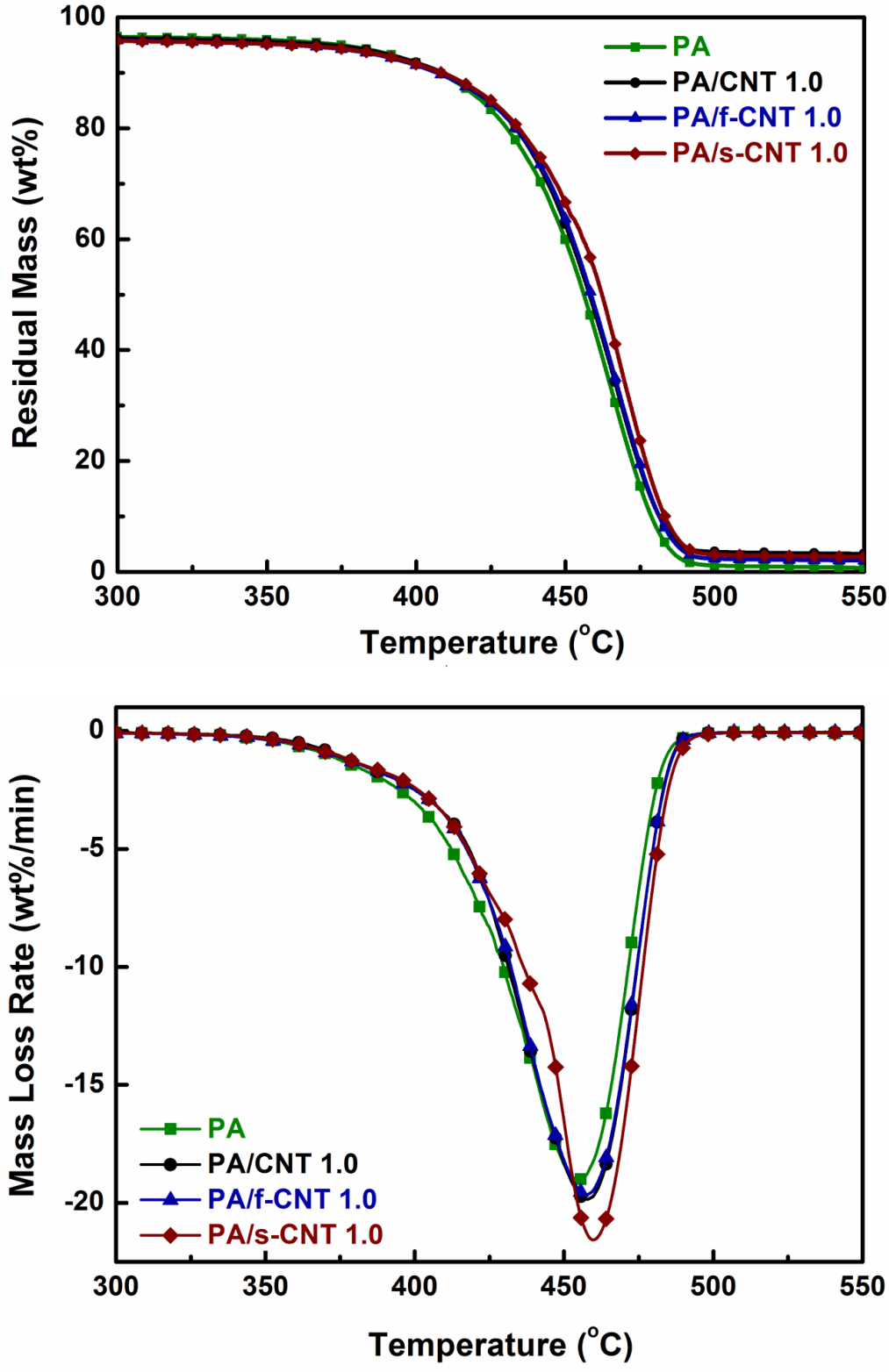

Figure 3.24 Thermogravimetric (TG) and Differential Thermogravimetric (DTG) Curves of PA6 and its Nanocomposites with 1.0 wt% Carbon Nanotubes

Figure 3.24 and Table 3.10 show that there are certain level of increases in the thermal degradation temperatures of neat PA6 when reinforced with CNTs. These improvements should be due to the physical barrier function of carbon nanotubes which prevent the diffusion of volatiles and decomposed products out of the polymer matrix during decomposition. Of course improved dispersion and interfacial bonding between the polymer matrix and functionalized CNTs lead to higher thermal degradation temperatures. For example, for the specimens of PA/s-CNT1.0, the increases in the $T_{25wt\%}$ and $T_{MLR\text{-}max}$ values are both as much as by 5°C. Again, it should be noted that, thermal properties might also increase due to the higher levels of crystallinity obtained by the heterogeneous nucleation effects of carbon nanotubes.

CHAPTER 4

CONCLUSIONS

The main conclusions drawn from the four stages of this study can be summarized as follows:

(i) Characterization of Oxidative Functionalized and Aminosilanized Carbon Nanotubes

- XPS of s-CNTs showed a distinct peak at binding energy of 101 eV, which was assigned to bridging silicon atoms. Deconvolution of silicon peak resulted in two peaks at 101.3 and 102.8 eV, which indicate two different chemical states of silicon.

- FTIR of s-CNTs exhibited the presence of Si–O–C stretching and Si–O vibration peak at wavenumbers of 1110 cm^{-1} and 1070 cm^{-1}, respectively, which confirm chemical interaction of aminosilane molecules with CNT surfaces.

- SEM revealed debundling and disentanglement of CNTs with respect to oxidative functionalization and aminosilanization. EDS results also showed the presence of silicon atom at around 1.8 keV, which could be an evidence of covalent attachment of aminosilane molecules on the surface of f-CNTs.

- XRD patterns of CNTs indicated that crystalline structure of CNTs remain almost unchanged after surface functionalization. TGA simply indicated that significant thermal degradation of unmodified CNTs started around 550°C while it was as low as 100°C for the f-CNTs and s-CNTs due to the lower temperature resistance of the chemical groups formed on the surfaces.

(ii) Effects of Oxidative Functionalization and Aminosilanization on the Dispersion of Carbon Nanotubes in Polyamide-6

- SEM and TEM analyses revealed that unmodified CNTs tend to form bundles and entanglaments leading to poor dispersion.

- Due to the increased chemical interactions between the matrix and carbon nanotubes, oxidative functionalization and aminosilanization resulted in rather much uniform dispersion of CNTs in PA6 matrix.

(iii) Effects of Oxidative Functionalized and Aminosilanized Carbon Nanotubes on the Crystallization Behavior of Polyamide-6 Nanocomposites

- Under isothermal crystallization condition, due to the heterogeneous nucleation effect, both increasing amount of carbon nanotubes and their oxidative functionalization and aminosilanization resulted in higher relative crystallinity X_c(an increase of up to 40%), and lower crystallization times $t_{max}$and $t_{1/2}$(decreases of up to 2 times for each) compared to neat PA6. Values of Avrami exponent n indicated that three-dimensional growth mechanism of PA6 spherulites might transform into two-dimensional growth mechanism when CNTs were incorporated, and Avrami rate constant K of PA6 could increase more than 24 times with only 1 wt% s-CNTs.

- Under non-isothermal crystallization condition, due to the same heterogeneous nucleation effect, increased content and surface functionalization of carbon nanotubes again resulted in up to 40% higher relative crystallinity X_c. In this case, all temperature parameters (T_o, T_p, $T_{1/2}$) shifted to higher temperatures, indicating that non-isothermal crystallization starts at higher temperatures. On the other hand, reciprocal of time ($1/t_{1/2}$) and modified Avrami rate constants K and $K_c$decreased with increasing CNT content and their surface functionalization, basically due to the delayed conformational mobility of polymer chains via act of physical hinderance of CNTs.

- Under injection molding condition, similarly, addition of all types of carbon nanotubes increased degree of crystallinity of neat PA6, reaching to a value of more than 2 times, due to again basically heterogeneous nucleation effect. Moreover, because of the constraints from carbon nanotubes imposed on the polymeric chains, formation of γ-phase was prevented leading to crystallization only in α-phase form.

(iv) Effects of Oxidative Functionalized and Aminosilanized Carbon Nanotubes on the Mechanical and Thermal Properties of Polyamide-6 Nanocomposites

- Both increasing CNT content and oxidative functionalization and aminosilanization of CNTs increased mechanical properties due to decreased matrix chain mobility and very efficient load transfer from the matrix to chemically bonded CNTs. For example, flexural strength and flexural modulus of nanocomposites with 1 wt% s-CNTs were as much as 30% and 40% higher compared to neat PA6, while their yield strength and Young's modulus were as much as 20% and 23% higher, respectively.

- Thermomechanical analysis by DMA indicated that surface modification of CNTs decreases mobility of both side groups and main backbone of PA6 chains significantly leading to improved storage modulus values as much as 25% and increased T_g (peak tan δ) by 19°C.

- TGA analysis also resulted in higher thermal degradation temperatures, as much as by 5°C, with the efficient physical barrier formation of surface treated CNTs preventing diffusion of volatiles and decomposed products from the matrix.

- Increases in the mechanical and thermal properties could be also originating from the increased relative crystallinity of PA6 due to the heterogeneous nucleation effects of CNTs.

REFERENCES

[1] Vinken E., Polyamides: Hydrogen Bonding, the Brill Transition, and Superheated Water, *Eindhoven University of Technology*, 2008.

[2] Kohan M.I., Mestemacher S.A., Pagilagan R.U. and Redmond K., Polyamides, *Ullmann's Encyclopedia of Industrial Chemistry*, 2003.

[3] Palmer R.J., Polyamides-Plastics, *Kirk-Othmer Encyclopedia of Chemical Technology*, John Wiley and Sons Inc., 2005.

[4] Fornes T.D., Paul D.R., Crystallization Behavior of Nylon 6 Nanocomposites, *Polymer*, 44(14): 3945-3961, 2003.

[5] Iijima S., Helical Microtubules of Graphitic Carbon, *Nature*, 354(6348): 56–58, 1991.

[6] Ajayan P.M., Nanotubes from Carbon, *Chemical Reviews*, 99(7): 1787–1799, 1999.

[7] Dai H.J., Carbon Nanotubes: Synthesis, Integration, and Properties, *Accounts of Chemical Research*, 35(12): 1035–1044, 2002.

[8] Popov V.N., Carbon Nanotubes: Properties and Application, *Materials Science and Engineering: R-Reports*, 43(3): 61–102, 2004.

[9] Demczyk B.G., Wang Y.M., Cumings J., Direct Mechanical Measurement of the Tensile Strength and Elastic Modulus of Multiwalled Carbon Nanotubes, *Materials Science and Engineering A-Structural Materials*, 334(1-2): 173–178, 2002.

[10] Thostenson E.T., Ren Z.F., and Chou T.W., Advances in the Science and Technology of Carbon Nanotubes and Their Composites: A Review, *Composites Science and Technology*, 61(13): 1899–1912, 2001.

[11] Lau K.T., and Hui D., The Revolutionary Creation of New Advanced Materials - Carbon Nanotube Composites, *Composites Part B-Engineering*, 33(4): 263–277, 2002.

[12] Ma P.C., Siddiqui N.A., Marom G., Dispersion and Functionalization of Carbon Nanotubes for Polymer - Based Nanocomposites: A Review, *Composites Part A-Applied Science and Manufacturing*, 41(10): 1345–1367, 2010.

[13] Coleman J.N., Khan U., Blau W.J., Small but Strong: A Review of the Mechanical Properties of Carbon Nanotube – Polymer Composites, *Carbon*, 44(9): 1624–1652, 2006.

[14] Sahoo N.G., Rana S., Cho J.W., Polymer Nanocomposites Based on Functionalized Carbon Nanotubes, *Progress in Polymer Science*, 35(7): 837–867, 2010.

[15] Moniruzzaman M., Winey K.I., Polymer Nanocomposites Containing Carbon Nanotubes, *Macromolecules*, 39(16): 5194–5205, 2006.

[16] Miyata Y., Maniwa Y. and Kataura H., Selective Oxidation of Semiconducting Single-Wall Carbon Nanotubes by Hydrogen Peroxide, *Journal of Physical Chemistry B*, 110(1): 25–29, 2006.

[17] Hernadi K., Siska A. and Thien-Nga L., Reactivity of Different Kinds of Carbon during Oxidative Purification of Catalytically Prepared Carbon Nanotubes, *Solid State Ionics*, 141: 203–209, 2001.

[18] Liang Y.M., Zhang H.M., and Yi B.L., Preparation and Characterization of Multi-walled Carbon Nanotubes Supported PtRu Catalysts for Proton Exchange Membrane Fuel Cells, *Carbon*, 43(15): 3144–3152, 2005.

[19] Zhang N.Y., Me J., and Varadan V.K., Functionalization of Carbon Nanotubes by Potassium Permanganate Assisted with Phase Transfer Catalyst, *Smart Materials and Structures*, 11(6): 962–965, 2002.

[20] Kim M., Hong C.K., Choe S., Synthesis of Polystyrene Brush on Multi-walled Carbon Nanotubes Treated with $KMnO_4$ in the Presence of a Phase-Transfer Catalyst, *Journal of Polymer Science Part A-Polymer Chemistry*, 45(19): 4413–4420, 2007.

[21] Najafi E., Kim J.Y., and Han S.H., UV-ozone Treatment of Multi-walled Carbon Nanotubes for Enhanced Organic Solvent Dispersion, *Colloids and Surfaces A-Physicochemical and Engineering Aspects*, 284: 373–378, 2006.

[22] Simmons J.M., Nichols B.M., and Baker S.E., Effect of Ozone Oxidation on Single-walled Carbon Nanotubes, *Journal of Physical Chemistry B*, 110(14): 7113–7118, 2006.

[23] Zhang X.F., Sreekumar T.V., and Liu T., Properties and Structure of Nitric Acid Oxidized Single Wall Carbon Nanotube Films, *Journal of Physical Chemistry B*, 108(42): 16435–16440, 2004.

[24] Rosca I.D., Watari F., and Uo M., Oxidation of Multi-walled Carbon Nanotubes by Nitric Acid, *Carbon*, 43(15): 3124–3131, 2005.

[25] Li X.H., Niu J.L., and Zhang J., Labeling the Defects of Single-walled Carbon Nanotubes Using Titanium Dioxide Nanoparticles, *Journal of Physical Chemistry B*, 107(11): 2453–2458, 2003.

[26] Zhang J., Zou H.L., and Qing Q., Effect of Chemical Oxidation on the Structure of Single-walled Carbon Nanotubes, *Journal of Physical Chemistry B*, 107(16): 3712–3718, 2003.

[27] Xia W., Wang Y., and Bergstraesser R., Surface Characterization of Oxygen-Functionalized Multi-walled Carbon Nanotubes by High-Resolution X-ray Photoelectron Spectroscopy and Temperature-programmed Desorption, *Applied Surface Science*, 254(1): 247–250, 2007.

[28] Serp P., Corrias M., and Kalck P., Carbon Nanotubes and Nanofibers in Catalysis, *Applied Catalysis A-General*; 253(2): 337–358, 2003.

[29] Cuentas-Gallegos A.K., Martinez-Rosales R., and Rincon M.E., Design of Hybrid Materials Based on Carbon Nanotubes and Polyoxometalates, *Optical Materials*, 29(1): 126–133, 2006.

[30] Li Y., Zhang X.B., and Luo J.H., Purification of CVD Synthesized Single-wall Carbon Nanotubes by Different Acid Oxidation Treatments, *Nanotechnology*, 15(11): 1645–1649, 2004.

[31] Xing Y.C., Li L., and Chusuei C.C., Sonochemical Oxidation of Multi-walled Carbon Nanotubes, *Langmuir*, 21(9): 4185–4190, 2005.

[32] Osorio A.G., Silveira I.C.L., and Bueno V.L., H_2SO_4/HNO_3/HCl-Functionalization and its Effect on Dispersion of Carbon Nanotubes in Aqueous Media, *Applied Surface Science*, 255(5): 2485–2489, 2008.

[33] Rosario-Castro B.I., Contes E.J., and Lebron-Colon M., Combined Electron Microscopy and Spectroscopy Characterization of As-received, Acid Purified, and Oxidized HiPCO Single-wall Carbon Nanotubes, *Material Characterization*, 60(12): 1442–1453, 2009.

[34] Murugesan S., Myers K., and Subramanian V., Amino-functionalized and Acid Treated Multi-walled Carbon Nanotubes as Supports for Electrochemical Oxidation of Formic Acid, *Applied Catalysis B-Environmental*, 103(3-4): 266–274, 2011.

[35] Chiang Y., Lin W., and Chang Y., The Influence of Treatment Duration on Multi-walled Carbon Nanotubes Functionalized by H_2SO_4/HNO_3 Oxidation, *Applied Surface Science*, 257(6): 2401–2410, 2011.

[36] Kathi J., Rhee K.Y., Surface Modification of Multi-Walled Carbon Nanotubes Using 3-Aminopropyltriethoxysilane, *Journal of Materials Science*, 43(1): 33–37, 2008.

[37] Zhou Z., Wang S., Lu L., Functionalization of Multi-Wall Carbon Nanotubes with Silane and its Reinforcement on Polypropylene Composites, *Composites Science and Technology*, 68(7-8): 1727–1733, 2008.

[38] Ma P.C., Kim J.K., Tang B.Z., Functionalization of Carbon Nanotubes Using a Silane Coupling Agent, *Carbon*, 44 (15): 3232–3238, 2006.

[39] Yu S.H., Yeh J.T., Huang B.C., Preparation of a HDPE/Carbon Nanotube Composite, *Polymer-Plastics Technology and Engineering*, 49 (15): 1534–1539, 2010.

[40] Shanmugharaj A.M., Bae J.H., Lee K.Y., Physical and Chemical Characteristics of Multi-walled Carbon Nanotubes Functionalized with Aminosilane and its Influence on the Properties of Natural Rubber Composites, *Composites Science and Technology*, 67(9): 1813–1822, 2007.

[41] Li J., Fang Z., Tong L., Improving Dispersion of Multi-walled Carbon Nanotubes in Polyamide 6 Composites through Amino-Functionalization, *Journal of Applied Polymer Science*, 106(5): 2898–2906, 2007.

[42] Aviles F., Cauich-Rodriguez J.V., Rodriguez-Gonzalez J.A., Oxidation and Silanization of MWCNTs for MWCNT/Vinyl Ester Composites, *Express Polymer Letters*, 5(9): 766–776, 2011.

[43] Yuen S.M., Ma C.C.M., Chiang C.L., Morphology and Properties of Aminosilane Grafted MWCNT/Polyimide Nanocomposites, *Journal of Nanomaterials*, Article Number: 786405 DOI: 10.1155/2008/786405, (2008).

[44] Fornes T.D., Paul D.R., Crystallization Behavior of Nylon 6 Nanocomposites, *Polymer*, 44(14): 3945-3961, 2003.

[45] Lincon D.M., Vaia R.A., and Krishnamurti R., Isothermal Crystallization of Nylon-6/Montmorillonite Nanocomposites, *Macromolecules*, 37(12): 4554, 2004.

[46] Liu X.H., and Wu Q.J., Non-isothermal Crystallization Behaviors of Polyamide 6/Clay Nanocomposites, *European Polymer Journal*, 38(7): 1383, 2002.

[47] Ma C.C., Kuo C.T., Kuan H.C., Effects of Swelling Agents on the Crystallization Behavior and Mechanical Properties of Polyamide 6/Clay Nanocomposites, *Journal of Applied Polymer Science*, 88(7): 1686–1693, 2003.

[48] Weng W., Chen G., and Wu D., Crystallization Kinetics and Melting Behaviors of Nylon 6/Foliated Graphite Nanocomposites, *Polymer*, 44(26): 8119–8132, 2003.

[49] Chae D.W., Oh S.G., and Kim B.C., Effect of Silver Nanoparticles on the Dynamic Crystallization Behavior of Nylon-6, *Journal of Polymer Science Part B: Polymer Physics*, 42(5): 790–799, 2004.

[50] Yang F., Ou Y., and Yu Z., Polyamide 6/Silica Nanocomposites Prepared by in situ Polymerization, *Journal of Applied Polymer Science*, 69(2): 355–361, 1998.

[51] Avella M., Errico M.E., and Gentile G., Nylon 6/Calcium Carbonate Nanocomposites: Characterization and Properties, *Macromolecular Symposium*, 234: 170–175, 2006.

[52] Zheng J., Siegel R.W., and Toney C.G., Polymer Crystalline Structure and Morphology Changes in Nylon-6/ZnO Nanocomposites, *Journal of Polymer Science Part B: Polymer Physics*, 41(10): 1033–1050, 2003.

[53] Chen E.C., and Wu T.M., Isothermal and Nonisothermal Crystallization Kinetics of Nylon 6/Functionalized Multi-walled Carbon Nanotube Composites, *Journal of Polymer Science Part B-Polymer Physics*, 46(2): 158–169, 2008.

[54] Li J., Fang Z., and Tong L., Effect of Multi-walled Carbon Nanotubes on Non-isothermal Crystallization Kinetics of Polyamide 6, *European Polymer Journal*, 42(12): 3230–3235, 2006.

[55] Li J., Fang Z., and Zhu Y., Isothermal Crystallization Kinetics and Melting Behavior of Multiwalled Carbon Nanotubes/Polyamide-6 Composites, *Journal of Applied Polymer Science*, 105(6): 3531–3542, 2007.

[56] Qui S., Zheng Y., and Zeng A., Non-isothermal Crystallization of Monomer Casting Polyamide 6/Functionalized MWNTs Nanocomposites, *Polymer Bulletin*, 67(9): 1945–1959, 2011.

[57] Mukherjee M., Nayak G., and Bose S., Improvement of the Properties of PC/LCP/MWCNT with or without Silane Coupling Agents, *Polymer-Plastics Technology andEngineering*, 48(11): 1107–1112, 2009.

[58] Yuen S.M., Ma C.C.M., Chiang C.L., Morphology and Properties of Aminosilane Grafted MWCNT/Polyimide Nanocomposites, *Journal of Nanomaterials*, Article Number: 786405 DOI: 10.1155/2008/786405, 2008.

[59] Wu S.Y., Yuen S.M., Ma C.C.M., Preparation, Morphology, and Properties of Silane-Modified MWCNT/Epoxy Composites, *Journal of Applied Polymer Science*, 115(6): 3481-3488, 2010.

[60] Kim M.T., Rhee K.Y., Park S.J., Effects of Silane-Modified Carbon Nanotubes on Flexural and Fracture Behaviors of Carbon Nanotube-Modified Epoxy/Basalt Composites, *Composites Part B-Engineering*, 43(5): 2298-2302, 2012.

[61] Lee J.H., Rhee K.Y., Park S.J., Silane Modification of Carbon Nanotubes and its Effects on the Material Properties of Carbon/CNT/Epoxy Three-Phase Composites, *Composites Part A-Applied Science and Manufacturing*, 42(5): 478-483, 2011.

[62] Zhou Z., Wang S., Lu L., Functionalization of Multi-Wall Carbon Nanotubes with Silane and its Reinforcement on Polypropylene Composites, *Composites Science andTechnology*, 68(7-8): 1727-1733, 2008.

[63] Jiang H.X., Ni Q.Q., and Natsuki T., Design and Evaluation of the Interface Between Carbon Nanotubes and Natural Rubber, *Polymer Composites*, 32(2): 236-242, 2011.

[64] Kathi J., and Rhee K.Y., Surface Modification of Multiwalled Carbon Nanotubes Using 3-aminopropyltriethoxysilane, *Journal of Materials Science*, 43(1): 33–37, 2008.

[65] Ma P.C., Kim J.K., and Tang B.Z., Functionalization of Carbon Nanotubes Using a Silane Coupling Agent, *Carbon*, 44(15): 3232–3238, 2006.

[66] Velasco-Santos C., Martinez-Hernandez A.L., and Lozada-Cassou M., Chemical Functionalization of Carbon Nanotubes Through an Organosilane, *Nanotechnology*, 13(4): 495–498, 2002.

[67] Yu S.H., Yeh J.T., and Huang B.C., Preparation of a HDPE/Carbon Nanotube Composite, *Polymer-Plastics Technology and Engineering*, 49(15): 1534–1539, 2010.

[68] Lee J.H., Kathi J., and Rhee K.Y., Wear Properties of 3-aminopropyltriethoxysilane-Functionalized Carbon Nanotubes Reinforced Ultra High Molecular Weight Polyethylene Nanocomposites, *Polymer Engineering and Science*, 50(7): 1433–1439, 2010.

[69] Zhou Z., Wang S., and Lu L., Functionalization of Multi-wall Carbon Nanotubes with Silane and its Reinforcement on Polypropylene Composites, *Composite Science and Technology*, 68(7–8): 1727–1733, 2008.

[70] Zhou Z., Wang S., and Lu L., Isothermal Crystallization Kinetics of Polypropylene with Silane Functionalized Multi-walled Carbon Nanotubes, *Journal of Polymer Science Part B-Polymer Physics*, 45(13): 1616–1624, 2007.

[71] Ma P.C., Kim J.K., and Tang B.Z., Effects of Silane Functionalization on the Properties of Carbon Nanotube/Epoxy Nanocomposites, *Composites Science and Technology*, 67(14): 2965–2972, 2007.

[72] Kathi J., Rhee K.Y., and Lee J.H., Effect of Chemical Functionalization of Multi-walled Carbon Nanotubes with 3-aminopropyltriethoxysilane on Mechanical and Morphological Properties of Epoxy Nanocomposites, *Composites Part A-Applied Science and Manufacturing*, 40(6–7): 800–809, 2009.

[73] Wu S.Y., Yuen S.M., and Ma C.C.M., Preparation, Morphology, and Properties of Silane-modified MWCNT/Epoxy Composites, *Journal of Applied Polymer Science*, 115(6): 3481–3488, 2010.

[74] Shanmugharaj A.M., Bae J.H., and Lee K.Y., Physical and Chemical Characteristics of Multi-walled Carbon Nanotubes Functionalized with Aminosilane and its Influence on the Properties of Natural Rubber Composites, *Composites Science and Technology*, 67(9): 1813–1822, 2007.

[75] Jiang M.J., Dang Z.M., and Xu H.P., Enhanced Electrical Conductivity in Chemically Modified Carbon Nanotube/Methylvinyl Silicone Rubber Nanocomposite, *European Polymer Journal*, 43(12): 4924–4930, 2007.

[76] Jiang M.J., Dang Z.M., and Yao S.H., Effects of Surface Modification of Carbon Nanotubes on the Microstructure and Electrical Properties of Carbon Nanotubes/Rubber Nanocomposites, *Chemical Physics Letters*, 457(4–6): 352–356, 2008.

[77] Ramanathan T., Fisher F.T., and Ruoff R.S., Aminofunctionalized Carbon Nanotubes for Binding to Polymers and Biological Systems, *Chemistry of Materials*, 17(6): 1290–1295, 2005.

[78] Aviles F., Cauich-Rodriguez J.V., and Moo-Tah L., Evaluation of Mild Acid Oxidation Treatments for MWCNT Functionalization, *Carbon*, 47(13): 2970–2975, 2009.

[79] Kuznetsova A., Mawhinney D.B., and Naumenko V., Enhancement of Adsorption Inside of Single-walled Nanotubes: Opening the Entry Ports, *Chemical Physics Letters*, 321(3-4): 292–296, 2000.

[80] Grossiord N., Loos J., and Regev O., Toolbox for Dispersing Carbon Nanotubes into Polymers to Get Conductive Nanocomposites, *Chemistry of Materials*, 18(5): 1089–1099, 2006.

[81] Satyanarayana N., Xie X.G., and Rambabu B., Sol-gel Synthesis and Characterization of the Ag_2O-SiO_2 System, *Materials Science and Engineering B-Solid State Materials For Advanced Technology*, 72(1): 7–12, 2000.

[82] Chen X.H., Chen C.S., and Chen Q., Nondestructive Purification of Multi-walled Carbon Nanotubes Produced by Catalyzed CVD, *Materials Letters*, 57(3): 734, 2005.

[83] Jeziorny A., Parameters Characterizing Kinetics of Non-isothermal Crystallization of Poly(Ethylene-Terephthalate) Determined by DSC, *Polymer*, 19(10): 1142-1144, 1978.

[84] Logakis E., Pandis C., and Peoglos V., Structure–property Relationships in Polyamide 6/Multiwalled Carbon Nanotubes Nanocomposites, *Journal of Polymer Science Part B-Polymer Physics*, 47(8): 764-774, 2009.

[85] Brosse A.C., Tence-Girault S., and Piccione P.M., Effect of Multi-walled Carbon Nanotubes on the Lamellae Morphology of Polyamide-6, *Polymer*, 49(21): 4680-4686, 2008.

[86] Xiang F., Shi Y., and Li X., Cocontinuous Morphology of Immiscible High Density Polyethylene/Polyamide 6 Blend Induced by Multiwalled Carbon Nanotubes Network, *European Polymer Journal*, 48(2): 350-361, 2012.

APPENDIX A

CRYSTALLIZATION BEHAVIOUR CURVES FOR PA6 AND ITS NANOCOMPOSITES WITH 0.1 AND 0.5 WT% CARBON NANOTUBES

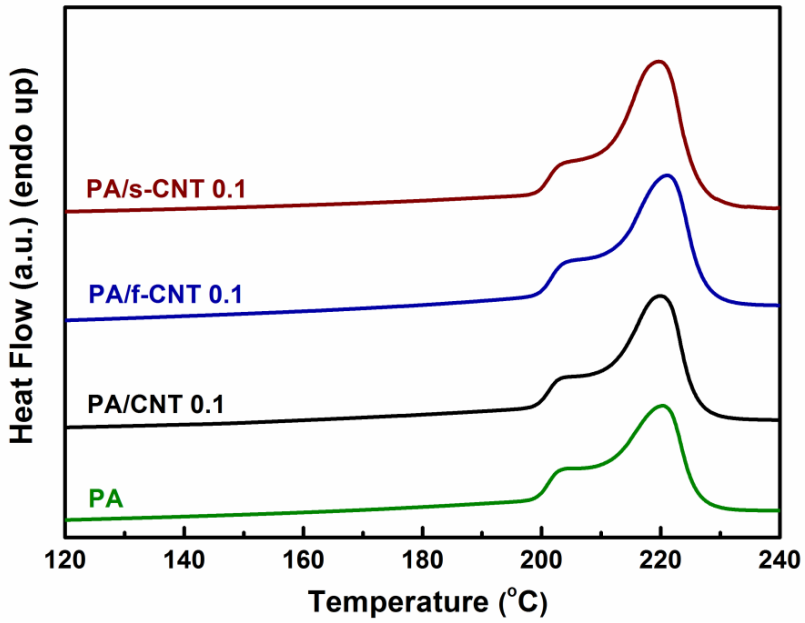

(a)

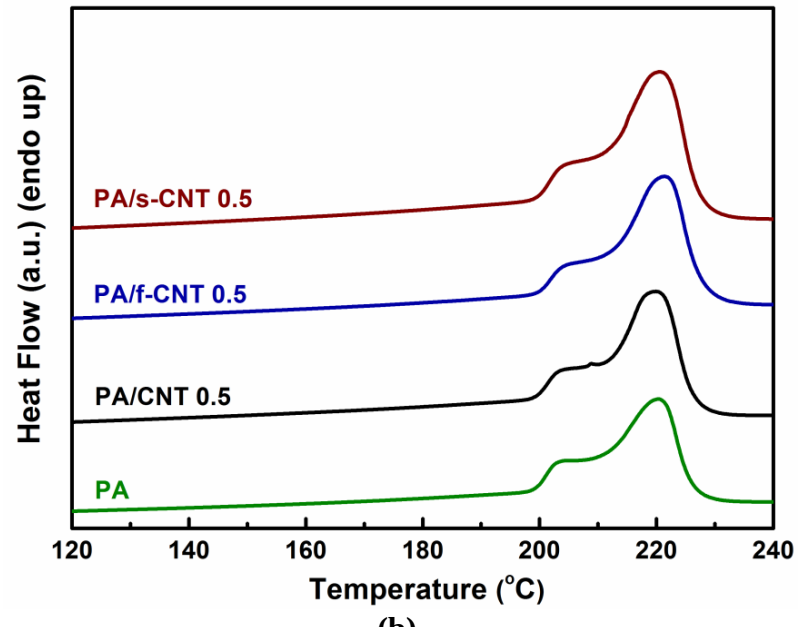

(b)

Figure A.1 DSC Heating Thermograms (at 20°C/min) for PA6 and its Nanocomposites with **(a)** 0.1 and **(b)** 0.5 wt% Carbon Nanotubes

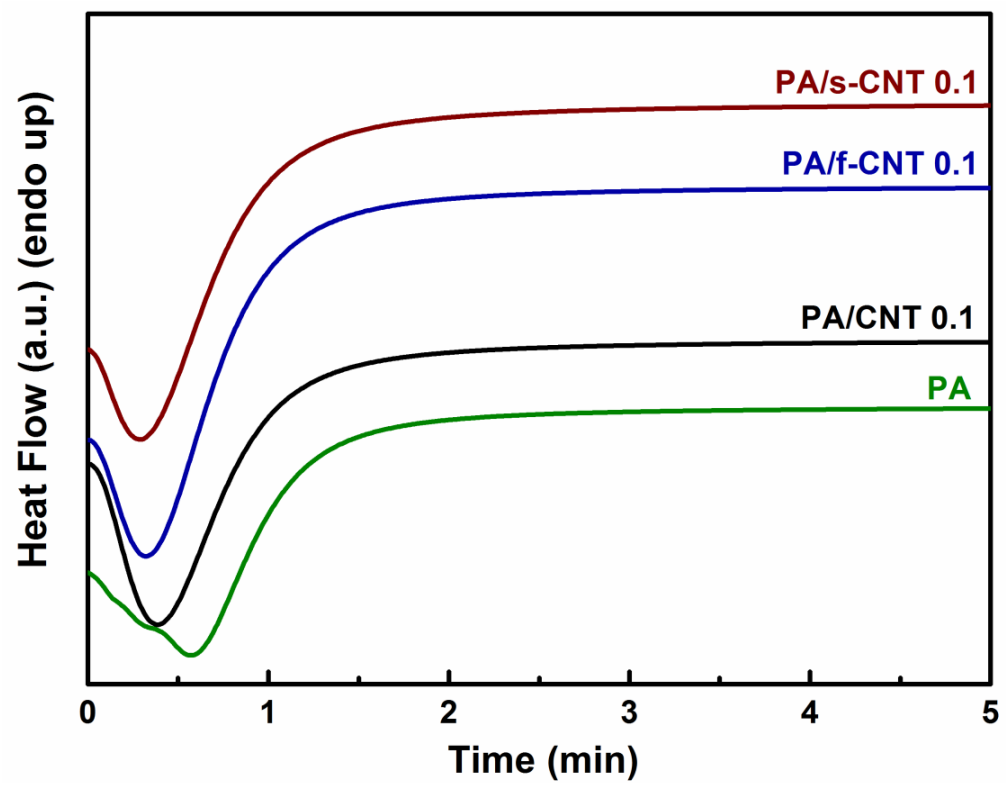

(a)

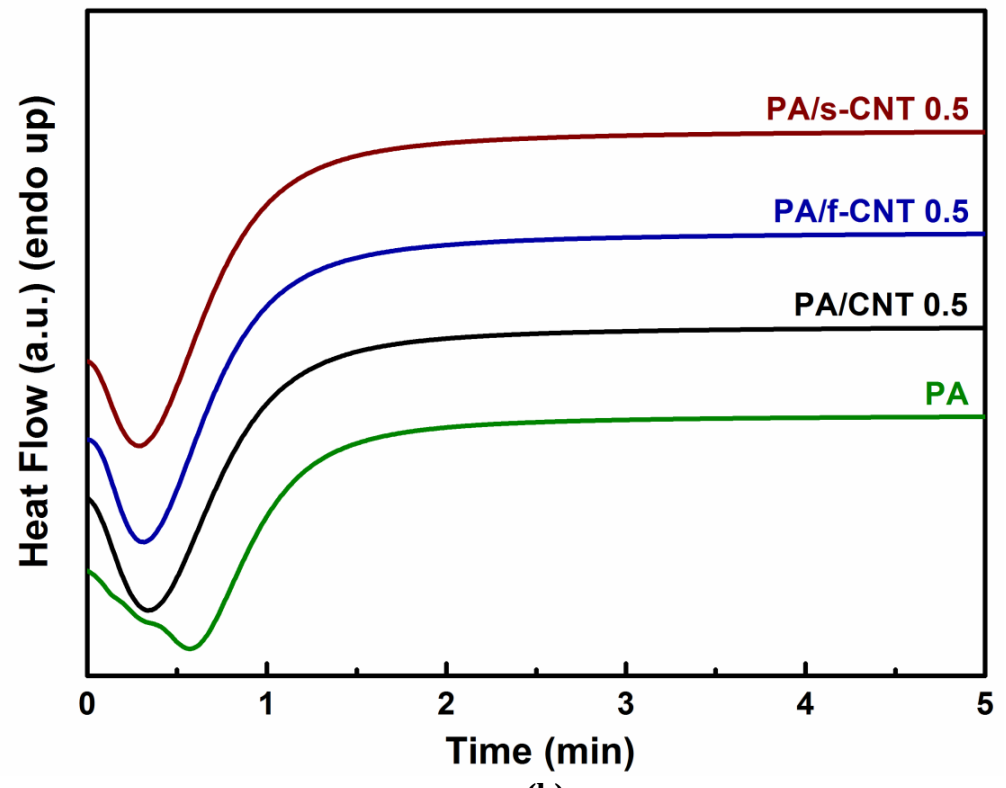

(b)

Figure A.2 Isothermal Crystallization Thermograms (at 195°C) for PA6 and its Nanocomposites with **(a)** 0.1 and **(b)** 0.5 wt% Carbon Nanotubes

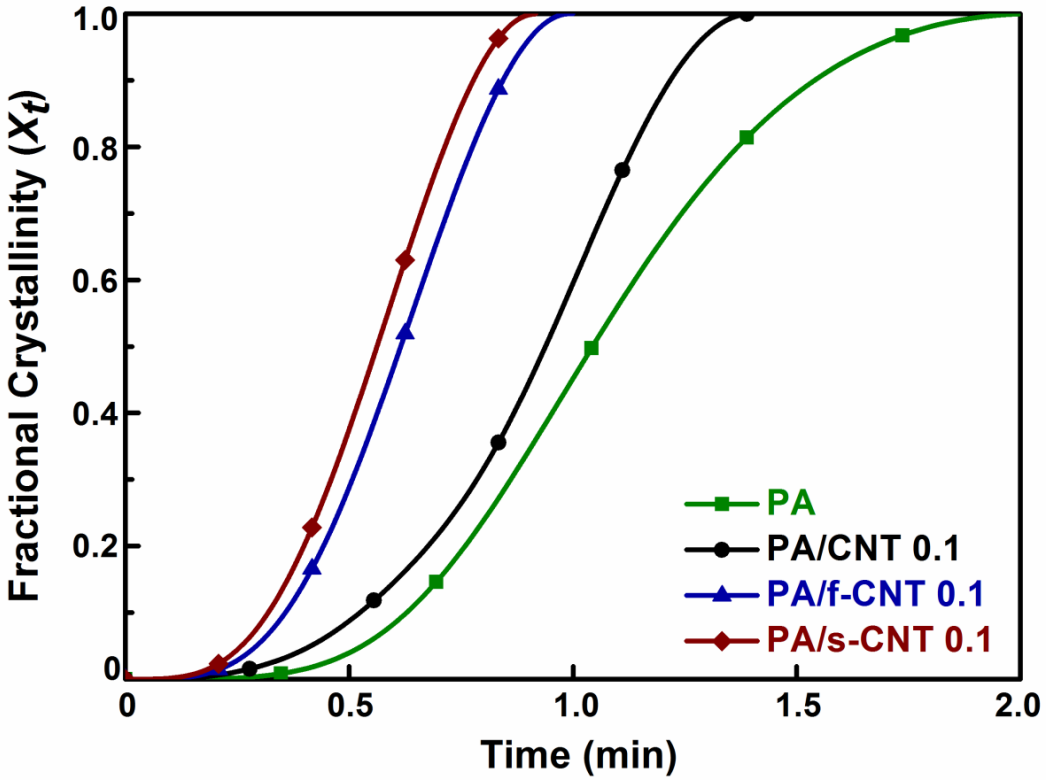

(a)

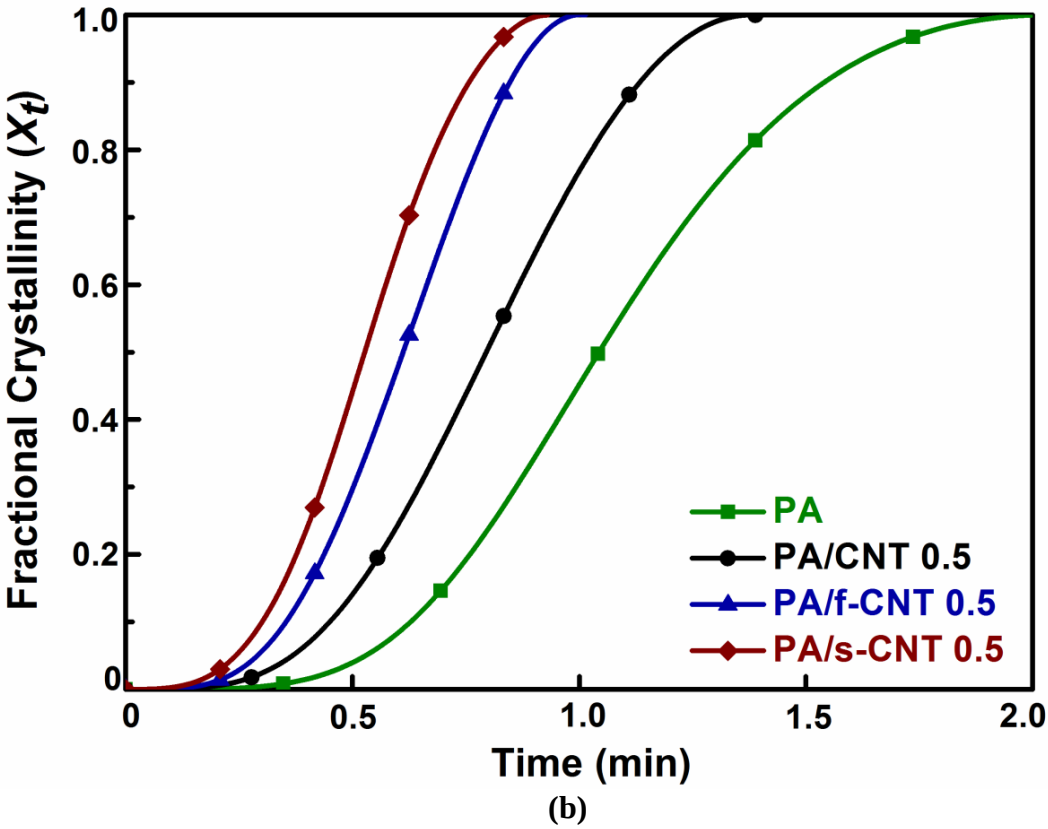

(b)

Figure A.3 Fractional Crystallinity versus Isothermal Crystallization Time Curves for PA6 and its Nanocomposites with **(a)** 0.1 and **(b)** 0.5 wt% Carbon Nanotubes

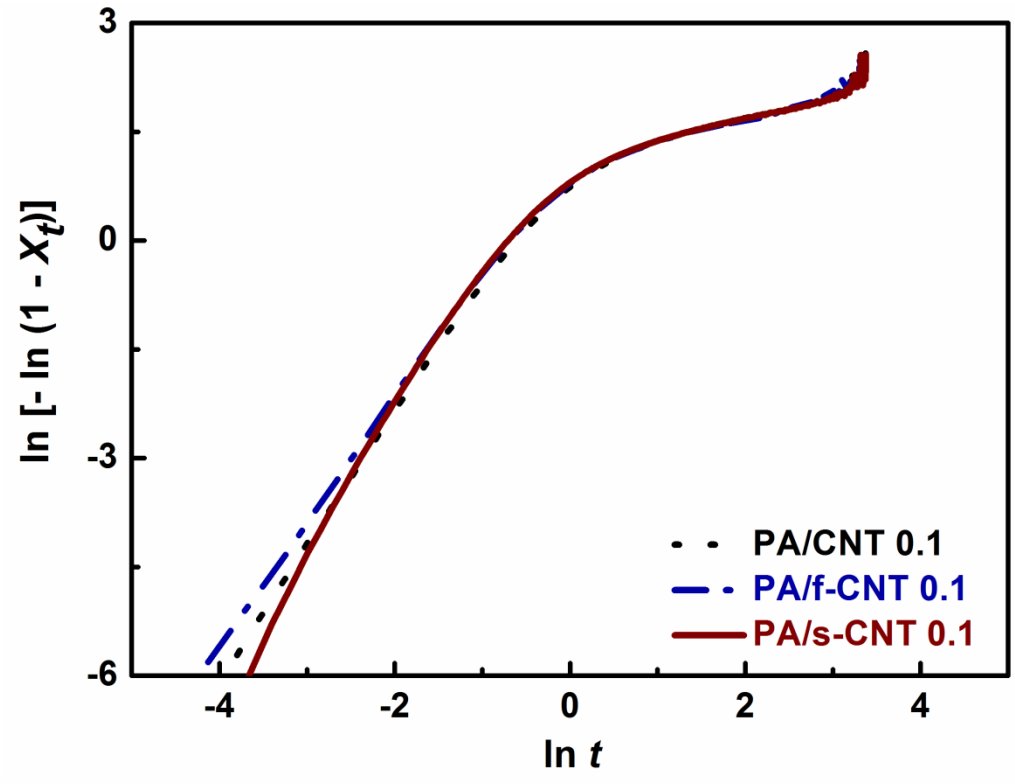

(a)

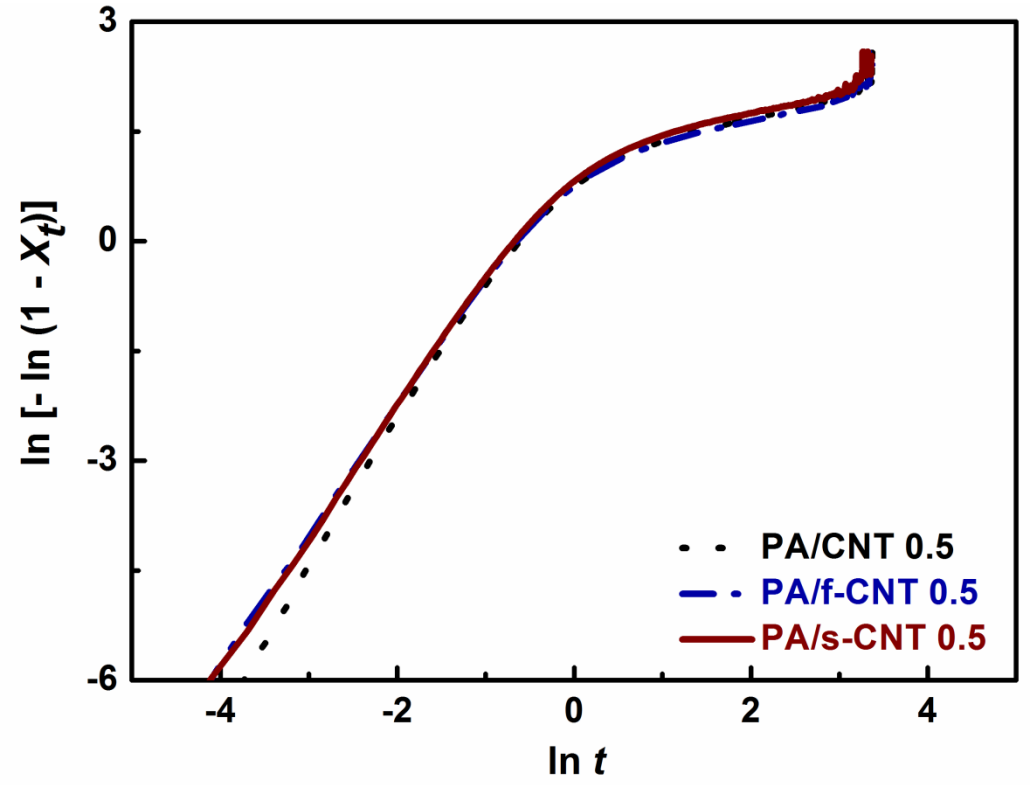

(b)

Figure A.4 Avrami Plots of ln [– ln (1 – X_t)] versus ln t during Isothermal Crystallization of Nanocomposites with **(a)** 0.1 and **(b)** 0.5 wt% Carbon Nanotubes

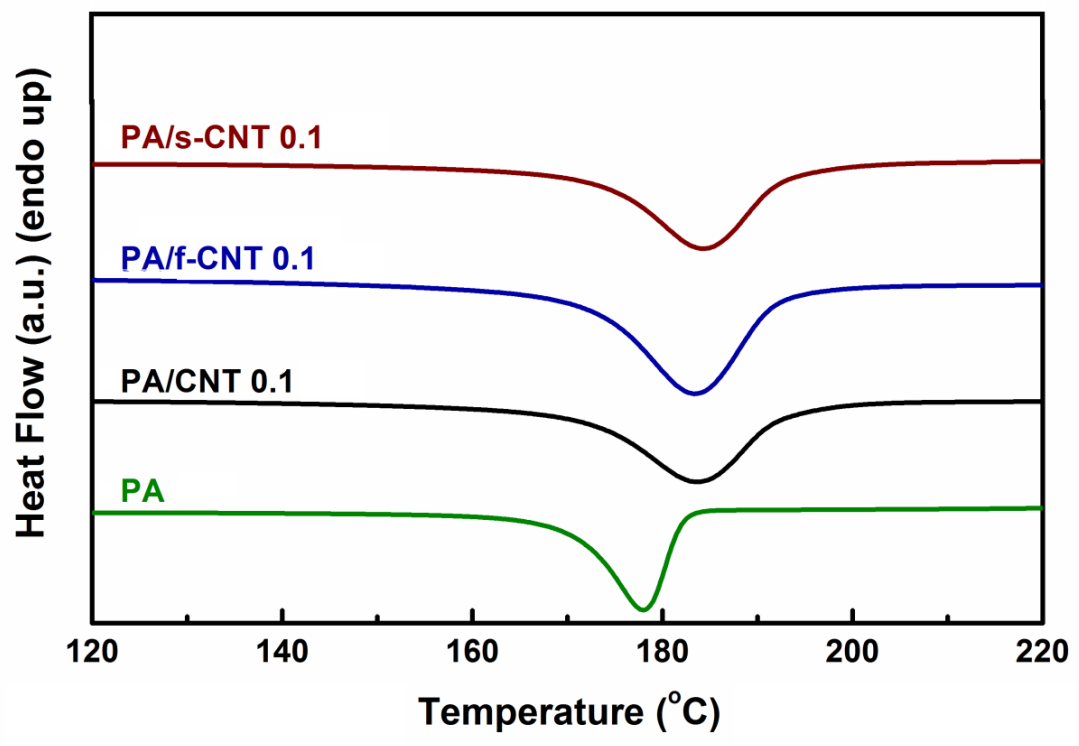

(a)

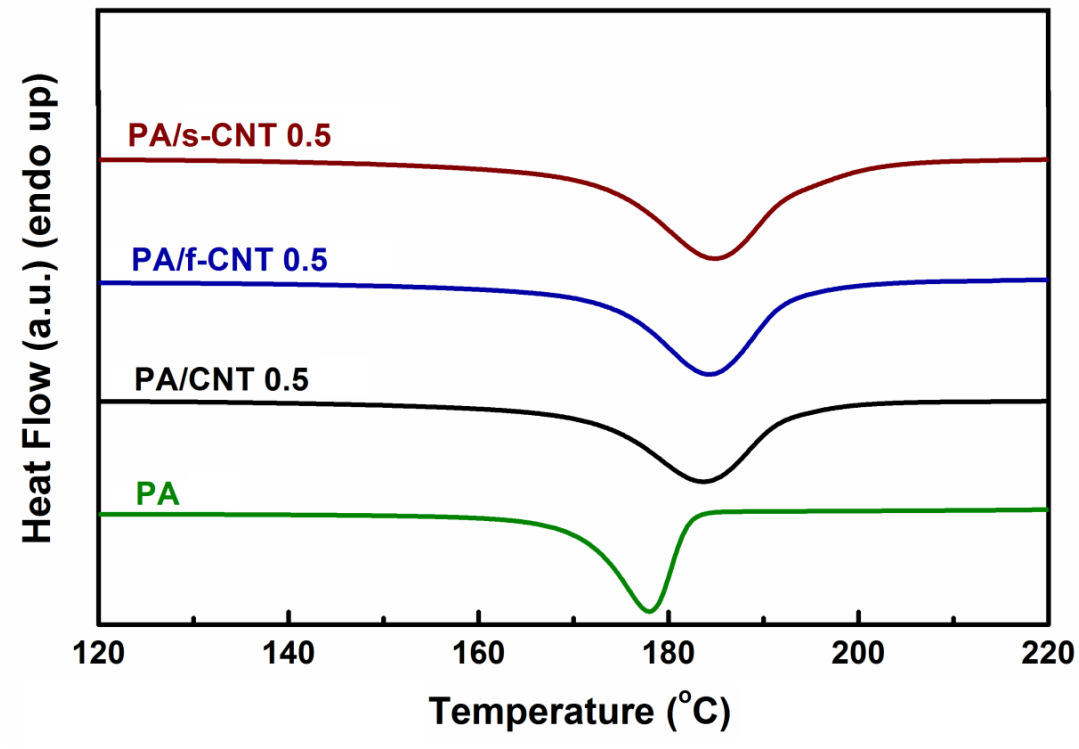

(b)

Figure A.5 DSC Cooling Thermograms (at 20°C/min) for PA6 and its Nanocomposites with **(a)** 0.1 and **(b)** 0.5 wt% Carbon Nanotubes

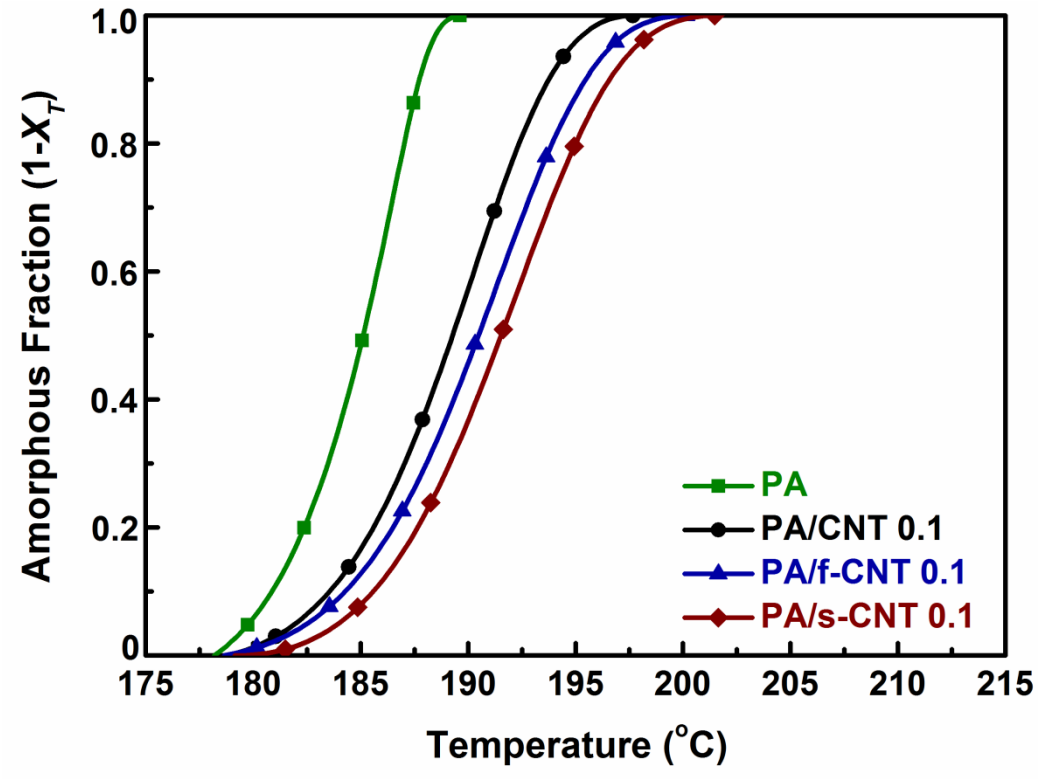

(a)

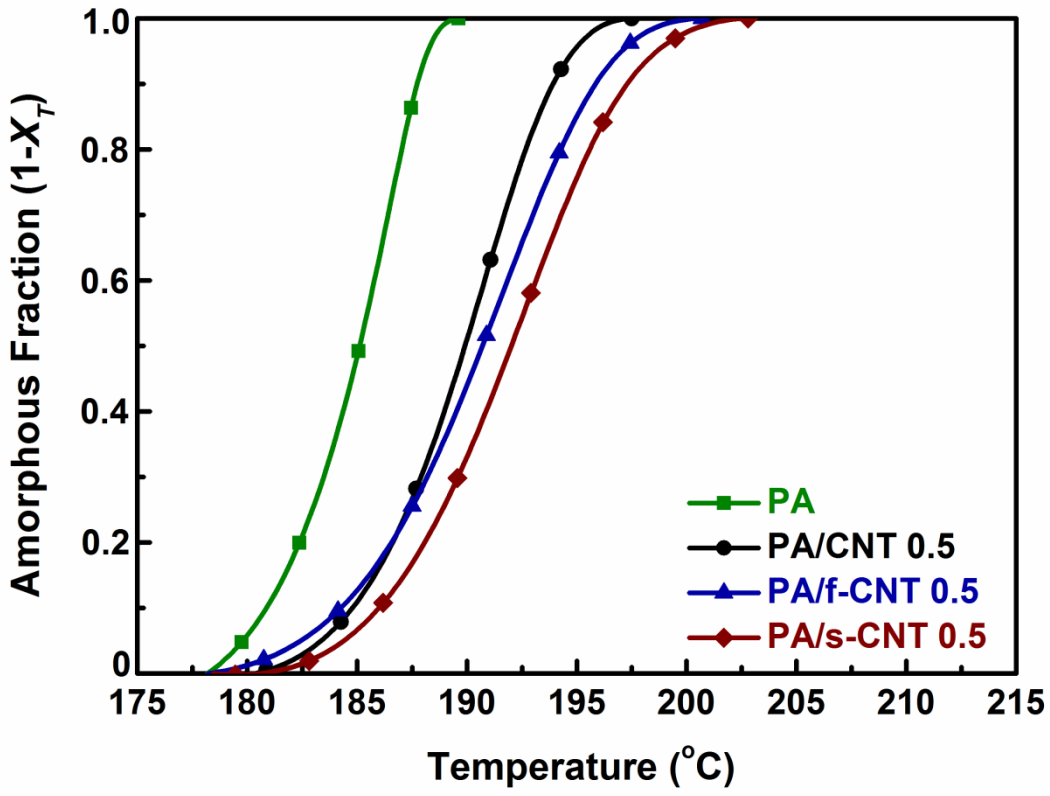

(b)

Figure A.6 Amorphous Fraction versus Non-isothermal Crystallization Temperature Curves for PA6 and its Nanocomposites with **(a)** 0.1 and **(b)** 0.5 wt% Carbon Nanotubes

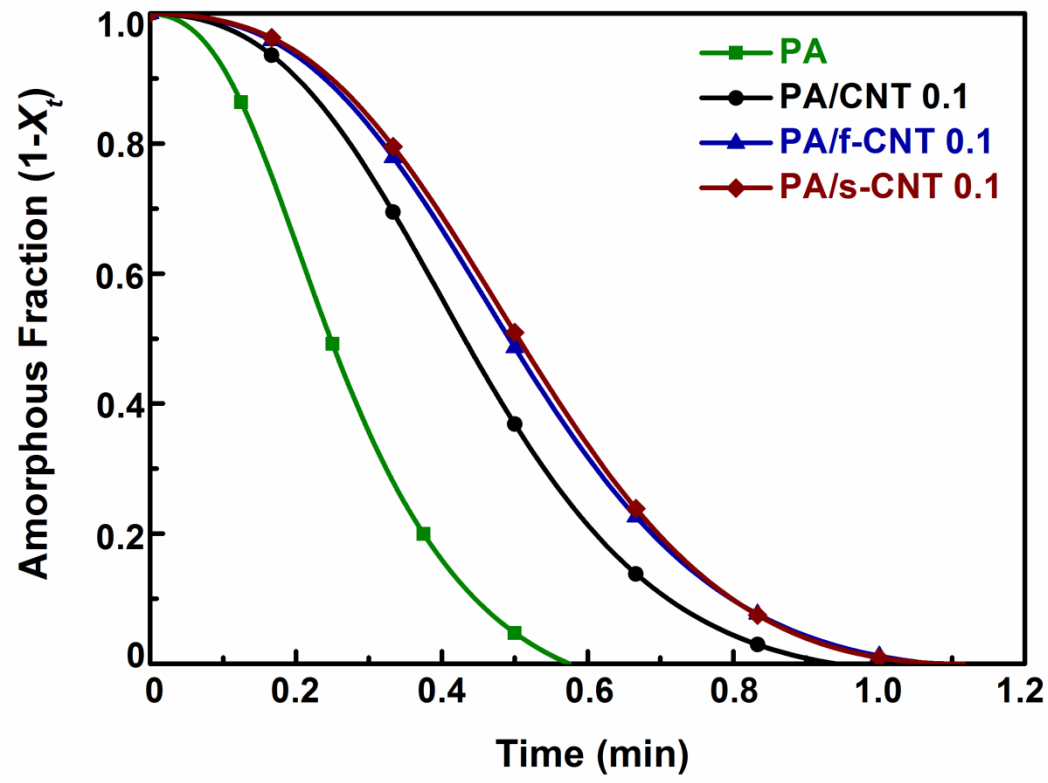

(a)

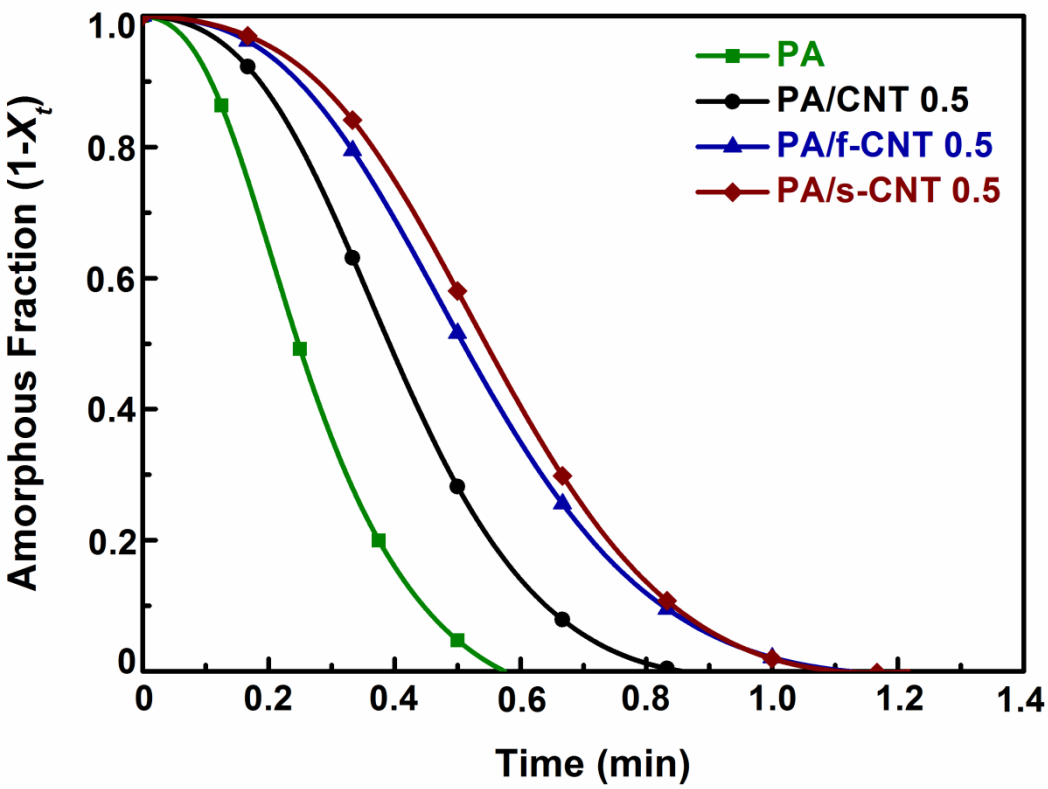

(b)

Figure A.7 Amorphous Fraction versus Non-isothermal Crystallization Time curves for PA6 and its Nanocomposites with **(a)** 0.1 and **(b)** 0.5 wt% Carbon Nanotubes

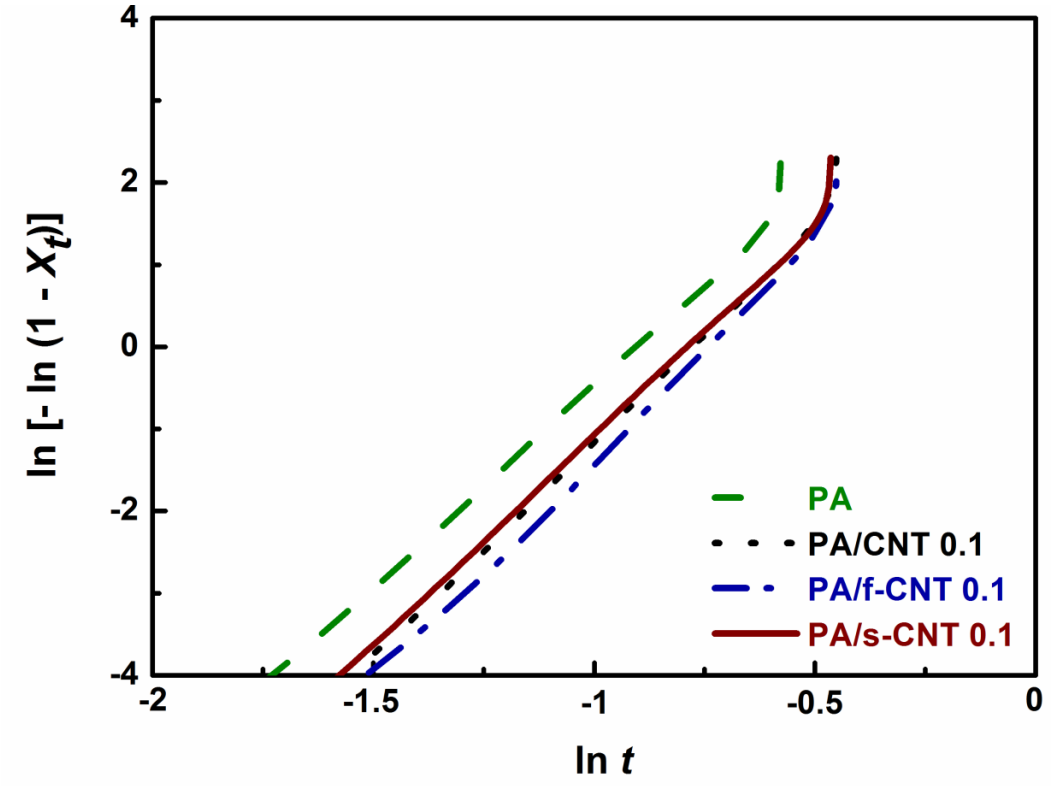

(a)

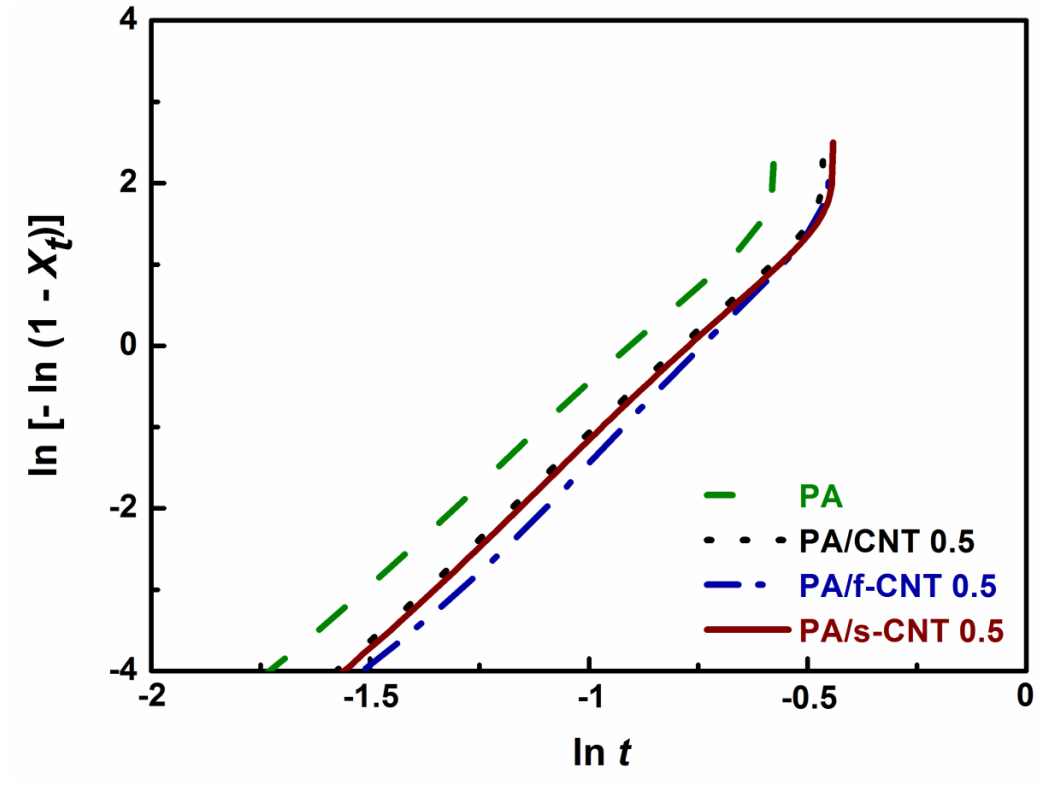

(b)

Figure A.8 Avrami Plots of ln [– ln (1 – X_t)] versus ln t during Non-isothermal Crystallization of PA6 and its Nanocomposites with **(a)** 0.1 and **(b)** 0.5 wt% Carbon Nanotubes

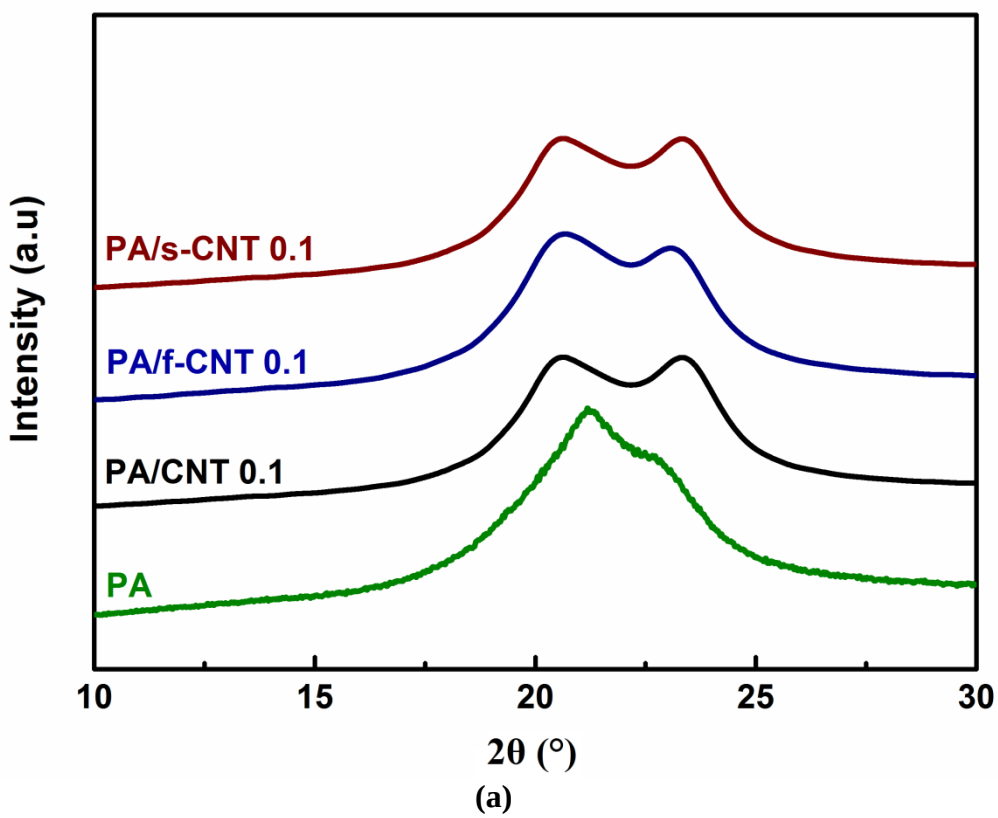

(a)

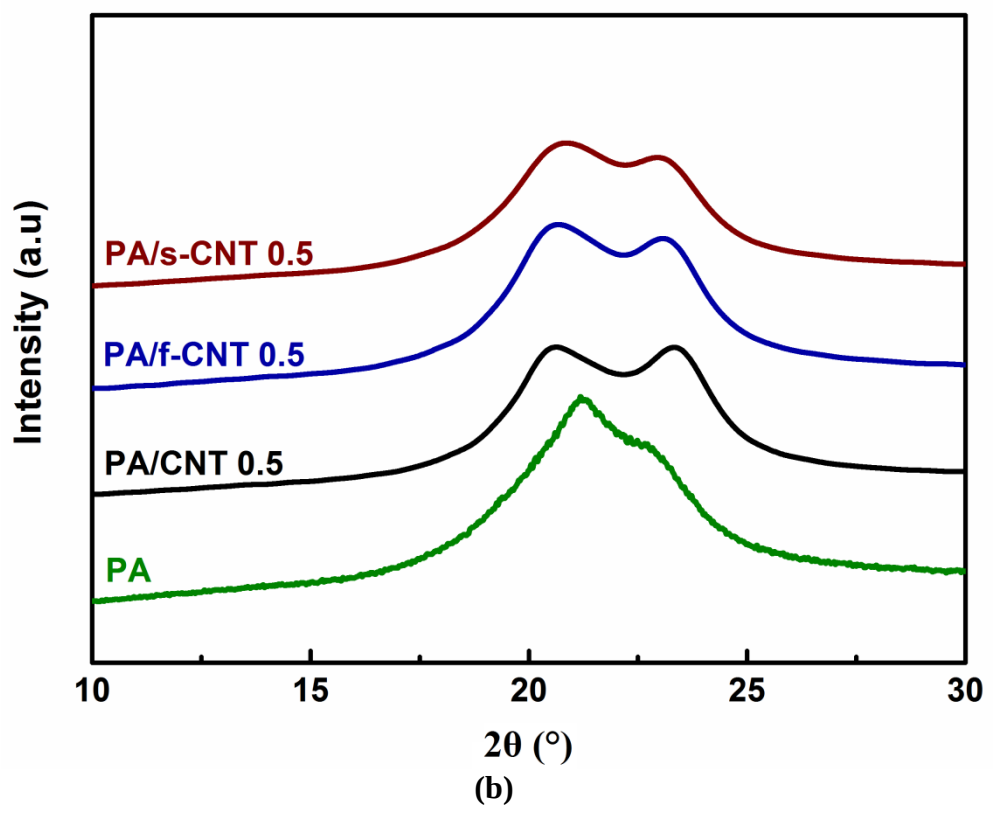

(b)

Figure A.9 XRD Patterns of Injection Molded PA6 and its Nanocomposites with **(a)** 0.1 and **(b)** 0.5 wt% Carbon Nanotubes

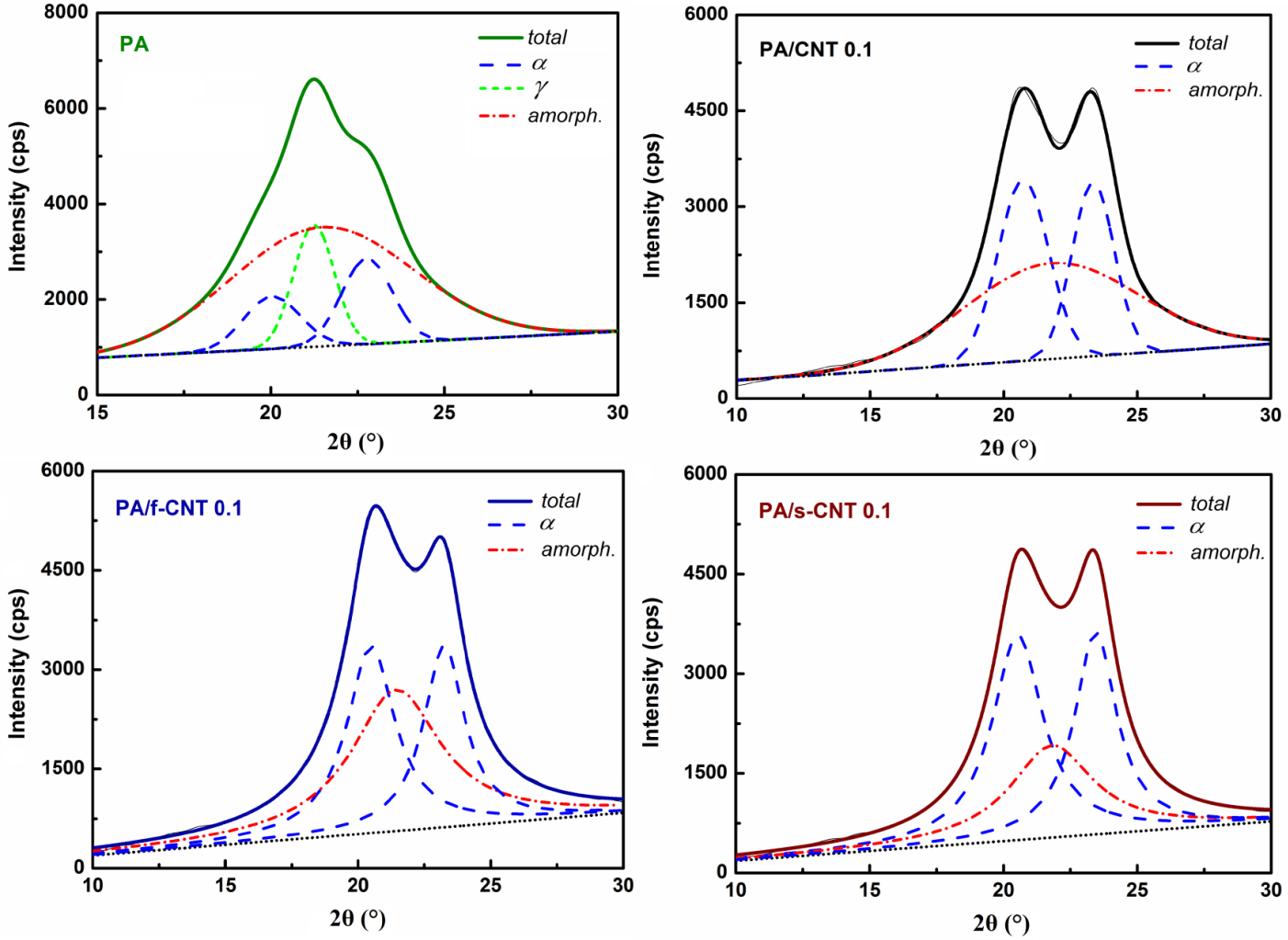

Figure A.10 Deconvoluted XRD Peaks of PA6 and its Nanocomposites with 0.1 wt% Carbon Nanotubes

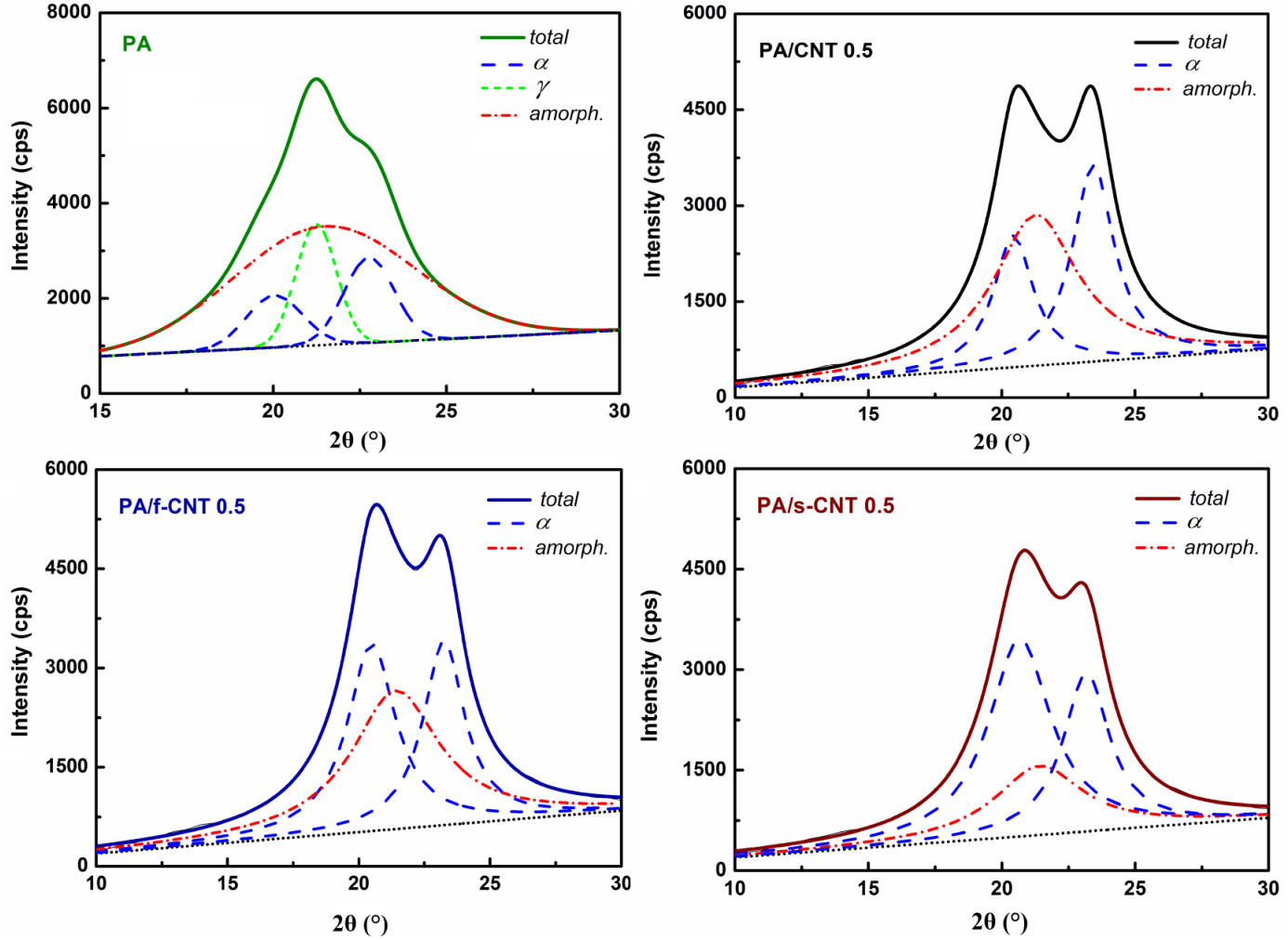

Figure A.11 Deconvoluted XRD Peaks of PA6 and its Nanocomposites with 0.5 wt% Carbon Nanotubes

APPENDIX B

MECHANICAL AND THERMAL BEHAVIOUR CURVES FOR PA6 AND ITS NANOCOMPOSITES WITH 0.1 AND 0.5 WT% CARBON NANOTUBES

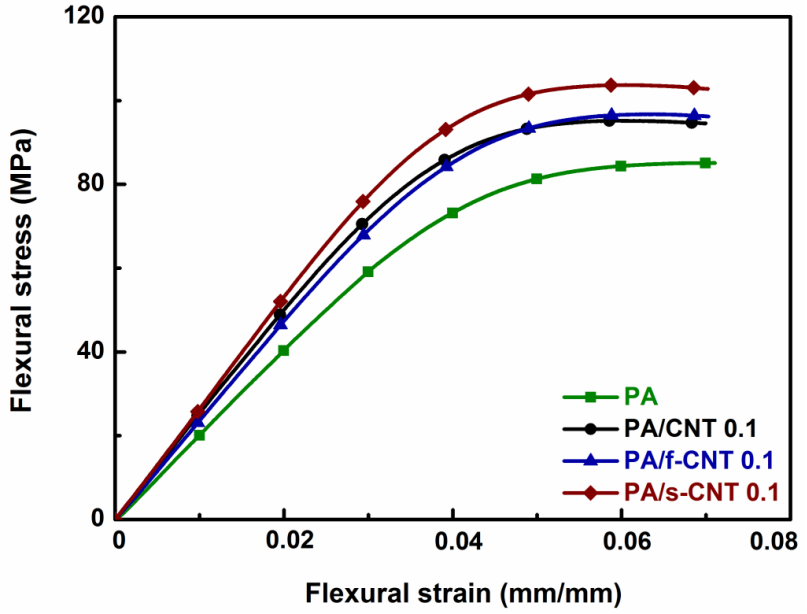

(a)

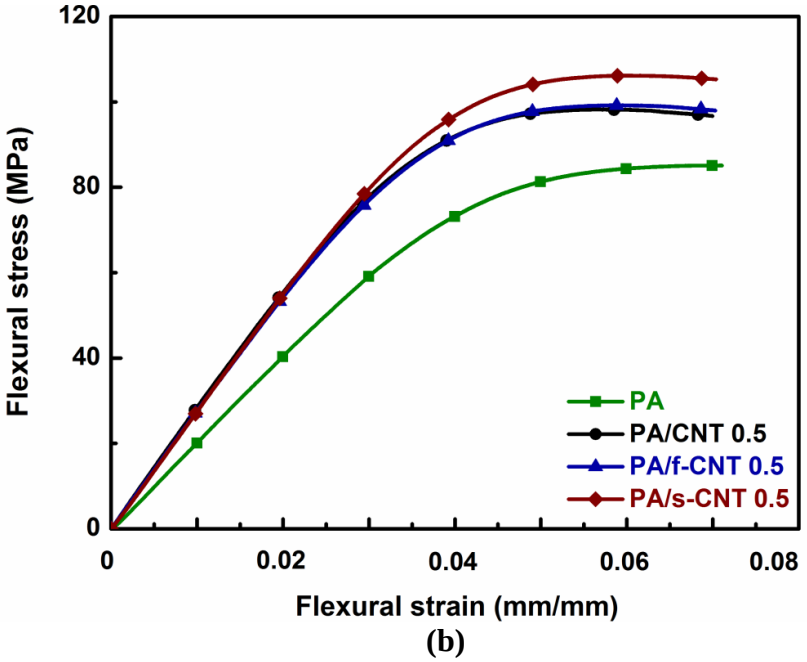

(b)

Figure B.1 Flexural Stress versus Flexural Strain Curves of PA6 and its Nanocomposites with **(a)** 0.1 and **(b)** 0.5 wt% Carbon Nanotubes

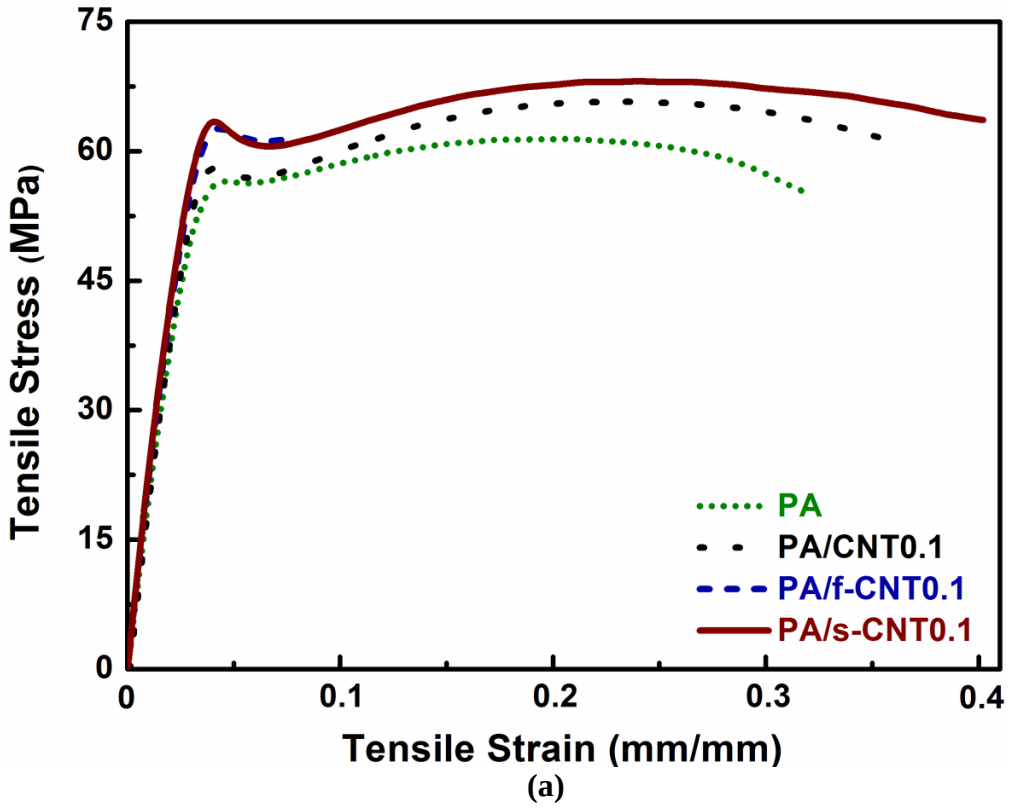

(a)

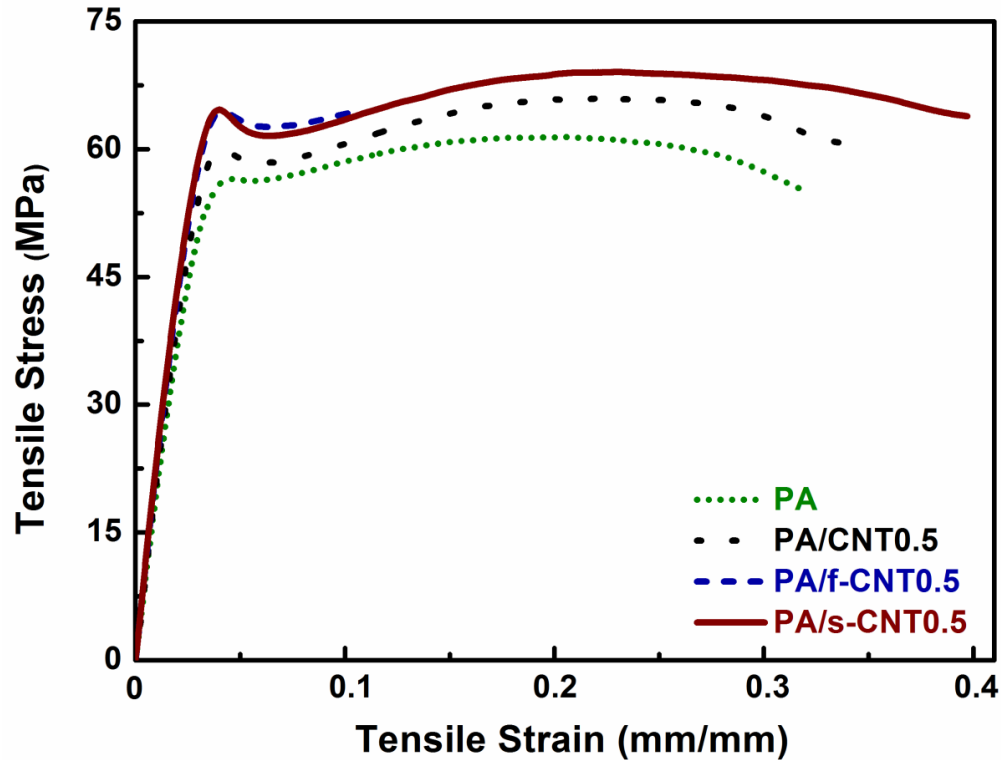

(b)

Figure B.2 Tensile Stress versus Tensile Strain Curves of PA6 and its Nanocomposites with **(a)** 0.1 and **(b)** 0.5 wt% Carbon Nanotubes

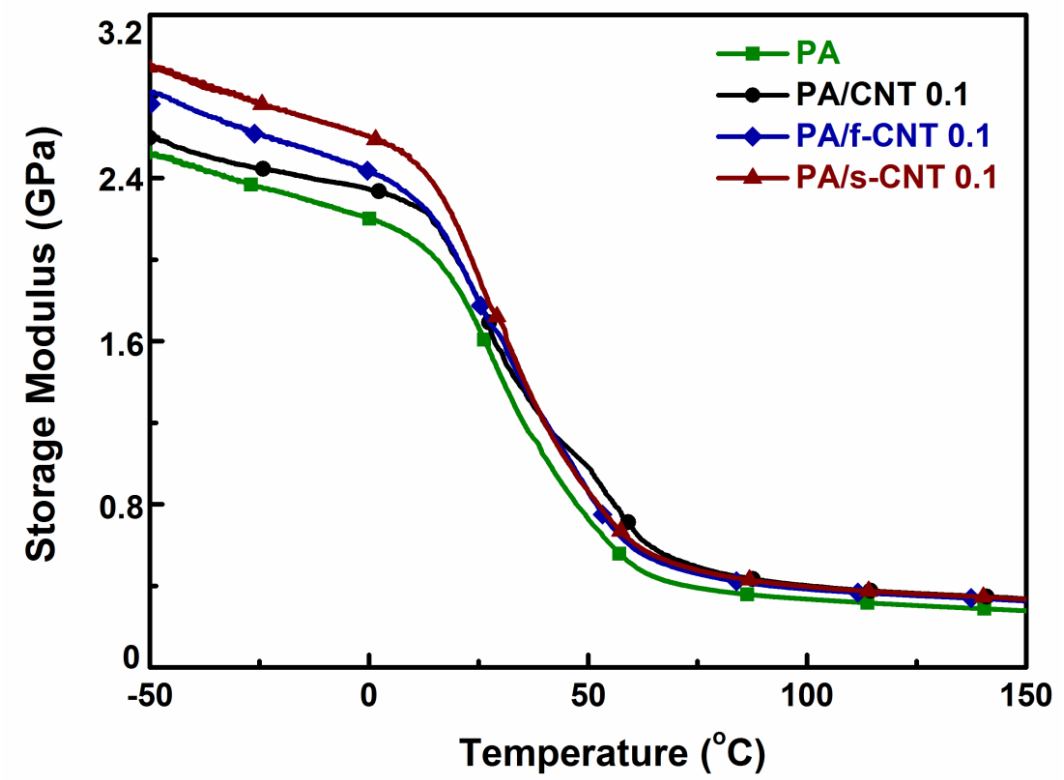

(a)

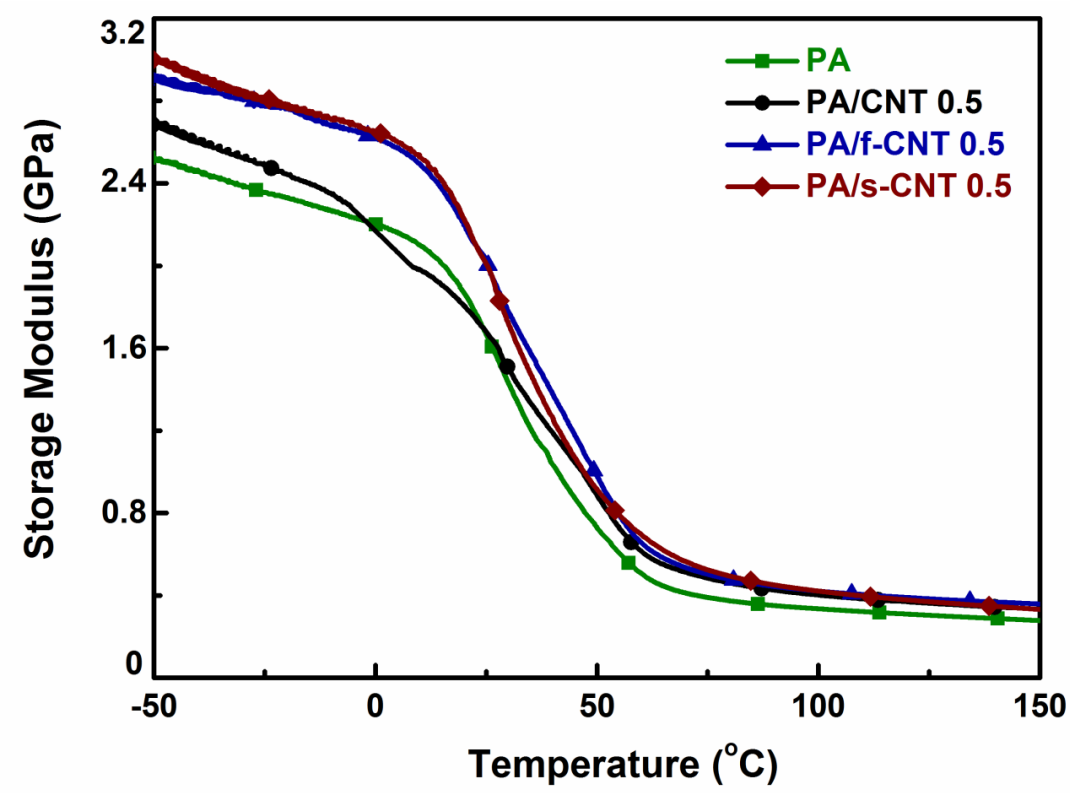

(b)

Figure B.3 Storage Modulus Curves of PA6 and its Nanocomposites with **(a)** 0.1 and **(b)** 0.5 wt% Carbon Nanotubes

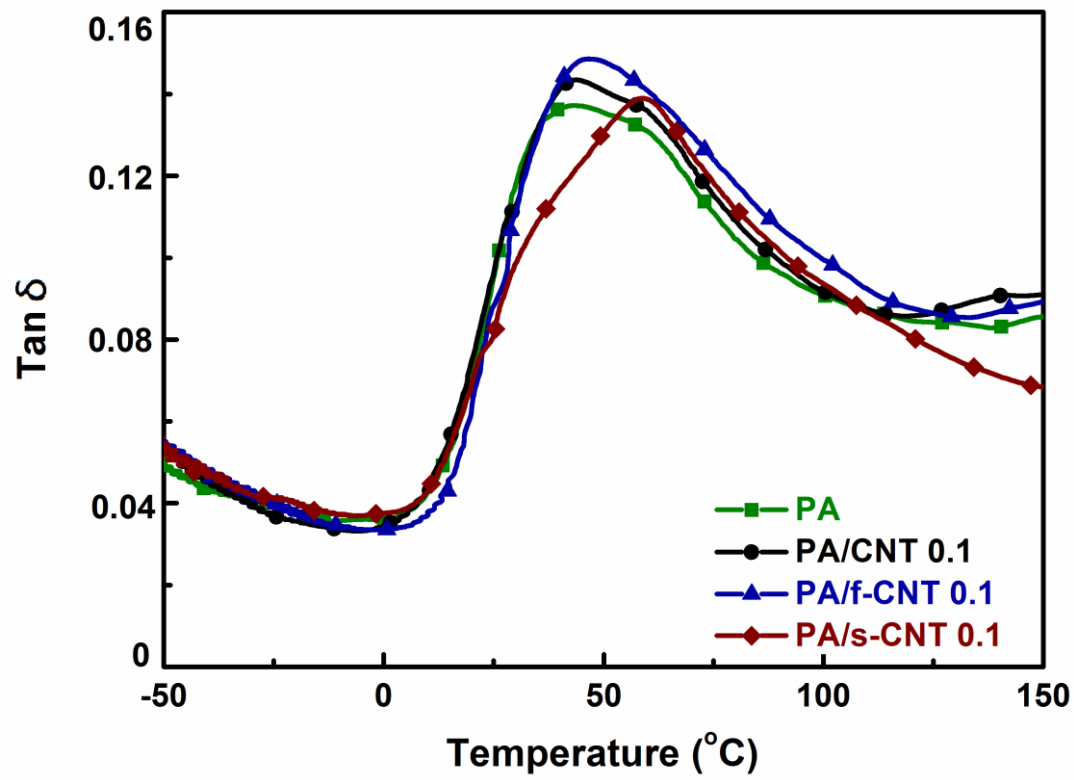

(a)

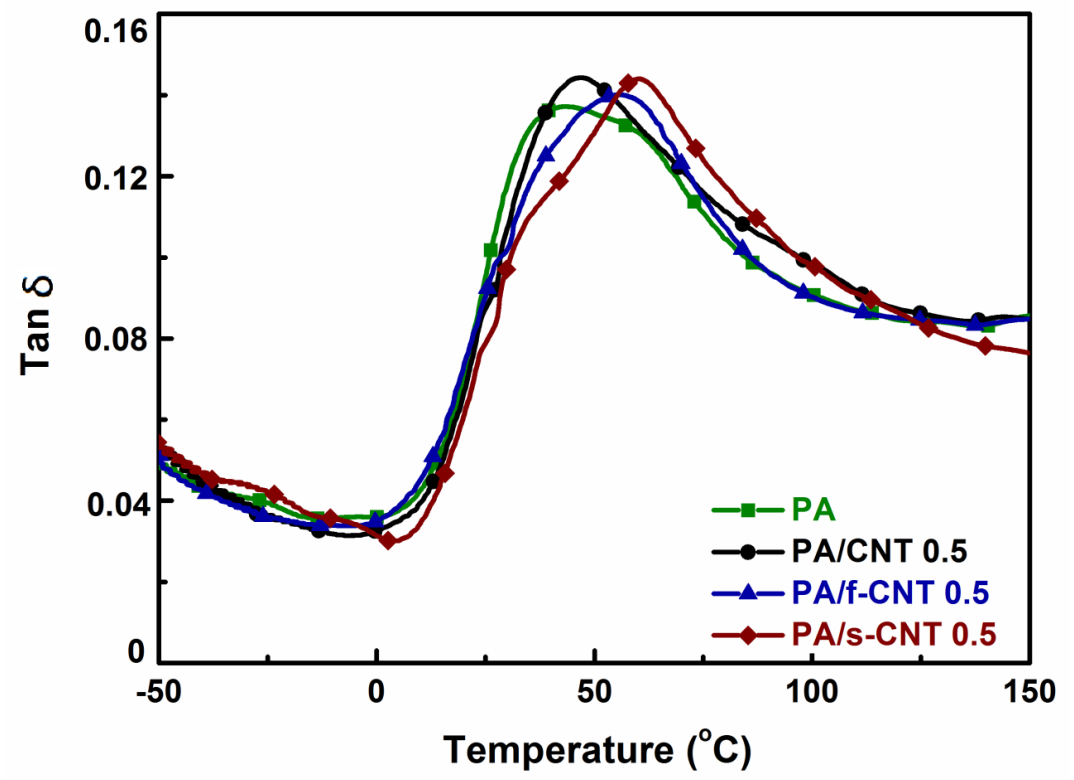

(b)

Figure B.4*tan δ* Curves of PA6 and its Nanocomposites with **(a)** 0.1 and **(b)** 0.5 wt% Carbon Nanotubes

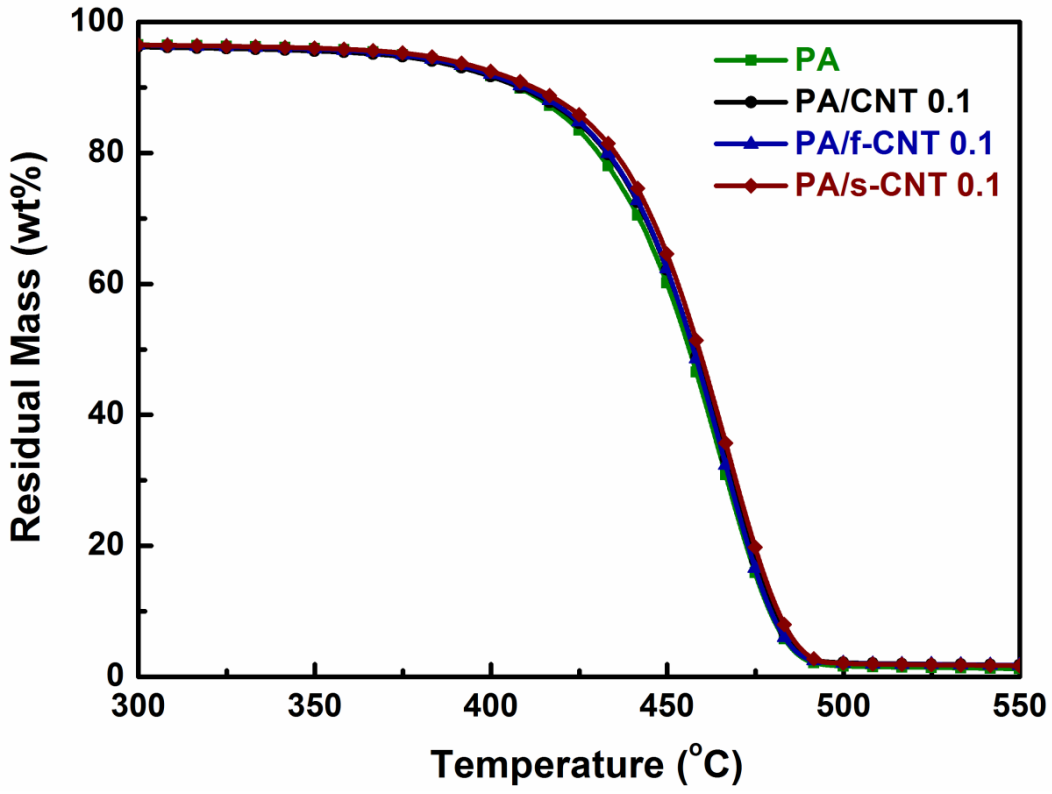

(a)

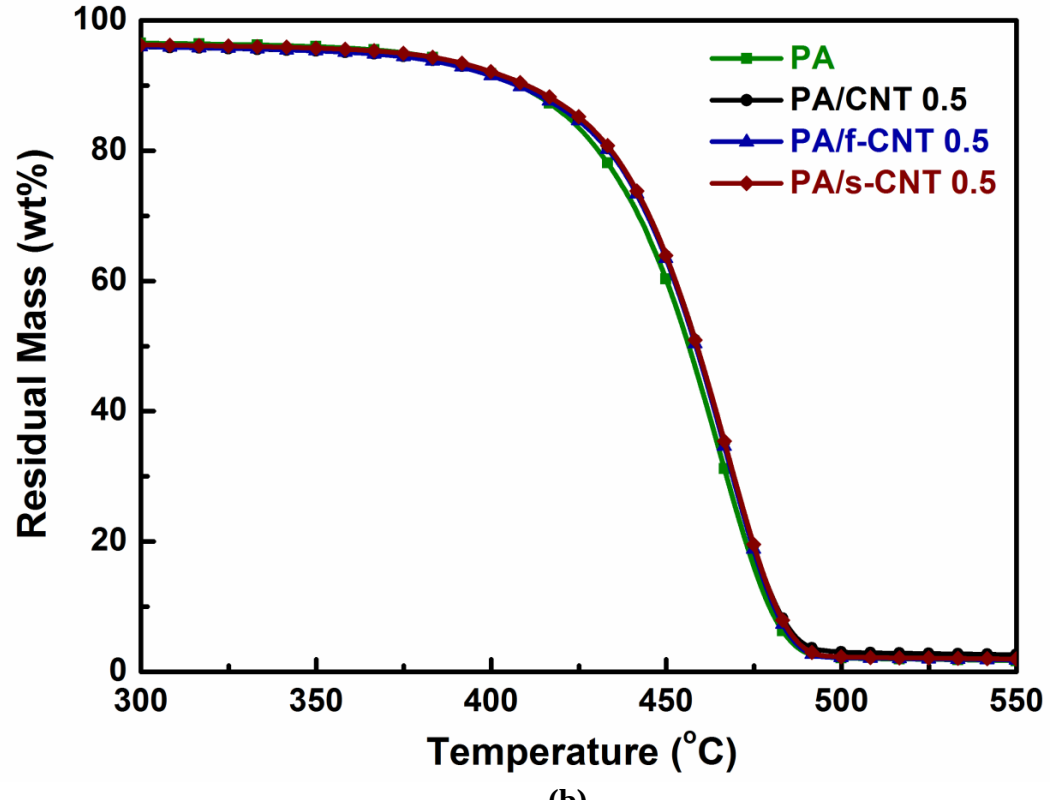

(b)

Figure B.5 Thermogravimetric (TG) Curves of PA6 and its Nanocomposites with **(a)** 0.1 and **(b)** 0.5 wt% Carbon Nanotubes

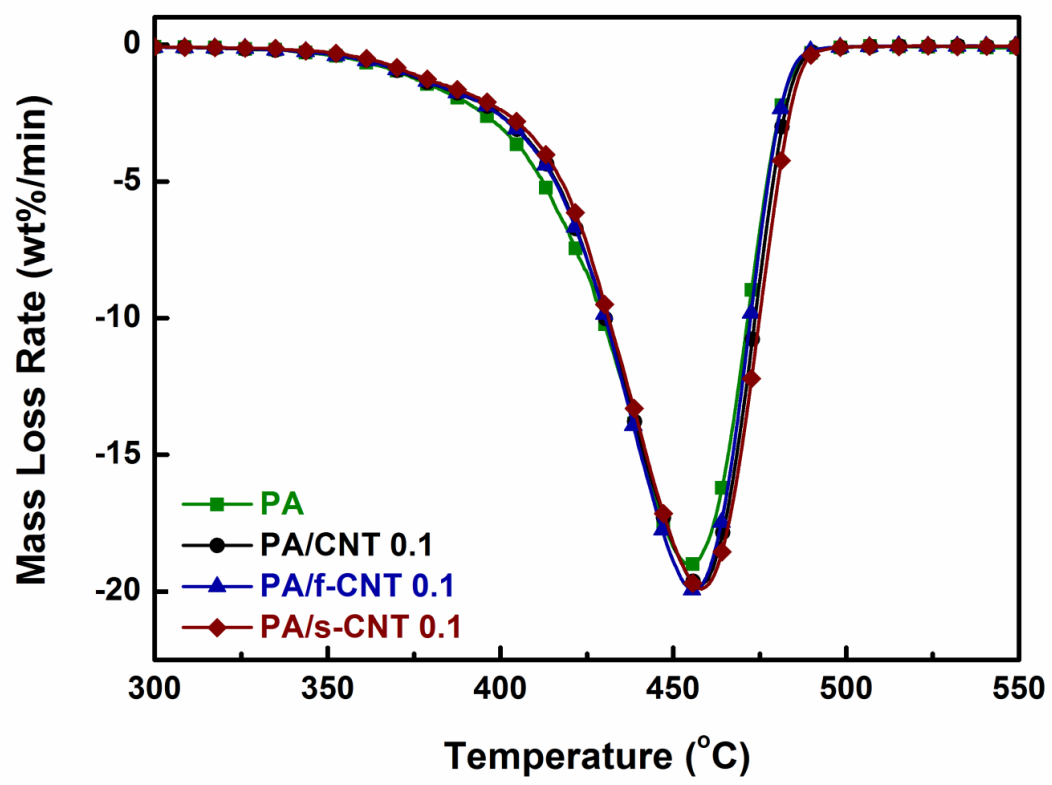

(a)

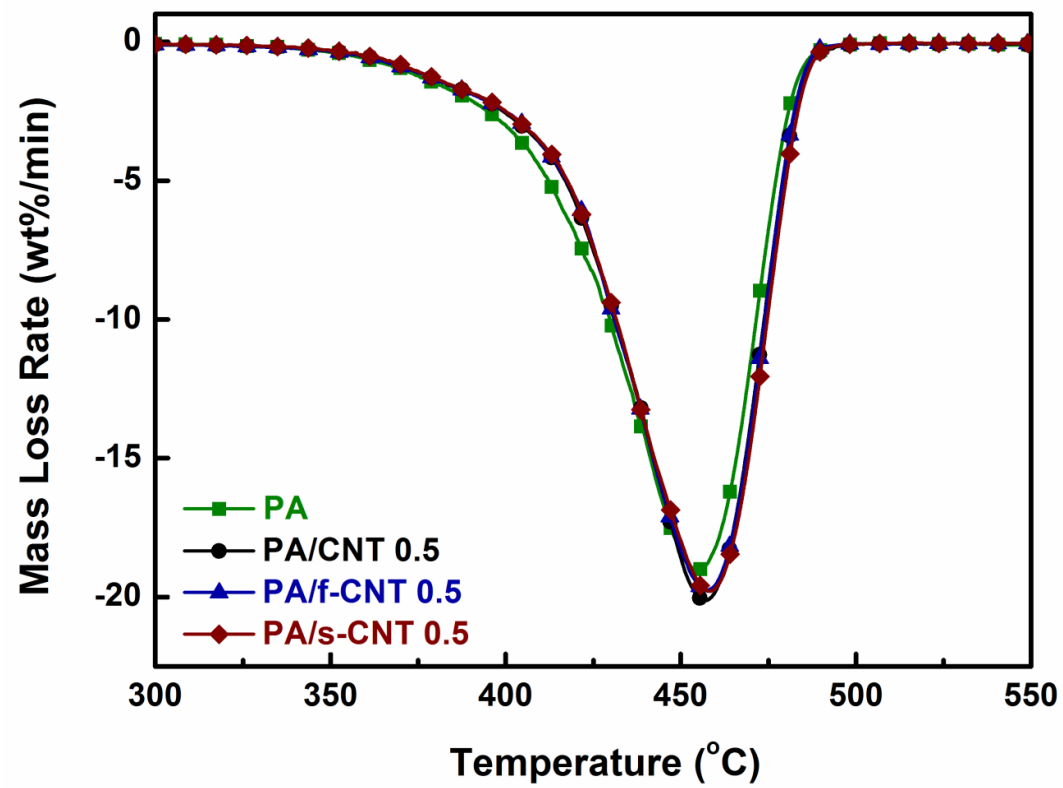

(b)

Figure B.6 Differential Thermogravimetric (DTG) Curves of PA6 and its Nanocomposites with **(a)** 0.1 and **(b)** 0.5 wt% Carbon Nanotubes